NASA CR-165572
PWA-5512-87

NASA

PERFORMANCE DETERIORATION DUE TO ACCEPTANCE TESTING AND FLIGHT LOADS

JT9D JET ENGINE DIAGNOSTICS PROGRAM

W. J. Olsson

UNITED TECHNOLOGIES CORPORATION
Pratt & Whitney Aircraft Group
Commercial Products Division

Prepared for

NATIONAL AERONAUTICS AND SPACE ADMINISTRATION

Lewis Research Center
Cleveland, Ohio 44135

Contract NAS3-20632

1. Report No.	2. Government Accession No.	3. Recipient's Catalog No.
NASA CR-165572		

4. Title and Subtitle	5. Report Date
Performance Deterioration due to Acceptance Testing and Flight Loads; JT9D Jet Engine Diagnostic Program	January 22, 1982
	6. Performing Organization Code

7. Author(s)	8. Performing Organization Report No.
W. J. Olsson	PWA-5512-87
	10. Work Unit No.

9. Performing Organization Name and Address	11. Contract or Grant No.
UNITED TECHNOLOGIES CORPORATION Pratt & Whitney Aircraft Group, Commercial Products Div. East Hartford, Connecticut 06108	NAS3-20632
	13. Type of Report and Period Covered Contractor Report

12. Sponsoring Agency Name and Address	14. Sponsoring Agency Code
NATIONAL AERONAUTICS AND SPACE ADMINISTRATION NASA Lewis Research Center Cleveland, Ohio 44135	

15. Supplementary Notes

Project Manager; D. L. Nored
Project Engineer; C. M. Mehalic
NASA Lewis Research Center, Cleveland, Ohio 44135

16. Abstract

This document presents the results of a Flight Loads Test of the JT9D-7 engine which was the final phase of the NASA JT9D Jet Engine Diagnostics Program. The objectives of this test program were to: measure aerodynamic and inertia loads on the engine during flight, explore the effects of airplane gross weight and typical maneuvers on these flight loads, simultaneously measure the changes in engine running clearances and performance resulting from the maneuvers, make refinements of engine performance deterioration prediction models based on analytical results of the tests, and make recommendations to improve propulsion system performance retention. The test program was conducted as a joint effort with the Boeing Commercial Airplane Company. Boeing provided the test airplane and made the flight loads measurements. Pratt & Whitney Aircraft provided the instrumented engines and made the engine clearance and performance measurements. The test program included a typical production airplane acceptance test plus additional flights and maneuvers to encompass the range of flight loads in revenue service. The test results indicated that aerodymanic loads, primarily at take-off, were the major cause of rub-induced deterioration in the cold section of the engine. Differential thermal expansion between rotating and static parts plus aerodynamic loads combined to cause blade-to-seal rubs in the turbine.

17. Key Words (Suggested by Author(s))	18. Distribution Statement
Nacelle Aerodynamic and Inertial Loads (NAIL) Engine/Module Performance Deterioration Thrust Specific Fuel Consumption (TSFC) JT9D-7A Engine Flight Load Effects	

19. Security Classif. (of this report)	20. Security Classif. (of this page)	21. No. of Pages	22. Price*
UNCLASSIFIED	UNCLASSIFIED	162	

* For sale by the National Technical Information Service, Springfield, Virginia 22161

NASA-C-168 (Rev. 10-75)

N82-27309#

PREFACE

The requirements of NASA Policy Directive NPD 2220.4 (September 14, 1970) regarding the use of SI Units have been waived in accordance with the provisions of paragraph 5d of that Directive by the Director of Lewis Research Center.

TABLE OF CONTENTS

TABLE OF CONTENTS (Cont'd.)

TABLE OF CONTENTS (Cont'd.)

LIST OF ILLUSTRATIONS

LIST OF ILLUSTRATIONS (Cont'd.)

LIST OF ILLUSTRATIONS (Cont'd.)

LIST OF ILLUSTRATIONS (Cont'd.)

LIST OF ILLUSTRATIONS (Cont'd.)

LIST OF TABLES

SECTION 1.0

SUMMARY

During the fourth and last phase of the JT9D Engine Diagnostics Program, JT9D-7A engines with special instrumentation were flight tested on a Boeing 747 airplane to determine the effects of production airplane acceptance testing and revenue service on running clearances in the fan and high-pressure turbine. The JT9D-7A engines installed with 747-200 nacelles were used in this test to be consistent with previous phases of the Engine Diagnostics Program. Thus, the beneficial effects of turbine clearance control and other engine and installation advances available in current engine models are not included in the test results.

Analysis of the flight test data, supplemented with engine test-stand performance calibrations and engine teardown inspection results, provided the following key findings:

- Maximum clearance closure of about 0.2 inch in the fan, which occurred during take-off rotation, climb, and incipient airplane stall conditions, is the combined effect of:
  - Deflection of the case under high aerodynamic loading of the nacelle,
  - Centrifugal growth of the rotor at high fan speed, and
  - Deflection of the case under high thrust loading.
- Fan clearance closures were essentially equal for inboard and outboard engine positions on the 747 airplane during all flight maneuvers.
- Maximum clearance closure of about 0.05 inch in the high-pressure turbine, which occurred during climb following take-off, is the combined effect of:
  - Differential thermal growth and deflection of the rotor and case at high temperatures,
  - Centrifugal growth of the rotor at high turbine speed,
  - Deflection of the case under thrust loading, and
  - Additional deflection of the case under aerodynamic loading of the nacelle.
- Dynamic vibration-induced flight loads have a negligible effect on fan and high-pressure turbine clearance closures.
- Rub-induced clearance changes cause a 0.8 percent increase in cruise thrust specific fuel consumption (TSFC) during production aircraft acceptance testing and an additional 0.3 percent during revenue service. This short-term effect combined with the

long-term deterioration effect results in a total of 2.1 percent increase in thrust specific fuel consumption in 2000 flight cycles for an unrepaired engine. These influences are illustrated in Figure 1-1.

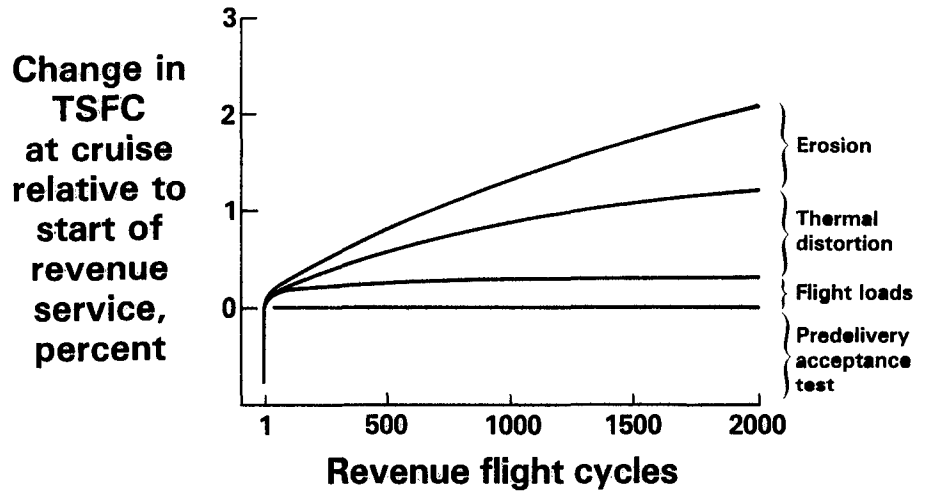

Figure 1-1 JT9D-7 Engine Performance Deterioration at Cruise - Combined short-term and long-term deterioration effects result in a total of 2.1 percent increase in thrust specific fuel consumption in 2000 flight cycles for an unrepaired engine. (J26216-21)

Based on the results of this Flight Loads Test program, the following recommendations are made, relative to current-engine operation and future-engine development:

Operation

- Use a derated power take-off when conditions permit to reduce hot section thermal distortion.
- Minimize high power operation immediately prior to start of take-off to prevent the combination of an increased thermal expansion-induced closure and the maximum load-induced closures at take-off, reducing the possibility of turbine rub.
- Minimize the possibility of turbine rubs due to snap accelerations with a hot rotor and cooler case.
- Minimize power increase during stall warning sequences in production acceptance testing.

Development

- o Optimize the use of turbine clearance control to open running clearances during pinch conditions and close these clearances during cruise conditions.

- o Structurally integrate the engine and nacelle design to reduce both the aerodynamic-load induced and thrust-bending induced closures in both the fan/low-pressure compressor and the high-pressure turbine.

- o Determine the cause of the apparent thermally induced asymmetric high-pressure turbine clearance closure. Correction of this asymmetry will permit more nearly uniform running clearances.

- o Develop abradable turbine seals such that rubs caused by the inevitable asymmetric closures will open clearances locally, where required, rather than wear blades and open clearances over the full circumference of the turbine.

- o Employ laser clearance monitoring probes to measure compressor and turbine running clearances during engine development testing to better understand symmetric and asymmetric clearance closures and thereby achieve an engine that retains tight running clearances.

SECTION 2.0

INTRODUCTION

2.1 BACKGROUND

The rapid rise in the cost of oil since the Organization of Petroleum Exporting Countries (OPEC) oil embargo in 1973 has resulted in a national effort to increase the availability of domestic oil, develop alternate sources of energy, and develop near-term and long-term means to reduce fuel consumption. To counteract the adverse impact of the world-wide fuel crisis on the aviation industry, NASA has initiated the Aircraft Energy Efficiency (ACEE) program. Included in this program are major propulsion projects which are addressing both near-term and long-term goals. The long-term activities are directed toward developing propulsion technology to reduce fuel consumption by at least 12 percent in the late 1980's and an additional 15 percent in the early 1990's. The near-term activities are a part of the Engine Component Improvement (ECI) Project which is directed toward improving the fuel consumption of selected current high bypass ratio turbofan engines and their derivatives by 5 percent over the life of these engines. The Engine Component Improvement project is divided into two subprojects, (1) Performance Improvement and (2) Engine Diagnostics. Performance Improvement is directed toward developing fuel saving component technology for existing engines and their derivatives to be introduced during the 1980 to 1982 time period. Engine Diagnostics is directed toward identifying and quantifying engine performance losses that occur during the engine's service life and developing criteria for minimizing these losses.

The first phase of the Engine Diagnostics project was the gathering, documentation, and analysis of historical data. The resulting information was used to establish performance deterioration trends at the overall engine and module level, establish probable causes contributing to performance deterioration, and identify areas and/or components where corrective action could be taken. That effort was completed in 1978, and the results are reported in Reference 1.

The second phase of the Engine Diagnostics project was directed toward expanding the understanding of engine deterioration by acquiring new in-service engine performance data from a selected sample of JT9D engines. This investigation was conducted during the period from February 1977 to February 1979. The main source of data was the Pan American World Airways JT9D-7A(SP) engines which are installed in their fleet of Boeing 747 Special Performance aircraft. These aircraft were introduced in service beginning in March 1976. Data were obtained from on-the-wing ground tests using expanded engine instrumentation, prerepair and postrepair test stand data, and in-flight cockpit monitored data. That effort was completed in 1979, and the results are reported in Reference 2.

The third phase of the Engine Diagnostics project was directed toward understanding the causes of short-term performance deterioration. During the first few flights of an aircraft, the performance of the engine deteriorates relative to its production performance level measured on the test stand. The effort to understand the causes of this phenomenon has been divided into several subphases or activities. The first activity was to test and analytically tear down a low time service engine. This activity was completed in June of 1978, and the results are reported in Reference 3. In summary, the results pointed to clearance changes as the major cause of the performance loss which were probably the result of loads imposed on the engine during flight. The second activity was, therefore, directed toward analytically investigating the impact of flight loads using an existing JT9D/747 Propulsion System NASTRAN Structural Model developed jointly by Pratt & Whitney Aircraft (P&WA) and Boeing Commercial Airplane Company (BCAC) prior to initiation of the Engine Diagnostics Contract. This activity resulted in two reports, References 4 and 5. In summary, these analytical studies confirmed that flight load-induced rubs were a primary cause of short-term performance deterioration and indicated that nacelle inlet aerodynamic pressures during flight maneuvers were a principal cause of these rubs. The last activity during the third phase was a Simulated Aerodynamic Loads Test. For this test, an inlet modified with a mechanical loading device was installed on a JT9D engine that was instrumented to monitor running clearances throughout the engine. Simulated aerodynamic loads were then applied mechanically through the inlet to the operating engine to simulate various flight maneuvers. Running clearances and engine performance were simultaneously monitored and recorded. The analytical results, as reported in Reference 6, established the effects of the simulated aerodynamic loads on each module of the engine.

2.2 OBJECTIVES

The results available from the first three phases of the Engine Diagnostics Program established the general causes of short-term and long-term engine performance deterioration and the magnitude of each cause. It remained for the Flight Loads Test program to establish the specific flight conditions and maneuvers which cause the engine case and rotor bending loads which, in turn, cause rubs and resulting performance loss. Thus, the specific objectives of this final program phase were:

- To measure aerodynamic and inertia loads during flight;
- To explore the effects of airplane gross weight, sink rate, pitch angle, and various typical maneuvers on nacelle loads;
- To simultaneously measure engine clearance closures and performance changes resulting from these airplane maneuvers; and
- To make a final refinement of engine performance deterioration prediction models based on the analytical results.

2.3 APPROACH

A cost/benefit feasibility study, Reference 7, was conducted to define the most effective approach to the conduct of this final test. This study considered cost (preparation, test, and refurbishment); data quality and quantity; technical risk and equipment availability in the selection of the test vehicle; the extent of engine preparation; the extent of instrumentation; and the test sequence.

The result of the feasibility study was a joint effort in which the Boeing Commercial Airplane Company (BCAC) was funded by the NASA Langley Research Center and Pratt & Whitney Aircraft (P&WA) was funded by the NASA Lewis Research Center. Boeing provided the RA001 747 test airplane, installed the flight loads instrumentation, and flew the test flights. Pratt & Whitney Aircraft provided the instrumented engines and monitored the engine running clearances.

The test program included a series of flight tests starting with a production acceptance test flight and subsequent take-off, maneuver, and landing conditions that were representative of the extremes likely to be encountered during revenue service. Engine calibrations between flight tests established the effect of each flight on engine performance. Finally, an analytical teardown of the instrumented engine confirmed the extent of wear incurred during the testing.

Subsequent to the analysis of the flight test data, an additional ground test was conducted at Pratt & Whitney Aircraft to better understand the effects of power and power transients on turbine running clearances. This test, which was run on a JT9D-7R4 engine, also identified improved characteristics with the more recent design.

SECTION 3.0

TEST PROGRAM

3.1 TEST PROGRAM DESCRIPTION AND OVERVIEW

The JT9D engine Flight Loads Test was the final task of the NASA-Lewis sponsored JT9D Jet Engine Diagnostics Program. It was conducted concurrently with the NASA-Langley sponsored Boeing Nacelle Aerodynamic and Inertial Loads (NAIL) program.

The selected test approach and degree of instrumentation were the result of a feasibility study which considered program goals, prior test results, cost, benefits, availability of test engines and airplane, and schedule. The selected approach was to use the Boeing test 747 airplane, RA001, shown in Figure 3-1, with the two right hand engines and nacelles instrumented to simultaneously measure flight conditions, aerodynamic and inertia loads, engine running clearances, and engine performance.

Figure 3-1 Flight Test Vehicle - The Boeing test 747, RA001, was selected for the flight tests on the basis of cost and availability. (J24018-5)

A spare JT9D-7 engine, serial number P-662204, from RA001 was returned to Pratt & Whitney Aircraft where it was partially disassembled and then reassembled with an analytically built and instrumented fan case and high-pressure turbine. Four laser proximity probes were installed around the fan case to measure fan running clearances. The high-pressure turbine case was modified to permit the installation of four laser proximity probes for the measurement of first-stage turbine running clearances. Also installed on the high-pressure turbine case were 20 thermocouples to measure transient and steady state temperatures around the case throughout the flight tests. Finally, the engine was equipped with expanded performance instrumentation to measure engine and engine-module performance before, during, and after the flight tests. These engine instrumentation systems are described in Section 3.4 of this document.

The analytically built engine was calibrated in a test stand, then shipped to Boeing where it was installed in the number 3 position on the test airplane, as shown in Figure 3-2. The laser clearance monitoring and recording system was connected to a Pratt & Whitney Aircraft read-out and recording system in the test airplane cabin. The temperature and performance instrumentation was connected to the Boeing Airborne Data Analysis and Monitoring System (ADAMS).

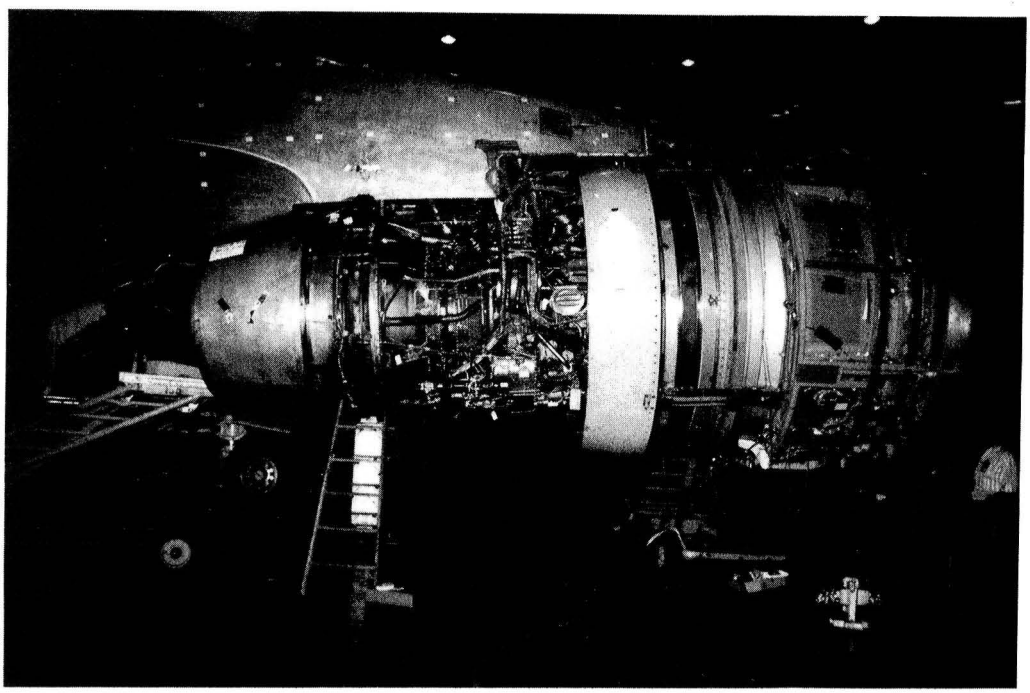

Figure 3-2 Primary Test Engine - The analytically built engine, serial number P-662204, with complete instrumentation was installed on the airplane in position number 3.
(Boeing, FA-122279)

A second fan case was analytically built and instrumented with laser clearance monitoring probes. This fan case was installed on the position number 4 engine, serial number P-662201, and the clearance monitoring instrumentation was connected to the read-out system in the test airplane cabin.

To measure the flight loads simultaneously with the engine data, Boeing, under the Nacelle Aerodynamic and Inertial Loads (NAIL) Program, installed pressure taps around the fan cowls and accelerometers and rate gyro's on the engines and mounts. Aerodynamic loads on the two engine inlets were mapped by 252 pressure probes on the position number 3 engine and by 45 pressure probes on the position number 4 engine. Accelerometers on the inlet, fan case, and engine mount struts monitored the inertia loads. Rate gyro's on the fan cases monitored the gyroscopic loads. The pressure and acceleration signals were scanned continuously and recorded by the ADAMS system. Descriptions of this Boeing NAIL Program instrumentation are presented in the Boeing Test Report for the NAIL Program, Reference 8.

Airplane flight conditions, flight loads, engine performance, turbine case temperatures, and engine running clearances were all recorded along with a time signal to the nearest 0.01 second. Thus, airplane condition, flight loads, and engine response can be compared at any steady state or transient condition.

The position number 3 engine was the primary data source. Lesser instrumentation on the position number 4 engine provided back-up data and the basis for comparing flight loads and engine responses for the inboard and outboard engine installations.

The JT9D Flight Loads Test/NAIL Flight Test Program was conducted by Boeing in October 1980, flying out of Glasgow, Montana. The NASA program included five test flights. However, Boeing concurrently conducted an additional development test program on a new engine installed in position number 2. The additional flights dedicated to and paid for by that program provided significant additional clearance data at no cost to the NASA program.

The flight test program started with the 747 production acceptance test, illustrated in Figure 3-3, since the acceptance test precedes delivery of the airplane to the operator, and data collected in earlier phases of the JT9D Diagnostics Program indicated that a performance loss occurred during the first flight of the airplane. Subsequently, the effects of heavier gross weight take-offs and variation of take-off flap settings were measured. High G turns were performed to simulate the effects of extreme avoidance maneuvers.

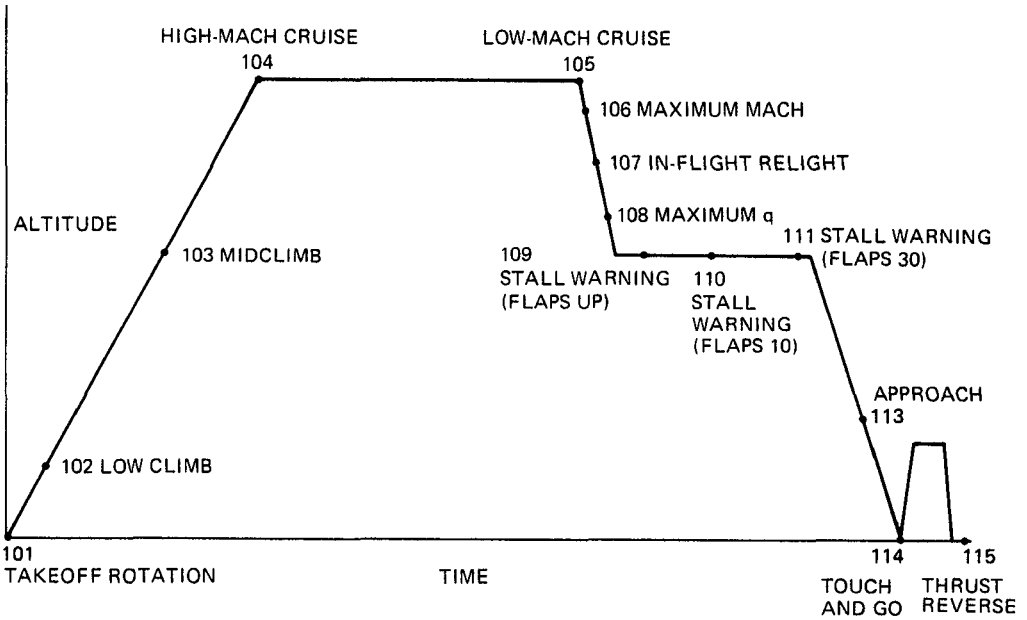

Figure 3-3 Production Acceptance Test Flight Profile - This test pattern was the initial test of the program since it had been indicated that a performance loss occurred on the first airplane flight.

Previous analysis had indicated the possibility of rubs occurring from dynamic vibration-induced loads which could be caused by an extreme air gust condition or a hard landing. No gust conditions were encountered; however, a heavy gross weight, hard landing test was accomplished.

Following completion of the tests, engine P-662204 was removed from the airplane and returned to Pratt & Whitney Aircraft where a final calibration test was conducted. The engine was then disassembled, the fan and high-pressure turbine were analytically inspected, and the engine was refurbished and returned to Boeing for use on test airplane RA001. The instrumented fan on engine P-662201 was replaced and returned to Pratt & Whitney Aircraft for inspection and refurbishment.

The test conditions and sequence are discussed in Section 3.2, and the test facility is described in Section 3.3 of this document. The data analysis methodology and results are presented in Sections 4 and 5. Final revisions of the JT9D performance deterioration models were made based on the analytical results and are presented in Section 6.

3.2 TEST CONDITIONS AND SEQUENCE

The test program included flight tests and ground engine calibrations. The ground test calibrations conducted and flight conditions monitored are listed chronologically on Table 3-I. The refurbished engine (serial number P-662204) was initially calibrated at the Pratt & Whitney Aircraft Middletown (Connecticut) test facility, then shipped to Seattle, Washington and installed on the RA001 test airplane in position number 3. The initial installed performance calibration on October 3, 1980 at Boeing Field, Seattle provided no useful performance data since the cabin bleed ports were inadvertently left open. However, the clearance probes and subsequent fan inspection indicated both fan and high-pressure turbine rubs. The airplane was then ferried to the remote test site (Valley Industrial Park, Glasgow, Montana) with the position number 3 engine operated at reduced power to prevent any further rubs prior to flight testing. The initial installed ground calibration was then repeated at the 2560-foot altitude test site.

The initial test flight on October 11, 1980 duplicated the production airplane acceptance flight with the exception of the take-off and the maximum Mach number and maximum dynamic pressure cruise conditions. An engine ground calibration and fan inspection were conducted following this initial flight of the test program.

The second test flight on October 19, 1980 included the acceptance test 10-degree flap setting take-off and climb-out with the anticipated higher aerodynamic loads. High G left turns, simulated avoidance maneuvers, and an airplane stall were also included in this test flight. Rubs were noted on the fan rub strips. The time spread between the first and second test flights resulted from inclement weather.

TABLE 3-I

TEST SEQUENCE

Date	Flight Condition Description	Number	Pressure Altitude (feet)	Mach Number	Location
06-24-80	Bare Engine Ground Calibration		Sea Level	0	East Hartford, Conn.
10-03-80 *	Installed Engine Ground Calibration	1-1	Sea Level	0	Boeing Field, Wash.
10-10-80	Installed Engine Ground Calibration	1-2	2,560	0	Glasgow, Montana
10-11-80	First Test Flight				Glasgow, Montana
	Acceptance Test Flight:				
	612,000 lb Take-Off with 20° Flaps	101-1	2,560	0.25	
	Mid-Climb	103	17,200	0.60	
	High Mach Number Cruise	104	35,500	0.86	
	Low Mach Number Cruise	105	35,500	0.77	
	In-Flight Relight	107	27,900	0.72	
	Stall Warning with Flaps Up	109	17,000	0.39	
	Stall Warning with 10° Flaps	110	16,200	0.35	
	Stall Warning with 30° Flaps	111	17,000	0.27	
	Idle Descent	112	8,500	0.44	
	Approach	113	6,000	0.27	
	Touch and Go	114	2,560	0.26	
	Thrust Reverse	115	2,560	0.18	
10-11-80	Installed Engine Ground Calibration	2	2,560	0	Glasgow, Montana
10-19-80	Second Test Flight				Glasgow, Montana
	538,000 lb Take-Off with 10° Flaps	101-2	2,560	0.24	
	Low-Climb	102	5,900	0.39	
	2.0-G Left Turn with Flaps Up	116	8,400	0.49	
	1.6-G Left Turn with 30° Flaps	117	8,200	0.26	
	Airplane Stall	123	9,000	0.21	
10-20-80	Third Test Flight				Glasgow, Montana
	647,000 lb Take-Off with 10° Flaps	101-3	2,560	0.25	
10-20-80	Installed Ground Calibration	3	2,560	0	Glasgow, Montana
10-25-80	Fourth Test Flight				Glasgow, Montana
	710,000 lb Take-Off with 10° Flaps		2,560	0.25	
	780,000 lb Take-Off with 10° Flaps (Simulated)	118	3,650	0.30	
	690,000 lb Landing				
10-25-80	Fifth Test Flight				Glasgow, Montana
	Maximum Mach Number Flight	106	37,000	0.91	
	Maximum Dynamic Pressure Flight	108	24,500	0.84	
	2.0-G Right Turn with Flaps Up	120	8,200	0.48	
	1.6-G Right Turn with 30° Flaps	121	8,300	0.27	
10-25-80	Installed Ground Calibration	4	2,560	0	Glasgow, Montana
11-05-80	Installed Ground Calibration	5	2,560	0	Glasgow, Montana
01-09-81	Bare Engine Ground Calibration, As-Received		Sea Level	0	East Hartford, Conn.
01-12-81	Bare Engine Ground Calibration after Vane Trim		Sea Level	0	East Hartford, Conn.

* Note: A check flight was made on 10-3-80 and a ferry flight was made on 10-6-80. However, both flights were conducted with reduced power on engine number 3 such that no close clearances occurred or were measured.

The third test flight included a higher gross weight take-off (647,000 pounds) with flaps set at 10 degrees. Additional fan rub was noted. The third ground calibration followed the flight.

The fourth test flight was conducted with take-off at the highest gross weight that was feasible for the airplane and conditions (710,000 pounds). At 1000 feet above ground, a 1.3-G pull-up was executed to simulate the aerodynamic loads which would occur during a 780,000-pound gross weight take-off to obtain data for the final take-off test condition. The airplane landed with a gross weight of 690,000 pounds at a high sink rate (5 feet/second) to establish a dynamic load condition. Rubs were noted on the fan rub strips.

The final test flight was then flown to conduct the remaining two acceptance flight conditions (maximum Mach number cruise and maximum dynamic pressure cruise) and the high G turns to the right which were added to the program. The fourth ground calibration followed this flight.

Two additional flights were then conducted to complete the companion test program on the position number 2 engine. Then a final installed calibration was conducted. The airplane was then ferried to Seattle, and the test engine (serial number P-662204) was removed and returned to Pratt & Whitney Aircraft.

The initial bare engine calibration was then repeated at Pratt & Whitney Aircraft on serial number P-662204 in the as-received condition. The fan blades were then washed, the vane trim was checked, and the calibration was repeated.

An analytical teardown and inspection were then conducted on the fan and high-pressure turbine from the primary test engine (serial number P-662204) and the instrumented fan case which was installed on the position number 4 engine (serial number P-662201).

3.3 TEST FACILITY

The Boeing-owned and operated 747-100, RA001 test bed aircraft, shown in Figure 3-1, was the basic test facility for the JT9D Flight Loads/Nacelle Aerodynamic and Inertial Loads test program. This airplane is powered by four Pratt & Whitney Aircraft-owned JT9D-7 engines. In this program, the two starboard engines and their nacelles and pylons were instrumented. In addition, an advanced model JT9D engine was installed in position number 2 for a development test program that was run concurrently with the NASA program.

The RA001 airplane is equipped with an Airborne Data Analysis and Monitoring System (ADAMS), shown in Figure 3-4, which can monitor, process, record, and print out data on aircraft flight conditions and engine performance as well as data from the various special instrumentation for a specific test program. The capability for print out of predetermined critical data immediately after completion of a flight test at a given condition for evaluation and flight decisions

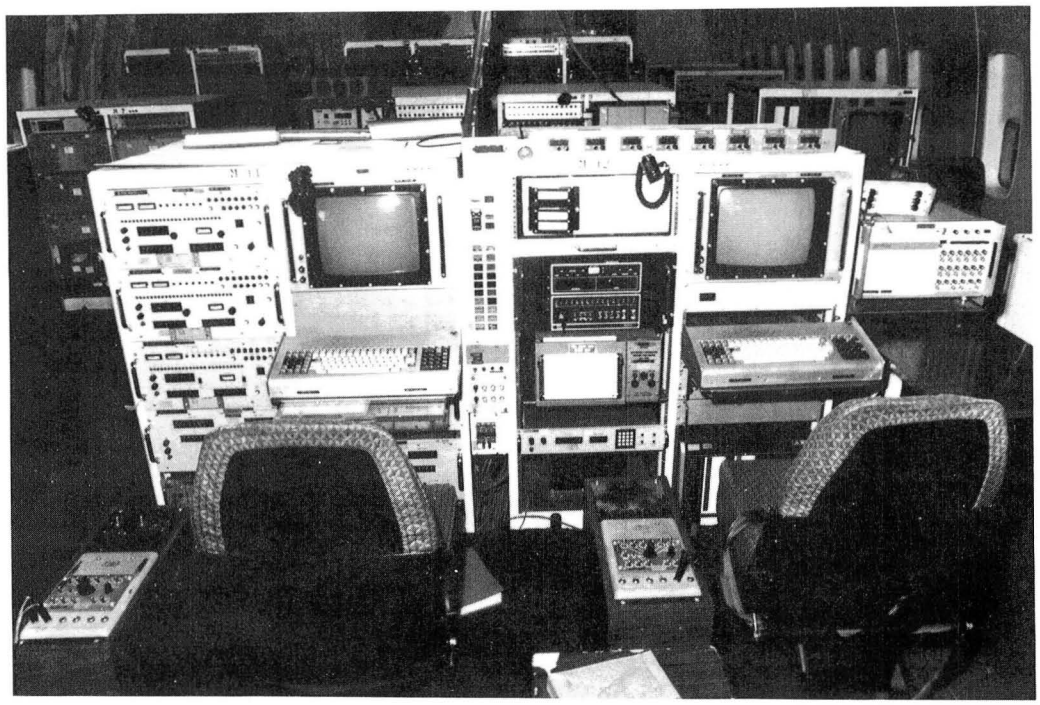

Figure 3-4 Airborne Data Analysis and Monitoring System (ADAMS) - This system can monitor, process, record, and immediately print out aircraft and engine data immediately after completion of a test condition. (Boeing, FA-123936)

was extremely beneficial to the efficient execution of this multitest program. Because 1023 channels of measurements were being recorded during this combined test program, a second ADAMS was installed in the RA001 test airplane. The ADAMS served as the primary data collection and processing system for all data collection for this program except the engine clearance monitoring data. Clearance data management was provided by a Pratt & Whitney Aircraft-installed and operated system on the RA001 airplane.

The Boeing-installed special instrumentation for this test included a pressure field mapping system on the position numbers 3 and 4 engine inlets to provide the data for computing aerodynamic loads plus accelerometers and rate gyro's on those engines, their mounts, and the fuselage to establish inertia loads.

Data for the aerodynamic loads were provided by 252 pressure taps installed on the position number 3 engine inlet, as shown in Figure 3-5, plus an additional 45 pressure taps on the position number 4 engine inlet. The pressure taps were connected to transducers mounted in the engine inlets, as illustrated in Figure 3-6, which, in turn, transmitted the electrical signals back to the ADAMS.

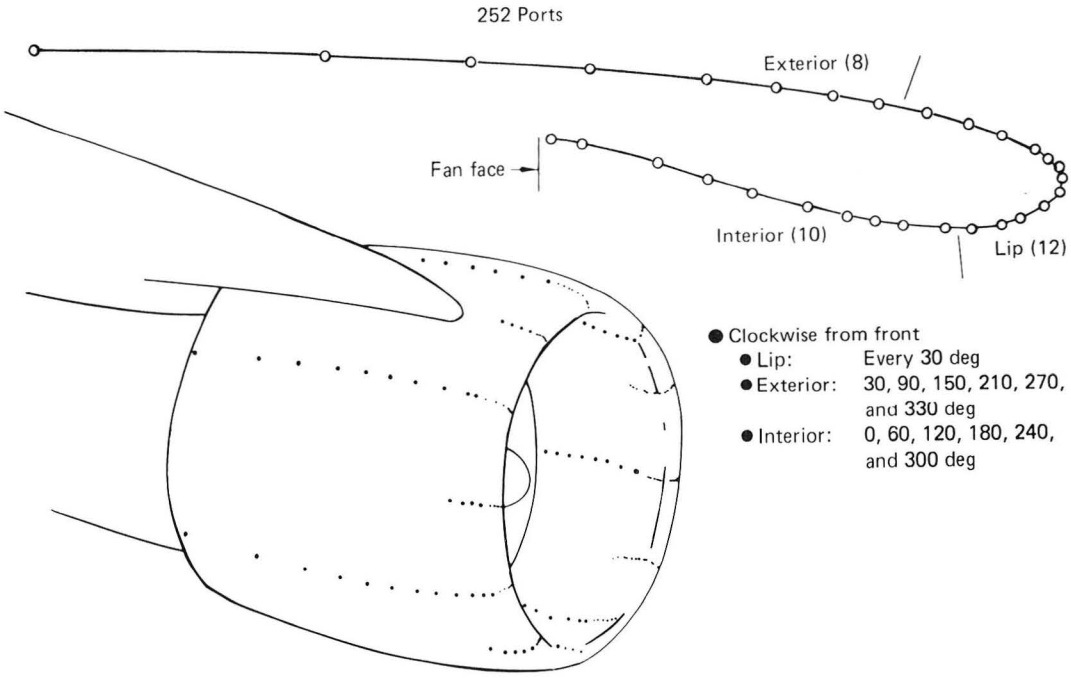

Figure 3-5 Position Number 3 Engine Pressure Tap Locations - A total of 252 pressure taps provided data for computing the aerodynamic loads.

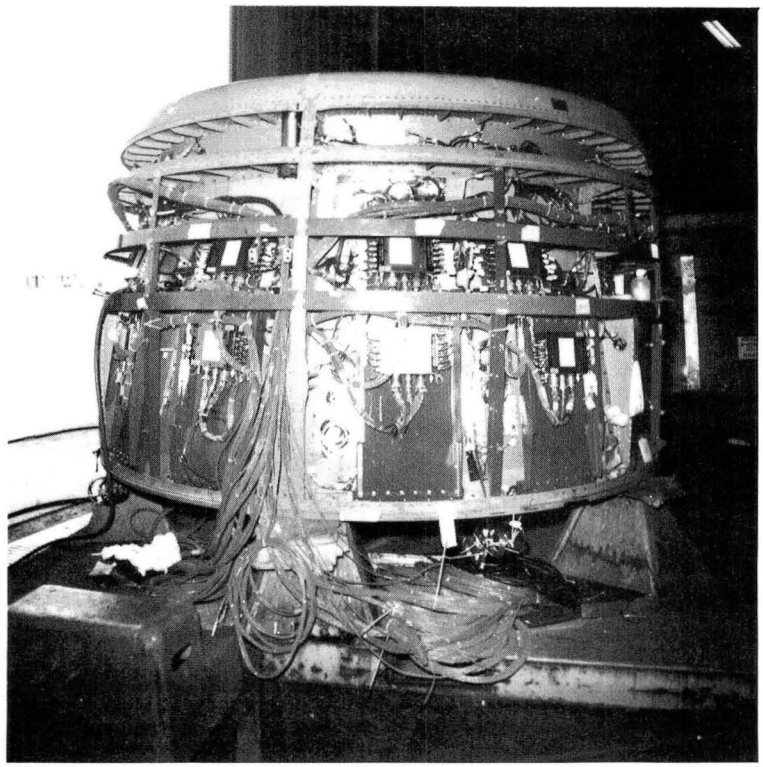

Figure 3-6 Pressure Transducer Installation - These transducers transmitted electrical signals, proportional to the pressure data, to the ADAMS for processing.
(Boeing, FA 122104)

Accelerometers mounted on the position numbers 3 and 4 engines and on the engine mounts, as shown in Figure 3-7, as well as at the airplane center of gravity monitored G loads in all directions. Similarly, gyroscopic effects were monitored by pitch and yaw rate gyro's mounted adjacent to the two instrumented fans.

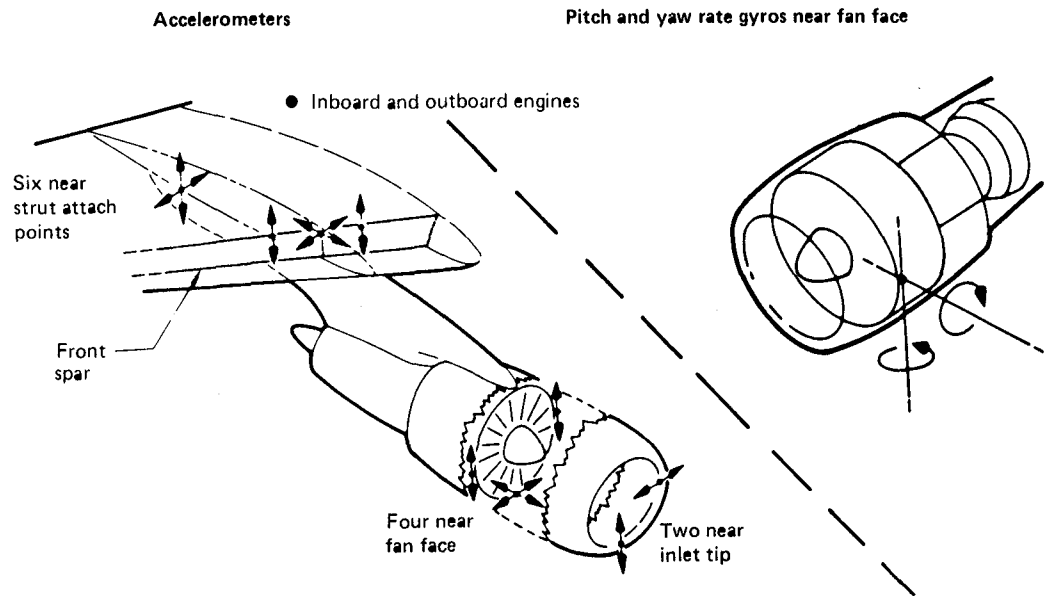

Figure 3-7 Location of Inertial Data Sensors - These sensors provided data for calculation of G loads and gyroscopic effects.

The ADAMS recorded all of these data and identified it with a time signal to permit later comparison of all of the simultaneous effects. This time signal as well as an engine speed signal were also transmitted to the clearance monitoring system and recorded with the clearances on video tape.

A more detailed description of the flight load measuring system is presented in Boeing's NAIL Project Test Report, Reference 8.

3.4 INSTRUMENTATION

Test engine instrumentation consisted of running clearance monitoring, case temperature monitoring, and performance monitoring systems which are described in Sections 3.4.1, 3.4.2 and 3.4.3, respectively. The location and quantity of this instrumentation are summarized in Table 3-II

TABLE 3-II

ENGINE INSTRUMENTATION LOCATION

Parameter	Engine Position Number	Instrumentation Location	Sensor Quantity
Performance:			
Engine Speed, N_1 and N_2	3	Low- & High-Pressure Rotors	2
Free Stream Temp., T_{T2}	3		1
Free Stream Press., P_{T1}	3		1
Gas-Path Static Pressures	3	Stations 3, 4 & 5i	5
Gas-Path Total Pressures	3	Stations 2.5, 3, & 7	15
Gas-Path Temperatures	3	Stations 3, 4.5, 6, & 7	16
Fuel Temperature	3		1
Fuel Totalizer and Elapsed Fuel	3		1
Fuel Control Positions	3	PLA, EVC, 5th IGV, Bleed Valve, Precooler Exit Valve, Cross Feed Valve	6
Thermal Loads:			
Engine Surface Thermocouples	3	M & N Flanges	18
Air-Path Thermocouples	3	6" Outboard of N Flange	2
Clearances:			
Laser Proximity Probes	3 & 4	Fan Case	8
	3	First-Stage High-Pressure Turbine Case	4

3.4.1 Clearance Measurement Instrumentation

Running clearances in the two fans and the high-pressure turbine in the position number 3 engine were monitored throughout each flight test using laser proximity probes of the type used in the Simulated Aerodynamic Loads Test program. A detailed explanation of the laser probe system is provided since this is a new concept with which the reader may not be familiar.

3.4.1.1 Laser Proximity Probe Location

Twelve laser probes were installed. Four were mounted to measure fan blade/outer air-seal clearances in an outboard engine. The locations are shown on Figure 3-8. An inboard engine was equipped with four similarly mounted fan clearance probes plus four probes to measure first-stage high-pressure turbine blade clearance. The turbine probe locations are shown on Figure 3-9. Four probes located 90 degrees apart would provide the desired clearance data in each location. However, limitations on probe location resulted in the selected positions shown on Figure 3-8 and 3-9. Bottom dead center (+10 degrees) was avoided due to the possible build-up of contaminants which would blind the probes. Various Pratt & Whitney Aircraft- and Boeing-mounted accessories further restricted the location of probes and leads.

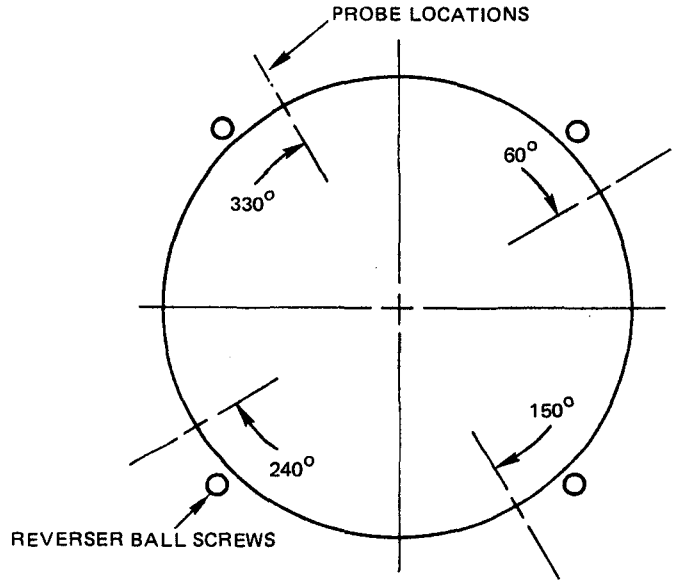

Figure 3-8 Angular Location of Fan Blade Laser Proximity Probes - Four probes, located 90 degrees apart, provided the desired clearance data.

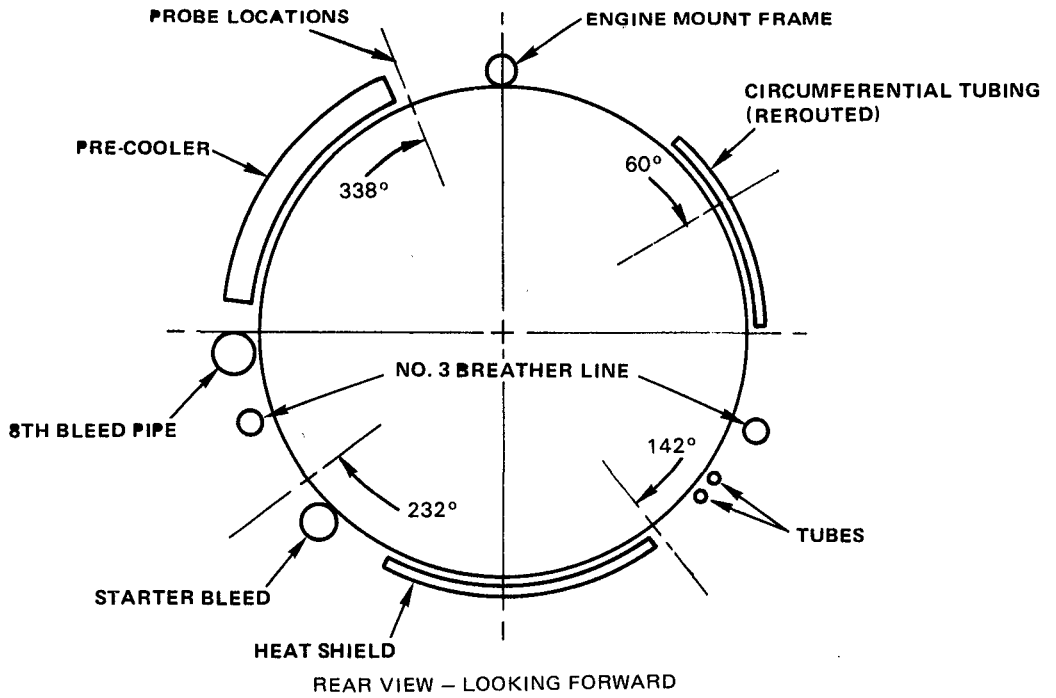

Figure 3-9 Angular Location of High-Pressure Turbine Blade Laser Proximity Probes - Four probes, located approximately 90 degrees apart, provided the desired clearance data.

3.4.1.2 Laser Proximity Probe System Description

A fan clearance monitoring system for one engine, as shown in Figure 3-10, consists of: 1) four helium-neon lasers which are installed in the cabin; 2) single input fiber optic mounted in conduits to transmit the laser light signal to the probes; 3) four probes (Figure 3-11) mounted over slots in the fan cases; 4) output fiber optic bundles to transmit the output signal to a video camera; 5) a video camera, mounted in the engine pylon (Figure 3-12), which simultaneously and continuously monitors the output signals from the four probes and transmits a video signal to; 6) a cabin-mounted display, processing, and recording system (Figure 3-13).

The coherent light from the helium-neon laser is focused onto a single 0.001-inch diameter input fiber optic. The light is carried along this fiber and emitted from the end of the fiber in the probe, acting as a point source of light. This point source of light is focused on the blades by the input lens in the probe. If the blades are at Position A, shown on Figure 3-11, the spot of light image will be focused by the output lens onto a coherent output fiber optic at Point A'; similarly,

if the blades are at Position B, the reflected spot will be focused onto the coherent output fiber optic at Point B'. It should be noted that the imaged spot positions at A' and B' do not depend on the reflectivity of the blades (specular or diffuse, absorptive or reflective) or on the angle of tilt of the blade with respect to the probe. It is a function of only the distance of the blade from the probe. The coherent fiber optic bundle transfers the imaged spot positions from the probe end to the other end where the spot position is viewed through a lens system by a video camera. The video camera image is displayed on a TV monitor, so that the position of the light spot on the raster of the TV is a measure of the position of the blade clearance. An illuminated reticle is attached to the output fiber optic and serves as a calibration reference for the system. The system is calibrated so that any given position along the scale corresponds to a given average blade clearance between the blades and the outer air-seal surface.

Time, date, and engine (N_1) speed are superimposed on the recorded video signal for reference.

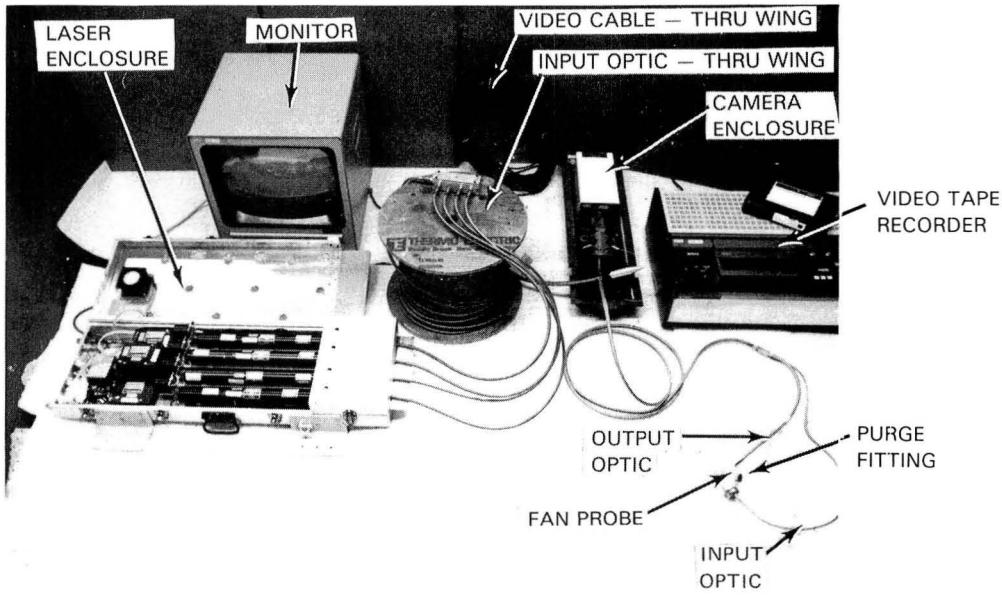

Figure 3-10 Laser Proximity Probe System - The system includes: 1) the laser, 2) input fiber optic, 3) the proximity probe, 4) output fiber optic bundle, 5) the pylon-mounted video camera, and 6) the monitor display screen. (80-441-0566-C)

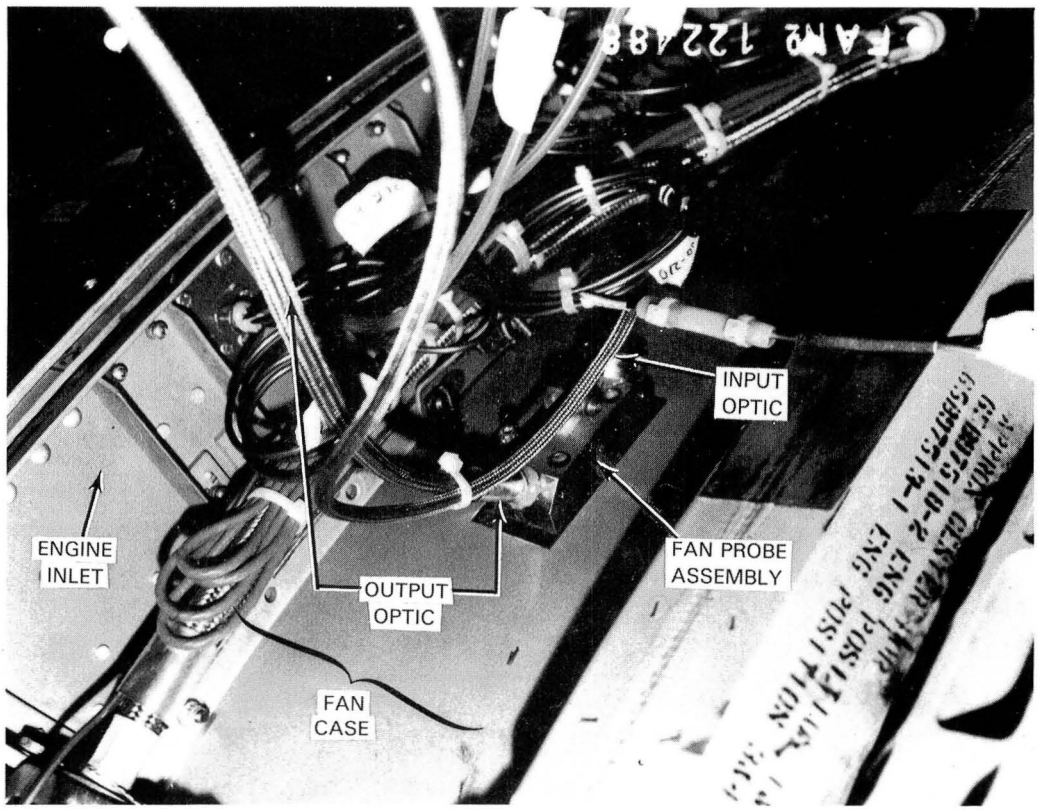

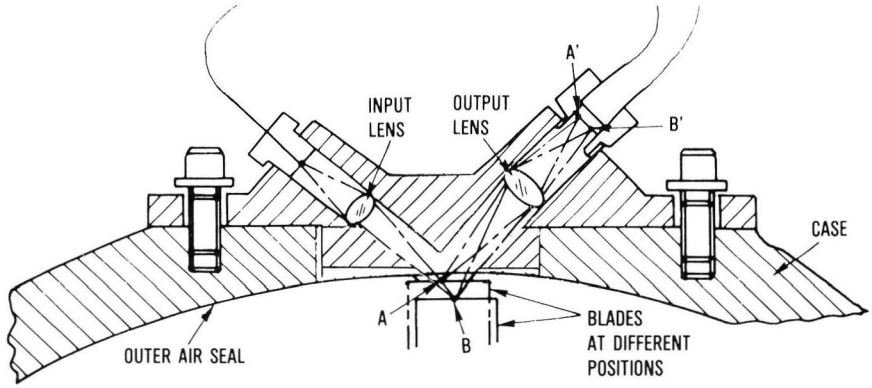

Figure 3-11 Installation of Laser Proximity Probe on the Fan Case and Sketch of Internal Structure of the Probe - The probe is designed for limited space in the fan cowl and the less hostile environment of the fan. (Boeing, FA-122488)

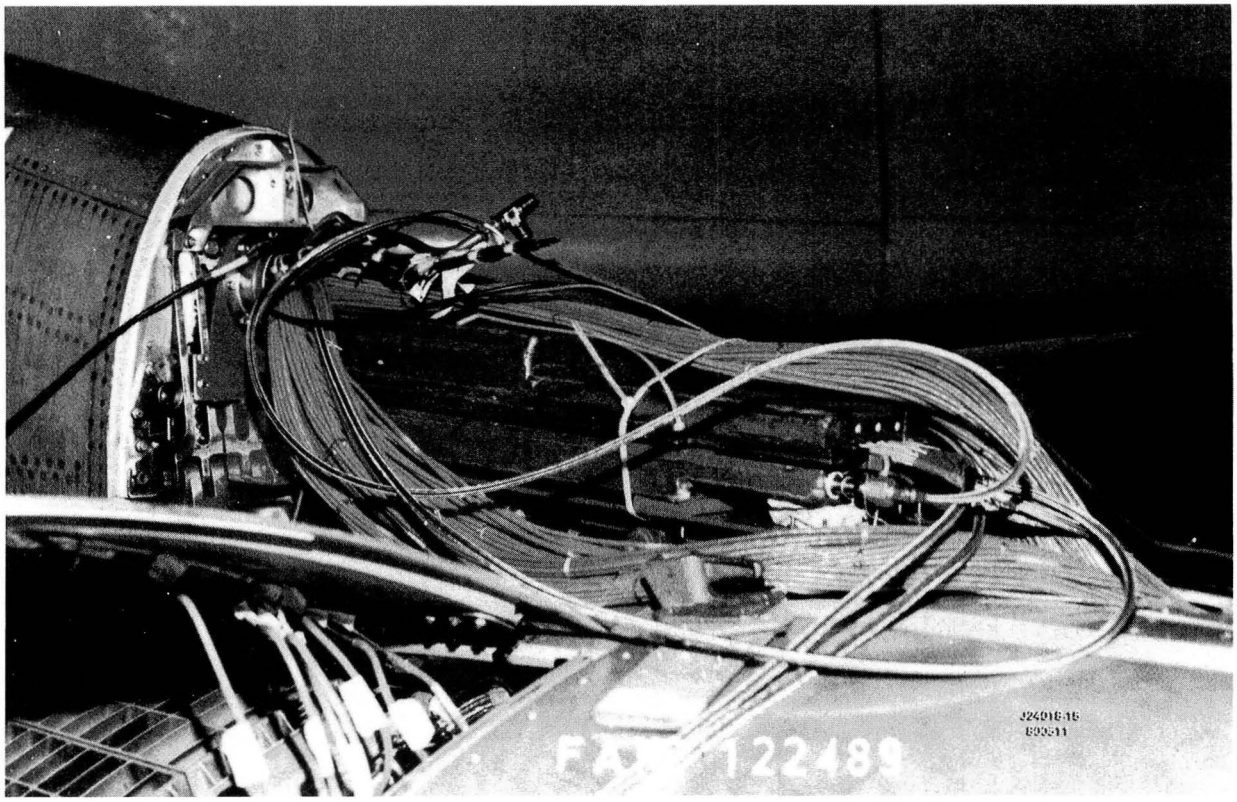

Figure 3-12 Fan Video Camera Installed in Pylon - Environmental control and shock mounting of the video camera were required. (J24018-15)

Figure 3-13 Clearance Monitoring System Console - Visual clearance read-out on a calibrated scale and a computerized digital read-out were provided. (J24018-16)

The video data is also processed by a laser proximity probe electronic read-out to provide a digital value of each of the measured clearances. These digital values are also displayed continuously on the monitor and are shown on Figure 3-14. This display of time, engine speed, and the four blade-tip clearances measured in the fan was continuously recorded on video tape throughout the test program for later analysis and comparison with the other system inputs.

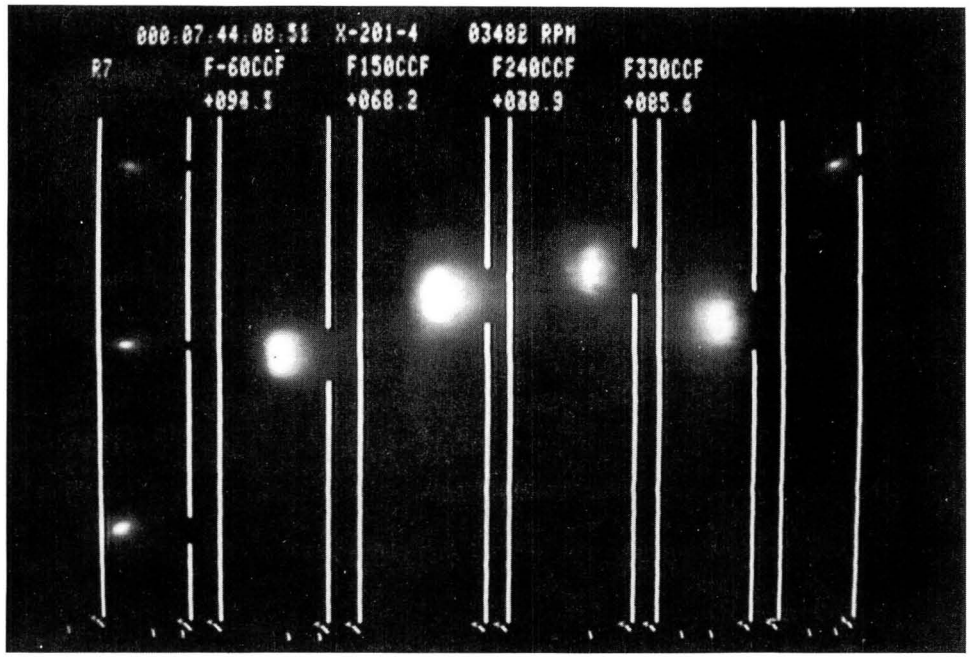

Figure 3-14 Display of Fan Clearance Indicated by Laser Proximity Probe - Visual and digital read-out provided redundancy. (J24018-31)

The high-pressure turbine laser probe system was essentially the same as the fan probe system with the exception that the turbine probe system was designed to operate in the high pressure, high temperature environment of the first-stage turbine gas path.

Due to the high temperature environment, the blade tips emit radiation which can be picked up by the video system. This "background radiation" is eliminated by using an optical band-pass interference filter which blocks out all light except for the laser light image. A folded optical system utilizing a prism at the base of the probe provides a system that is built into a cylindrical form. The probe is cylindrical so that it can be effectively sealed at the outer case with a piston-ring type seal. The probe is bayonetted into the rub strip so

that the probe moves with the rub strip, resulting in measurements relative to the rub strip, as illustrated in Figure 3-15. A typical high-pressure turbine probe system display of four clearances, time, and high-pressure rotor (N_2) speed is shown in Figure 3-16.

The turbine probe was purged with nitrogen to cool it and prevent the accumulation of contaminants on the probe optics. Nitrogen was flowed through each probe at a rate of 10 to 20 pounds/hour per probe, depending on engine power level. After cooling the probe optics and washing the prism face, the nitrogen flowed into the primary gas stream.

A gaseous nitrogen system with sufficient capacity for 13 hours of continuous engine operation was assembled by Boeing with 56 nitrogen gas bottles stored in the cargo hold of the airplane, as shown in Figure 3-17. Flow rate, controlled from the laser proximity probe monitoring station, was based on the thermocouple measured temperature at each of the four high-pressure turbine probes.

3.4.1.3 Laser Proximity Probe System Calibration

The final calibration of the proximity probe system prior to the flight test was a two-step process. The first step, after installation of each serialized probe in its assigned location in the assembled high-pressure turbine case or fan case, was to measure, using a depth micrometer, how far the probe head was recessed from the outer air-seal surface. Following installation of the assembled clearance monitoring system on the airplane and removal of each probe from its fan or turbine case, the second step was to calibrate the system using the digital micrometer calibration tool shown in Figure 3-18, factoring in the previously measured depth of probe recess. Both the visual dot location and the digital read-out were calibrated. This two-step calibration resulted in the preparation of a transparent overlay screen for each clearance monitoring station for subsequent comparisons of the visual and digital clearance readings.

After completion of this calibration procedure, the 12 proximity probes were reinstalled in their assigned locations. A final "zero-clearance" check of the eight installed fan probes was conducted by holding a piece of shim stock against the outer air seal at each probe location in the fans and monitoring the system output.

System accuracies of $\pm$0.004 inch and $\pm$0.001 inch, respectively, were achieved for the 0.400-inch depth-range fan probes and the 0.100-inch depth-range high-pressure turbine probes.

Replacement of failed components in the fan proximity probe system for the position number 3 engine during the test program required two recalibrations of that system.

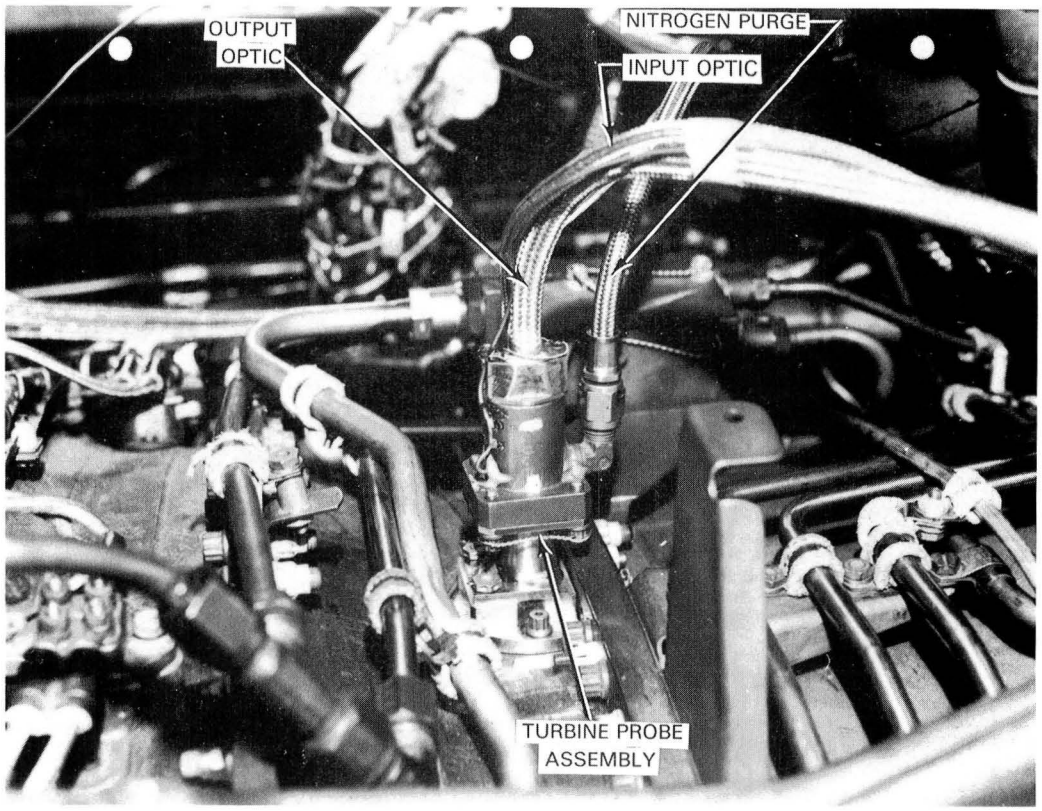

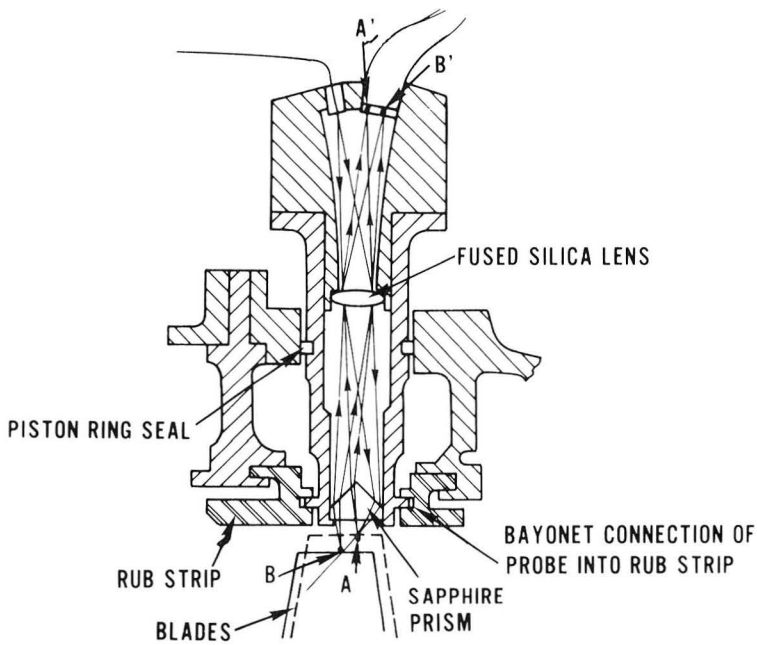

Figure 3-15 Installation of Laser Proximity Probe on the High-Pressure Turbine Case and Sketch of Internal Structure of the Probe - The probe is designed to penetrate the double-wall case and operate in a more hostile environment.
(Boeing, FA-122738)

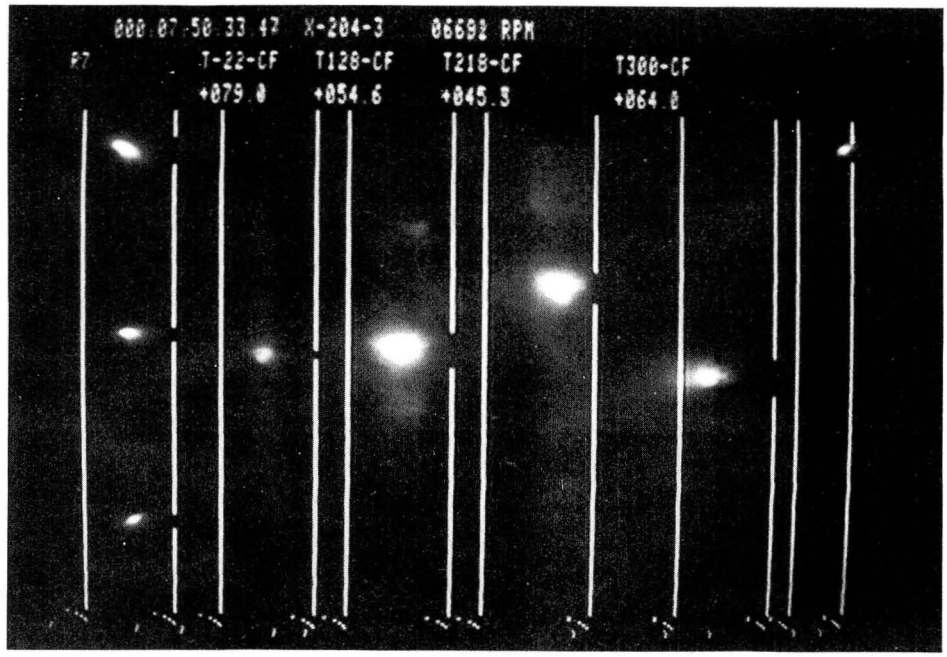

Figure 3-16 Display of High-Pressure Turbine Clearance Indicated by Laser Proximity Probe - Visual and digital read-out provided redundancy; high-pressure rotor speed is also displayed. (J24018-32)

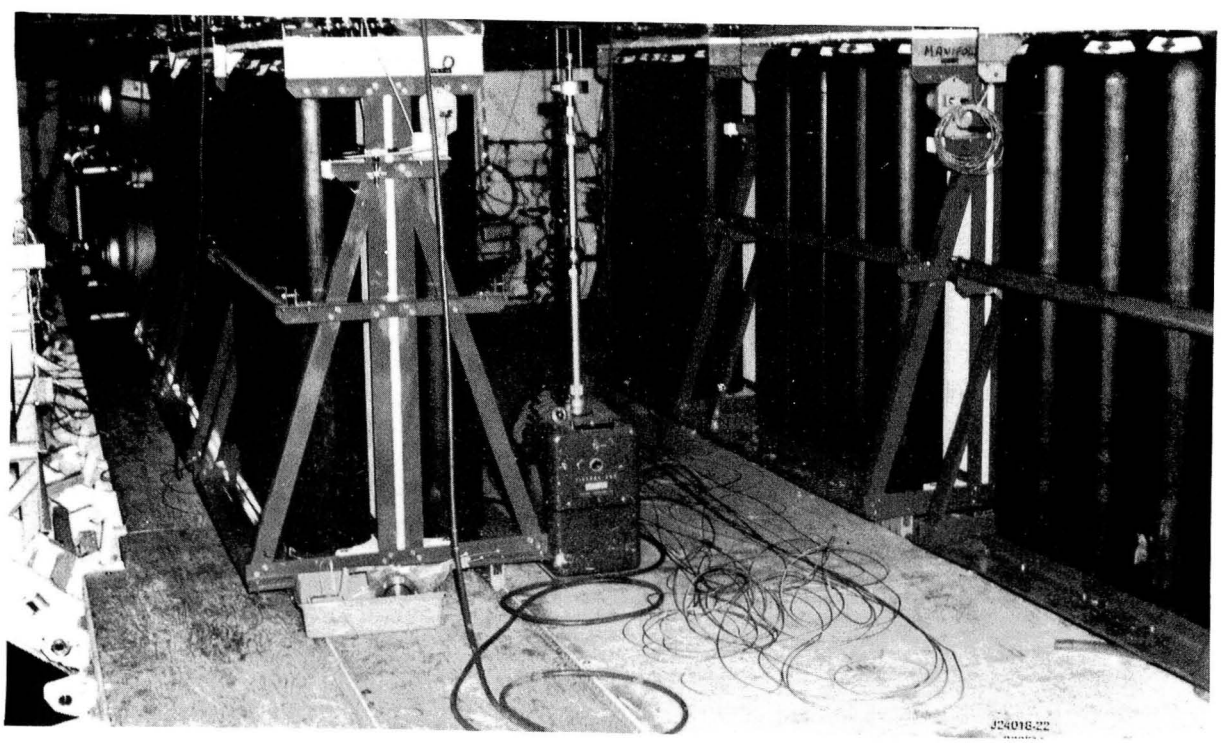

Figure 3-17 Purge Nitrogen Supply - Sufficient capacity for 13 hours of continuous engine operation was provided ty 56 nitrogen bottles in the cargo hold. (J24018-22)

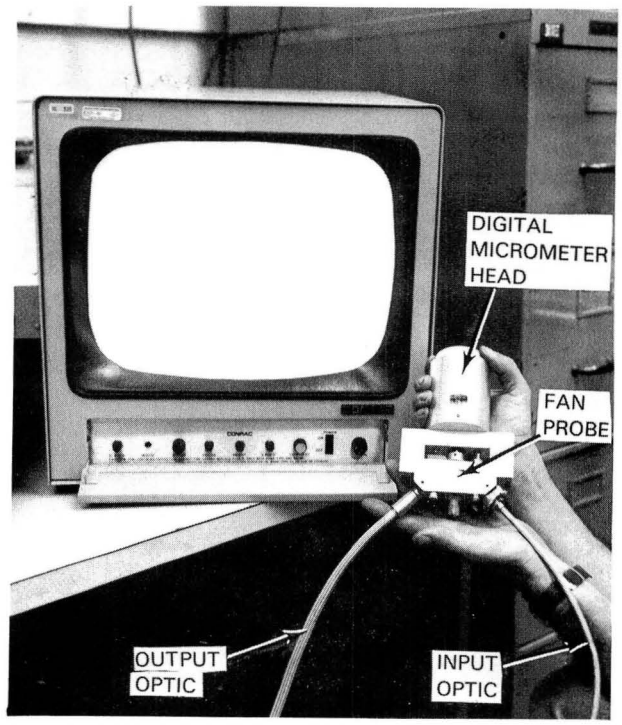

Figure 3-18 Digital Micrometer Calibration Tool - The digital head provides good accuracy of the indicated clearances.
(80-441-0566-D)

3.4.2 High-Pressure Turbine Case Temperature Instrumentation System

3.4.2.1 System Description and Thermocouple Locations

The major temperature excursions and corresponding influences on the JT9D engine blade tip clearances occur in the high-pressure compressor, high-pressure turbine, and low-pressure turbine with the largest influence in the high-pressure turbine. The laser probes measured the total running clearance change. Simultaneous monitoring and analysis of the high-pressure turbine case temperatures during flight and ground testing provided a better understanding of case growth and its influence on running clearances.

Radial, axial, and circumferential temperature patterns in the high-pressure turbine case of the position number 3 engine, under steady state and transient conditions, were established by 18 thermocouples installed around the turbine case front and rear (M and N) flanges plus two thermocouples mounted in the air space above and below the case, as shown in Figures 3-19 and 3-20. Leads from these 20 chromel-alumel thermocouples were routed from the point of installation on the engine to an interface located in a cooler zone above the engine. Connections were made from the interface through airplane-installed leads to the on-board ADAMS data read-out and recording equipment.

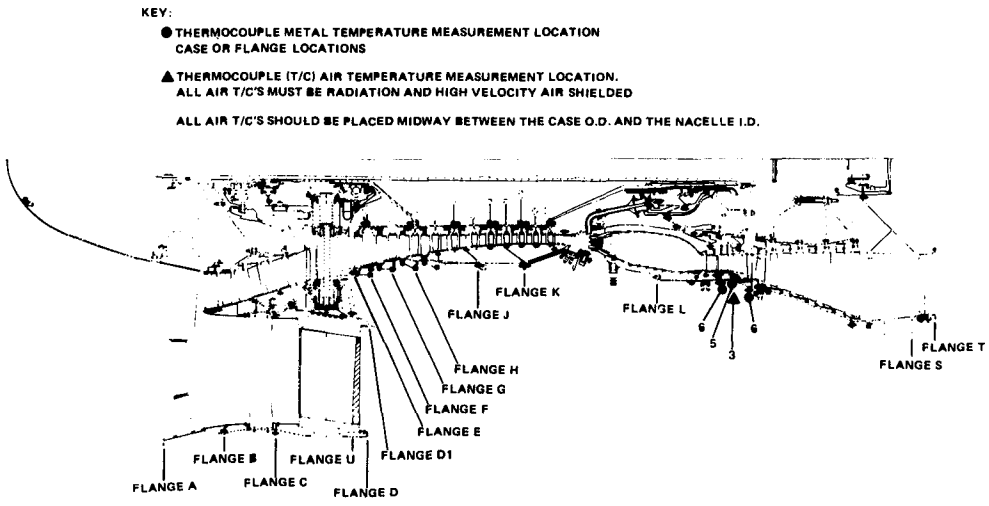

Figure 3-19 High-Pressure Turbine Case Thermocouple Locations - 18 thermocouples were installed around the front and rear flanges of the turbine case and two were located in the air space above and below the case. (J21627-26)

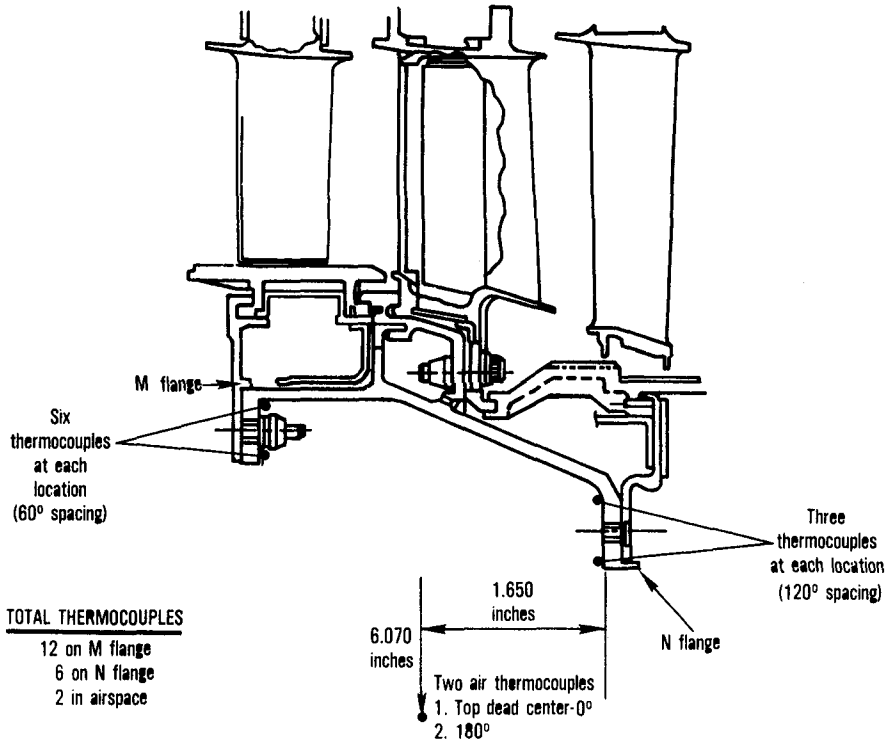

Figure 3-20 High-Pressure Turbine Case Thermocouple Detailed Locations - All circumferential locations are measured clockwise, from top dead center, looking forward. (J24018-24)

The ADAMS equipment sensed the output of each thermocouple every 0.2 second and recorded the case temperatures along with engine performance and flight data on a time synchronized master tape for later analysis of selected test conditions. The system also printed out "quick-look" transient and 30-second averaged case temperature data as required during the test program. A typical print-out of case temperatures is shown in Figure 3-21.

Thermocouple Number	Case Temperature (°F)	Location	Time Record
			07:18:54.5
			00:00:00.0

	MEAS	UL	LL	VALUE	UNITS	TITLE LIST# 5551 POS# 2 RIP STS
	5180			741.01	DEGF	TEMP M-FLNGE TIP 0 RAD
	5181			684.98	DEGF	TEMP M-FLNGE TIP 60 RAD
	5182			661.10	DEGF	TEMP M-FLNGETIP 120 RAD
	5183			749.58	DEGF	TEMP M-FLNGETIP 180 RAD
	5184			719.53	DEGF	TEMP M-FLNGETIP 240 RAD
	5185			606.50	DEGF	TEMP M-FLNGETIP 300 RAD
	5186			790.13	DEGF	TEMP M-FLNGE ROOT 0 RAD
	5187			762.42	DEGF	TEMP M-FLNGEROOT 60 RAD
	5188			756.14	DEGF	TEMP M-FLNGEROOT 120 RAD
*	5189			-1494.9	DEGF	TEMP M-FLNGEROOT 180 RAD
	5190			777.35	DEGF	TEMP M-FLNGEROOT 240 RAD
	5191			730.28	DEGF	TEMP M-FLNGEROOT 300 RAD
	5192			887.23	DEGF	TEMP N-FLNGE ROOT 0 RAD
	5193			824.06	DEGF	TEMP N-FLNGEROOT 120 RAD
	5194			838.84	DEGF	TEMP N-FLNGEROOT 240 RAD
*	5196			-280.01	DEGF	TEMP N-FLNGETIP 120 RAD
	5197			785.87	DEGF	TEMP N-FLNGETIP 240 RAD
	5198			239.51	DEGF	TEMP N-FLNGE AMB 0 RAD
*	5195			1148.7	DEGF	TEMP N-FLNGE TIP 0 RAD
*	5199			-8854.2	DEGF	TEMP N-FLNGEAMB 180 RAD

Figure 3-21 Typical Print-Out of High-Pressure Turbine Case Temperatures - The instrumentation system would provide case temperature as required during the test program.

3.4.2.2 Case Temperature System Calibration Accuracy

The 20 thermocouples were installed on the turbine case prior to engine assembly. During the subsequent engine assembly, shipment, and installation on the airplane, three thermocouples were damaged. The remaining thermocouples functioned as expected.

The assessment of the accuracy with which these temperatures were measured in the installed engine during the ground and flight test program is based on combined accuracies of the thermocouples, junctions, lead wires, and Boeing data recording system. The absolute accuracy of the airplane-installed high-pressure turbine case thermal measurements was estimated to be +14°F. The back-to-back precision over the flight test period was ±10°F.

3.4.3 Engine Performance Instrumentation

Expanded performance instrumentation as described below was installed on the inboard engine during the preprogram and postprogram calibrations and throughout the ground and flight testing.

3.4.3.1 Performance Instrumentation and Location

The engine performance instrumentation used in the bare engine calibration and in the flight test program is listed on Table 3-III with the various probe locations shown on Figure 3-22. The measurements in the test stand and on the airplane are essentially the same with the principle difference being that thrust is directly measured in the test stand but not on the airplane.

TABLE 3-III

PERFORMANCE TEST INSTRUMENTATION

Parameter	No. of Probes	No. of Measurements	When Used In Test Cell	When Used Installed On Airplane
Pamb	-	1	x	x
Pt1	1	1		x
Pt2	8	8	x	
Pt2, Ps2	8	8	x	
Pt2.5	6	1	x	x
Pt3	3	1	x	x
Ps3	3	1	x	x
Ps4	1	1	x	x
Ps5i	1	1	x	
Pt7	6	1	x	x
Pcell fan	8	1	x	
Pcell primary	4	1	x	
Tamb	-	1	x	x
Tt2	8	8	x	
Tt3	1	1	x	x
Tt4.5	3	1	x	x
Tt6	6	7	x	x
Tt7	6	7	x	x
Tf	-	1	x	x
Specific humidity	-	1	x	
Thrust	-	1	x	
Wf	-	2	x	x
N1	-	1	x	x
N2	-	1	x	x
Vane Angle (β)	-	1	x	
EVC	-	1	x	x
Condition Lever Angle	-	1	x	
Bleed Valve Positions	-		x	x
Cross feed Valve	-	1		x
Precooler Exit Valve	-	1		x

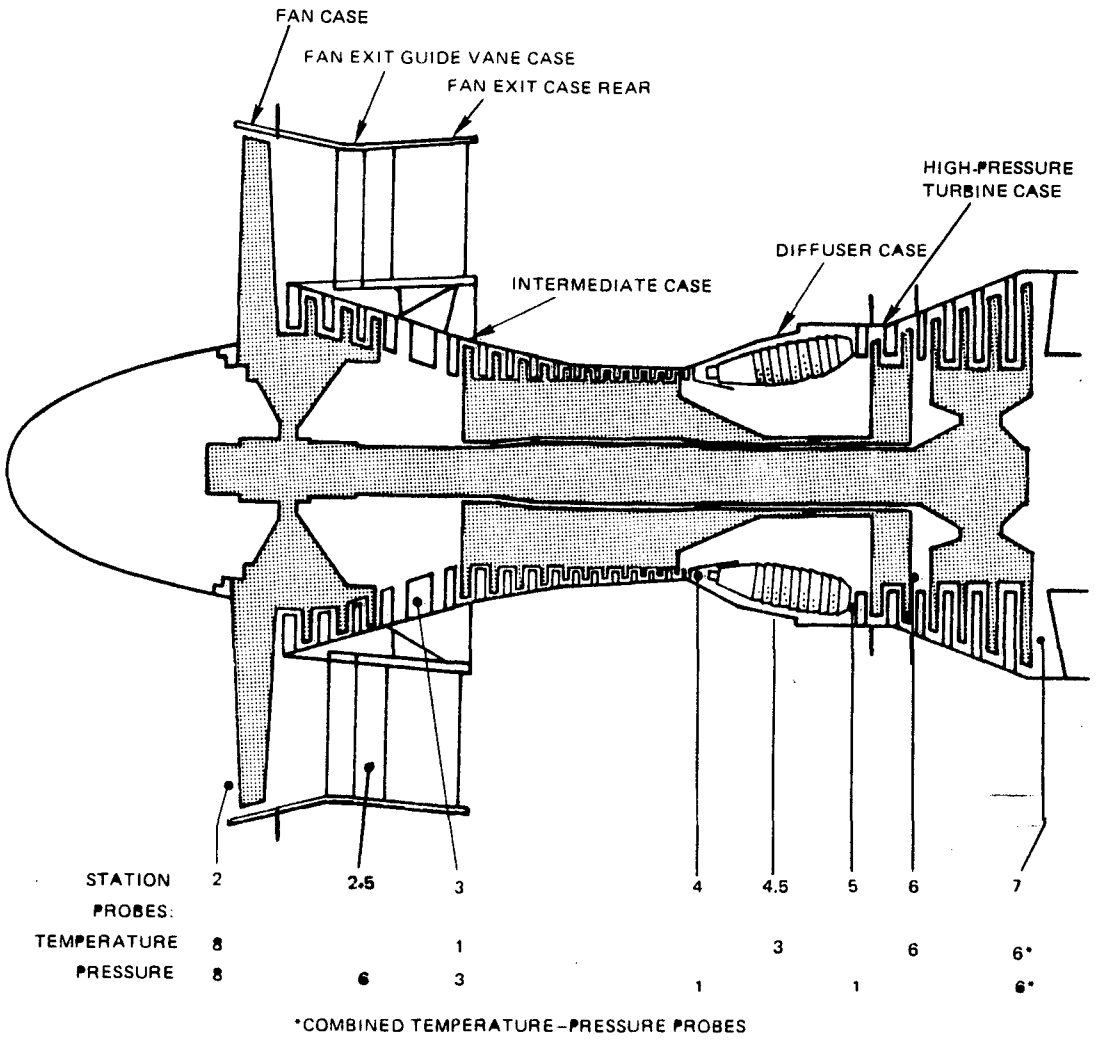

Figure 3-22 Performance Instrumentation Probe Locations - The instrumentation shown provides complete performance data.

When the engine was in the test stand, the various engine mount sensors as well as the ambient and inlet condition sensors all input into an Automatic Production Test Data Acquisition and Control (APTDAC) system which was designed, procured, and programmed by Pratt & Whitney Aircraft. Descriptions of a typical Pratt & Whitney Aircraft production test stand and the APTDAC system are presented in References 3 and 6, respectively.

When the instrumented engine was installed on the wing, the performance sensors were connected into the Boeing, RA001 747 airplane Airborne Data Analysis and Monitoring System (ADAMS) which was described briefly in Section 3.3 of this document. These engine data plus the airplane performance and environmental data provide the basis for the installed performance monitoring.

3.4.3.2 System Calibration and Accuracy

The initial and final calibrations were conducted in different test stands. The resulting total uncertainty between the initial and final calibrations is as follows:

Parameter	Total Uncertainty
N1	±0.1%
N2	±0.1%
Performance pressures	±0.4% of full scale
Performance Temperatures:	
Tt amb	±1°F
Tt3	±3°F
Tt4.5	±3°F
Tt6	±10°F
Tt7	±7°F
Tt fuel	±1°F
Fuel flow	±0.5% of full scale
Thrust	±0.5% of full scale

The airplane installed engine performance monitoring system incorporating the engine mounted probes and the Boeing ADAMS equipment had the following total uncertainties:

Parameter	Total Uncertainty
N1	±0.1%
N2	±0.1%
Performance pressures	±0.16% of full scale
Performance temperatures	±0.8% of full scale
Fuel flow	±0.25% of full scale

SECTION 4.0

DATA ANALYSIS METHODOLOGY

4.1 CLEARANCE CLOSURE DATA

Clearance changes were measured in the fan and first stage of the high-pressure turbine of a JT9D-7A engine in the number 3 position and in the fan of a JT9D-7A engine in the number 4 position of a 747 airplane for 25 discrete flight conditions using four laser proximity probes per stage. The measured clearance change at any probe location refers to the difference between the clearance measured at specific time points in the flight cycle and the clearance measured at a stabilized ground idle condition. For the transient flight conditions, such as take-offs and stall warnings, the clearance change was recorded continuously throughout the transient. The analytical interpretation of these measured blade-to-case closures can be described as the combination of engine power-induced effects and flight load effects.

Engine power-induced closure is the result of:

- o Blade and disk axisymmetric growth caused by power-induced centrifugal and thermal loads,
- o Case axisymmetric and asymmetric growth caused by power-induced thermal loads, and
- o Thrust-induced asymmetric bending of the engine.

Flight load-induced closure is the result of:

- o Asymmetric bending of the engine due to aerodynamic loads on the inlet cowl, and
- o Gravitational (G) loads and gyroscopic (gyro) loads associated with airplane maneuvers.

The power-induced axisymmetric closure was measured both on the ground and at altitude for different stabilized engine speeds. It was necessary to measure these closures at both conditions since fan clearance is significantly less at altitude as a result of reduced gas loading on the blades and reduced ambient air temperature.

The power-induced closure at a particular time in the flight cycle, together with the cold build clearance, defines the gaps available for the accommodation of additional deflection due to external flight loads.

All asymmetric closures were recorded for each flight condition; however, only the maximum asymmetric closures which would contribute to engine deterioration were fully explored.

The asymmetric closure due to thrust and flight load-induced engine bending was isolated using the NASTRAN (NASA STRuctural ANalysis) finite element mathematical model of the JT9D/747 propulsion system with the measured loads and calculated thrust levels as input. The mathematical model was jointly developed by Pratt & Whitney Aircraft and Boeing and began with an identification of below-the-wing propulsion system substructures which were provided by each party. Since primary emphasis in the study was on behavior of the engine, the wing was not included. By excluding the wing, the nacelle/strut combination could reasonably be assumed to be symmetric about a vertical plane through the engine centerline, and the engine behavior could then be calculated with a half model for much less cost than for a full model.

Substructure interfaces were chosen where subassemblies were mechanically joined (that is, mount points, flanges, etc.). Detailed finite-element models of the engine static structure (cases and bearing support frames), rotors, and thrust yoke were provided by Pratt & Whitney Aircraft. Rotors were modeled as beams with discrete masses input directly. Boeing provided the inlet, strut, and tail-cone models.

Secondary structural components (fan and core cowls, fan and turbine reversers, stator assemblies), accessories, and plumbing were included as discrete or distributed masses as appropriate to bring the mass properties of the model to within 5 percent of the actual hardware. The final static model consisted of eight substructures with approximately 11,000 degrees of freedom, as shown in Figure 4-1.

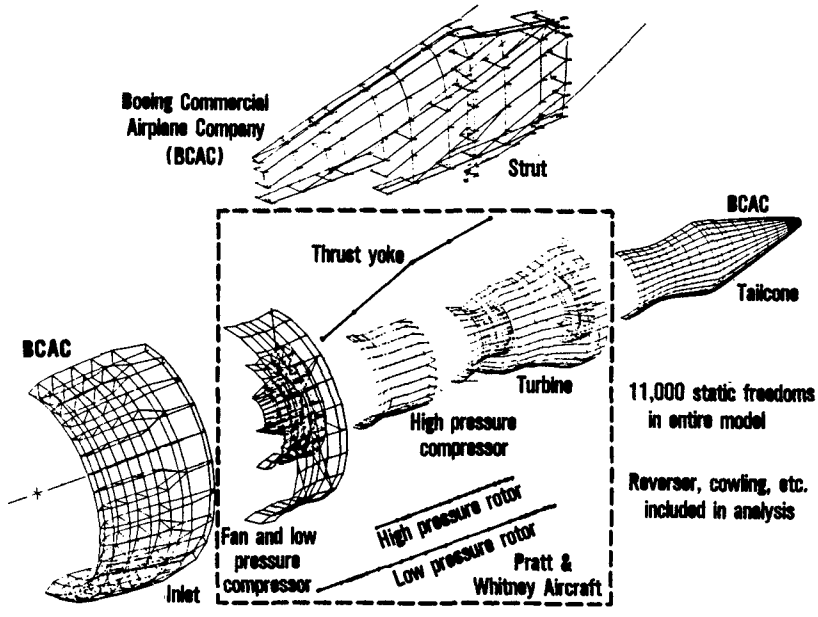

Figure 4-1 JT9D/747 Integrated NASTRAN Finite Element Structural Model - The model consists of eight substructures with approximately 11,000 degrees of freedom. (J20152-9)

The flight acceptance profile incorporated in the model includes the proper combination of measured nacelle loadings, engine thrust, inertia and gyroscopic effects, thermal expansion effects, base-line clearances, and air-seal/blade abradability factors. Exposure to thrust and maneuver loads results in deformation of propulsion system structural members and leads to relative motion between static and rotating components of flow-path seals (this is termed closure). If the motions are larger than can be accommodated by the available clearances, rubs and wear (air-seal/blade tip rubbing) will occur and result in increased operating clearances between blade tips and outer air seals. Abradability factors determine the relative blade tip and outer seal wear. Performance influence coefficients for each engine stage are then used to determine the performance loss due to these increased operating clearances.

4.2 CASE TEMPERATURE DATA

High-pressure turbine case metal temperatures at the front and rear flanges, shown previously in Figure 3-20, were recorded simultaneously with performance and clearance parameters during each of the test conditions. The case temperature data were recorded on the Boeing Airborne Data Analysis and Monitoring System (ADAMS). The data tapes were then processed by Pratt & Whitney Aircraft to define transient and steady state temperature patterns in the radial, axial, and circumferential directions.

Analytical models for predicting the steady state and transient thermal growth characteristics of the turbine assembly were validated and, where necessary, corrected using the case temperature, gas temperature, and directly-measured clearance data. Turbine case response to thermal transients was found to be faster than predicted by the analytical models, which were subsequently revised. The revised models were then used in the analysis to establish and quantify the various causes of clearance closure at the critical ground test and flight conditions.

4.3 PERFORMANCE DATA

A preflight performance calibration of the newly assembled engine was made in the Pratt & Whitney Aircraft test facility in Middletown, Connecticut. After the engine was installed in the number 3 position on the airplane, a five-point installed base-line ground calibration was conducted at Boeing Field, Washington. This base-line calibration was repeated after a functional check flight and the ferry flight to Glasgow, Montana when it was learned that cabin air was inadvertently being bled from the engine during the original installed calibration. Each of the subsequent test flights was followed by a ground calibration. Upon completion of the NAIL program flight testing, several additional flights were made for the JT9D-7R4 engine development program being conducted in conjunction with the NAIL program. Then a final installed calibration of the NAIL engine was

conducted prior to the ferry flight back to Boeing Field and removal of the engine. Two postflight performance calibrations were conducted in the Middletown test facility, one in the as-received condition and a second calibration after a vane trim check and fan blade wash.

A comparison of the postflight performance calibrations with the preflight performance base-line calibrations was made. The engine performance deterioration [thrust specific fuel consumption (TSFC) increase] was noted along with changes in certain other gas generator characteristics and in calculated component performance parameters. The impacts of the component efficiency and flow capacity changes on thrust specific fuel consumption and gas generator characteristics were estimated from a mathematical simulation of the engine. These estimated impacts were then compared with the measured changes in thrust specific fuel consumption and gas generator characteristics to verify the component efficiency and flow capacity changes.

Each of the installed calibrations was compared with the second (first test with no air bleed) installed calibration. These comparisons indicated no measurable change in engine performance, so that no component deterioration is attributed to the flight testing after calibration. Finally, a comparison of the installed performance and postflight test-stand performance with the preflight test-stand base-line performance was made to determine which test events produced the engine deterioration. This comparison was based primarily on turbine discharge temperature at constant engine pressure ratio and fuel flow at constant engine pressure ratio.

After completion of the performance data analysis, performance changes were assessed based on the condition of gas-path hardware observed during the analytical teardown of the test engine as compared to engine build conditions. The fan and high-pressure turbine modules were inspected extensively, since these modules had been refurbished prior to the test program. Build measurements of these two modules were also compared with nominal blueprint measurements to determine how these modules compared with typical new or refurbished parts.

SECTION 5.0

RESULTS

5.1 INTRODUCTION

The previously defined objectives of this program were to measure the flight loads on the nacelle/engine combination and the effects of these loads on the fan and high-pressure turbine clearance closures. However, it is the total closure in running clearances that causes the rubs and, hence, opening of running clearances and loss of performance. Therefore, the total axisymmetric and asymmetric closures in the fan and high-pressure turbine at the critical running clearances as well as the factors contributing to each type of closure in each module must be known. Only with this knowledge can methods be formulated to minimize clearance closure-induced rubs.

In the fan, there appear to be five types of loads that influence clearance closure, as shown in Figure 5-1 along with the causes of these loads. In the turbine there are six types of loads, as shown in Figure 5-2 along with their causes.

The laser proximity probes in the fans of the positions number 3 and 4 engines and in the first-stage high-pressure turbine of the position number 3 engine measured the absolute clearances, and recorded these measurments on video tape, 30 times per second. By comparing various combinations of these data and the corresponding flight conditions from more than 100 engine hours of video tape data, it was possible to segregate the effects of rotor speed, altitude, thrust, aerodynamic and inertia loads, and thermal expansion.

The effects of power-induced loads and flight loads on the fan clearances, as determined from laser probe data and subsequent inspections, as well as comparisons of current and previous test results are presented in Section 5.2. Similar information on the high-pressure turbine is presented in Section 5.3.

An analytical study conducted as part of an earlier phase of the JT9D Engine Diagnostics program assessed that time-dependent (dynamic) loads as might be caused by a vertical gust or a hard landing would have only a small effect on rub-induced wear. However, it was left to this Flight Loads Test program to experimentally verify these conclusions. In the 40 hours of flying in the combined program, no significant gusts were encountered. However, a heavy gross weight (690,000-pound), high sink rate (5 feet/second) landing was experienced. The results of this landing are compared with analytical predictions in Section 5.4.

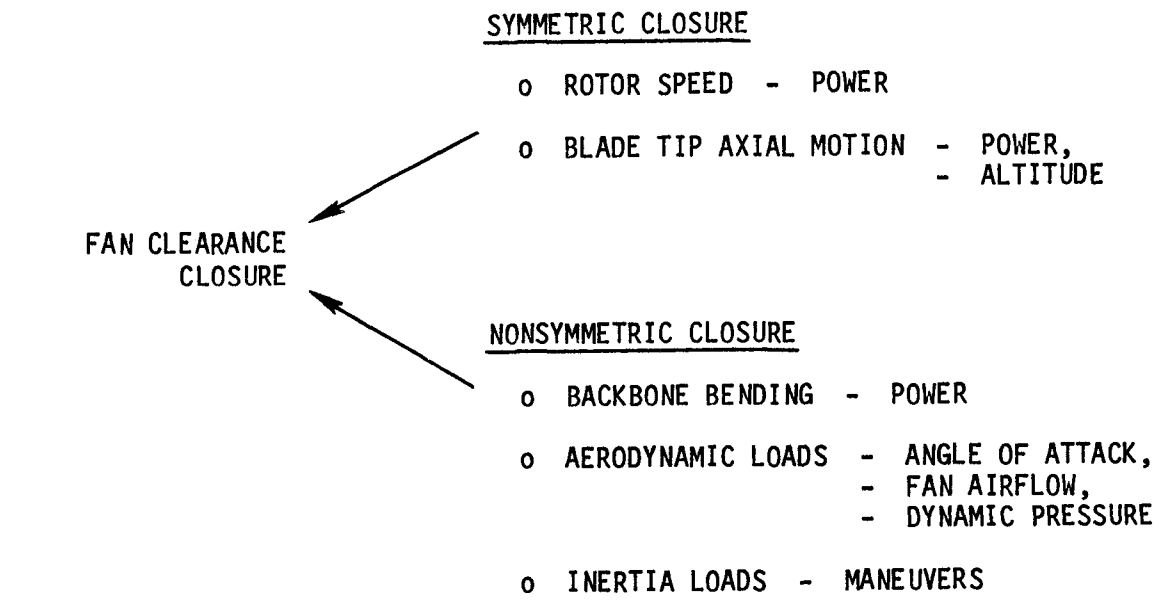

Figure 5-1 Fan Clearance Closure - Closure in the fan results from engine power, altitude, angle of attack, fan airflow, dynamic pressure, and maneuvers.

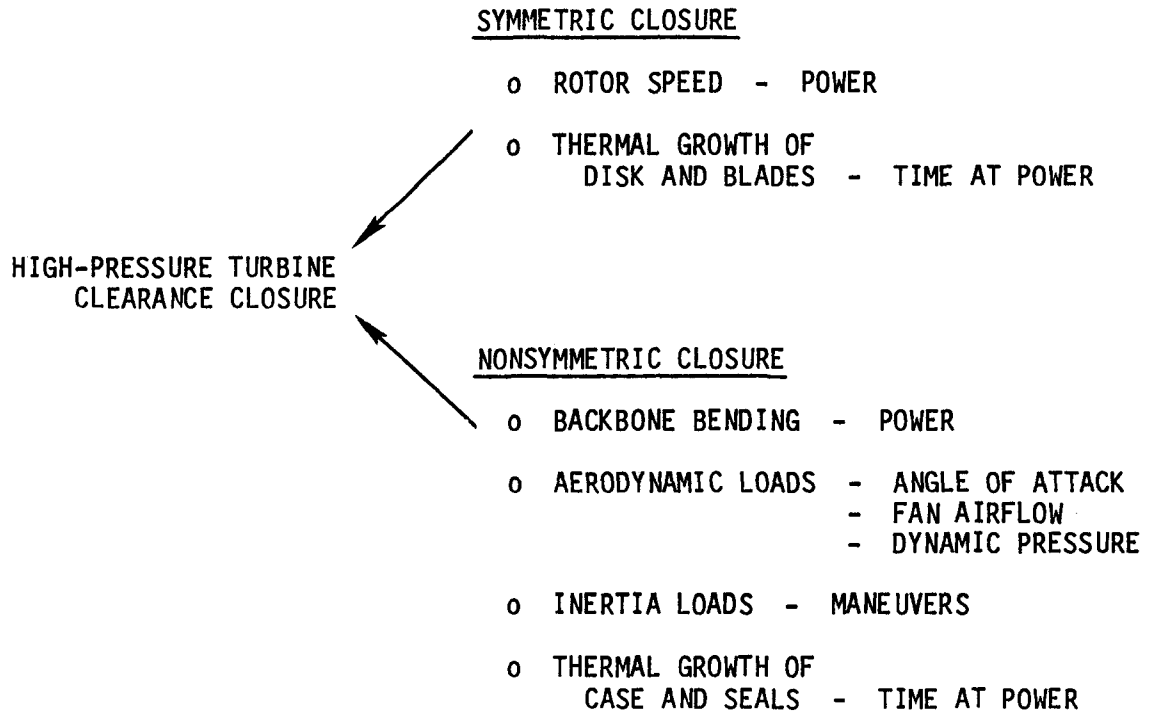

Figure 5-2 High-Pressure Turbine Clearance Closure - Closure in the turbine results from engine power, time at power, angle of attack, fan airflow, dynamic pressure, and maneuvers.

The position number 3 engine, serial number P-662204, with its refurbished fan and high-pressure turbine was calibrated on a Pratt & Whitney Aircraft production engine test stand before installation on RA001 airplane and after its removal from the airplane upon completion of the test flights. While installed on the airplane, it was calibrated five times on the ground as listed on Table 3-I. These calibrations were analyzed to determine the extent of engine and module deterioration caused by this test program and when during the program the performance loss occurred. These analytical results are presented in Section 5.5.

5.2 FAN EFFECTS

5.2.1 Summary of Fan Effects

Running clearance closure between the fan blades and the outer air seal was a maximum during take-off, immediately following rotation. The pinch point was slightly inboard of bottom center of the engine. Tight clearances at the bottom also occurred during the airplane stall, stall warning, and high g turn maneuvers.

Analysis of the test data established that fan clearance closures are a combination of axisymmetric closures and asymmetric closures, as previously outlined on Figure 5-1. Axisymmetric closures are caused by engine power-induced loads. The combination of centrifugal growth and axial deflection of the rotor/blade assembly establishes the axisymmetrical closures. Asymmetric closures are caused by both engine and externally generated forces. Backbone bending forces due to thrust deflect and ovalize the fan case, reducing running clearance at the bottom. Aerodynamic loads further deflect and ovalize the fan case. Finally, inertia loads cause additional asymmetric closures.

Axisymmetric closure is a maximum at altitude conditions when rotor speed is high and the thrust bending load on the blades is low. Asymmetric closure is a maximum at take-off when the combined effect of thrust backbone bending and aerodynamic loads is greatest.

Measured fan clearance closures on the position numbers 3 and 4 engines were essentially the same under all flight conditons, indicating that rub-induced fan performance deterioration is essentially independent of engine position on the 747 airplane.

Section 5.2.2 compares the measured clearance closures due to power-induced loads and flight loads at the various test conditions. Section 5.2.3 discusses the inspection results of fan wear observed at the post-test inspection. Section 5.2.4 compares the results of this test program with prior test data.

5.2.2 Measured Clearance Closures

5.2.2.1 Power Effects

Fan blade-to-case closure due to power effects is a combination of axisymmetric growth associated with low-pressure rotor (N_1) speed and asymmetric, thrust-induced, engine bending. Axisymmetric closure consists of fan blade and hub centrifugal and thermal growth, fan blade deflection due to gas-path loads, and case thermal growth.

The geometry of the fan outer air seal is such that forward axial bending of the fan blades, caused by gas-path loads, opens the blade tip clearance. However, at altitude lower gas-path loads, compared to sea level operation, are imposed on the fan blades, resulting in tighter axisymmetric running tip clearance.

Measured axisymmetric fan clearance change from a stabilized ground idle is presented in Figure 5-3 as a function of low-pressure rotor (N_1) speed, both on the ground and at altitude, based on ground and flight calibration data. The net thermal expansion effect on the fan rotor and case is also included in Figure 5-3. Axisymmetric clearance closures for the position number 3 fan at each of the test conditions are summarized on Table 5-I, column 1.

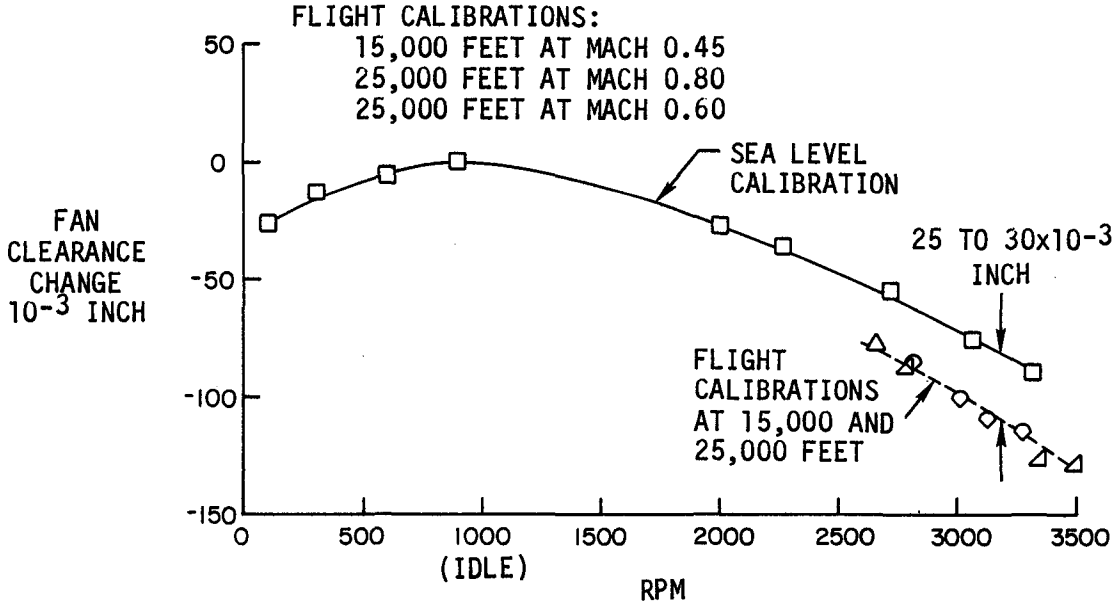

Figure 5-3 Measured Axisymmetric Fan Clearance Change - Ground and flight calibration data show that clearances are tighter at altitude compared to sea level for a given engine speed.

TABLE 5-I

POSITION NUMBERS 3 AND 4 FAN CLEARANCE CLOSURES (INCH) RELATIVE TO GROUND IDLE

Flight Condition Description	Number	Mach number	Position No. 3 Fan							Position Number 4 Fan	
			Power Induced Closure		Flight Loads Closure	Total Closure	Other Closures	Measured Total Closure	Pinch Location*	Measured Total Closure	Pinch Location*
			Axisymmetric	Asymmetric (Thrust)							
612,000 lb Take-Off with 20° Flaps	101-1	0.25	-0.086	-0.032	-0.125	-0.243	+0.022	-0.221	203°	-0.223	193°
538,000 lb Take-Off with 10° Flaps	101-2	0.24	-0.087	-0.037	-0.139	-0.263	+0.025	-0.238	197°	-0.251	195°
647,000 lb Take-Off with 10° Flaps	101-3	0.25	-0.087	-0.037	-0.147	-0.271	+0.016	-0.255	--	-0.263	195°
780,000 lb Take-Off with 10° Flaps (Simulated)	118	0.30	-0.088	-0.041	-0.149	-0.278	+0.008	-0.270	--	-0.285	194°
Low-Climb	102	0.37	-0.082	-0.036	-0.074	-0.192	-0.025	-0.217	206°	-0.208	198°
Mid-Climb	103	0.60	-0.085	-0.025	-0.056	-0.166	-0.026	-0.192	207°	-0.181	196°
High Mach Number Cruise	104	0.86	-0.107	-0.016	-0.033	-0.156	+0.008	-0.148	220°	-0.145	198°
Low Mach Number Cruise	105	0.77	-0.099	-0.011	-0.049	-0.159	+0.007	-0.152	216°	-0.153	198°
Maximum Mach Number Flight	106	0.91	-0.117	-0.016	-0.012	-0.145	-0.005	-0.150	219°	-0.140	194°
In-Flight Relight	107	0.72	-0.059	-0.008	-0.045	-0.112	--	**	--	Not Shut Down	
Maximum Dynamic Pressure Flight	108	0.84	-0.124	-0.034	+0.023	-0.135	-0.027	-0.162	220°	-0.126	212°
Stall Warning with Flaps Up	109	0.37	-0.094	-0.025	-0.086	-0.205	--	**	--	-0.124	203°
Stall Warning with 10° Flaps	110	0.35	-0.090	-0.027	-0.108	-0.225	--	-0.171	204°	-0.199	199°
Stall Warning with 30° Flaps	111	0.27	-0.113	-0.028	-0.075	-0.216	+0.018	-0.198	206°	-0.113	212°
Idle Descent	112	0.44	0.0	-0.001	-0.054	-0.055	-0.012	-0.067	199°	-0.063	206°
Approach	113	0.27	-0.117	-0.038	-0.069	-0.224	+0.028	-0.196	204°	-0.182	202°
Touch and Go	114	0.26	0.087	-0.047	-0.085	-0.219	+0.030	-0.189	210°	-0.145	206°
Thrust Reverse	115	0.18	-0.070	-0.036	-0.009	-0.043	-0.025	-0.068	240°	-0.068	248°
2.0-G Left Turn with Flaps Up	116	0.49	-0.095	-0.017	-0.100	-0.212	+0.011	-0.201	208°	-0.139	194°
1.6-G Left Turn with 30° Flaps	117	0.26	-0.057	-0.036	-0.137	-0.230	--	**	--	-0.103	199°
2.0-G Right Turn with Flaps Up	120	0.48	-0.068	-0.016	-0.081	-0.165	+0.018	-0.147	196°	-0.158	188°
1.6-G Right Turn with 30° Flaps	121	0.27	-0.100	-0.028	-0.080	-0.208	-0.009	-0.217	193°	-0.173	206°
Airplane Stall	123	0.21	-0.116	-0.036	-0.094	-0.246	-0.014	-0.260	190°	--	--

* Measured clockwise from top of engine, as viewed from the rear.
** Insufficient laser proximity probe data to define pinch point.

Note: Negative values of closure may be interpreted as reduced clearance and increased chance of rubs.

Since the thrust reaction is carried through the thrust frame, which is offset 30 degrees above the engine horizontal centerline, there is a backbone bending moment generated about the engine horizontal axis. The resulting engine bending (as illustrated in Figure 5-4) causes the front flange of the fan case to deflect upward more than the front section of the low-pressure rotor which results in reduced fan blade clearance at the bottom of the engine. The thrust load effects on blade clearances in the position number 3 fan for each of the test conditions are shown on Table 5-I, column 2.

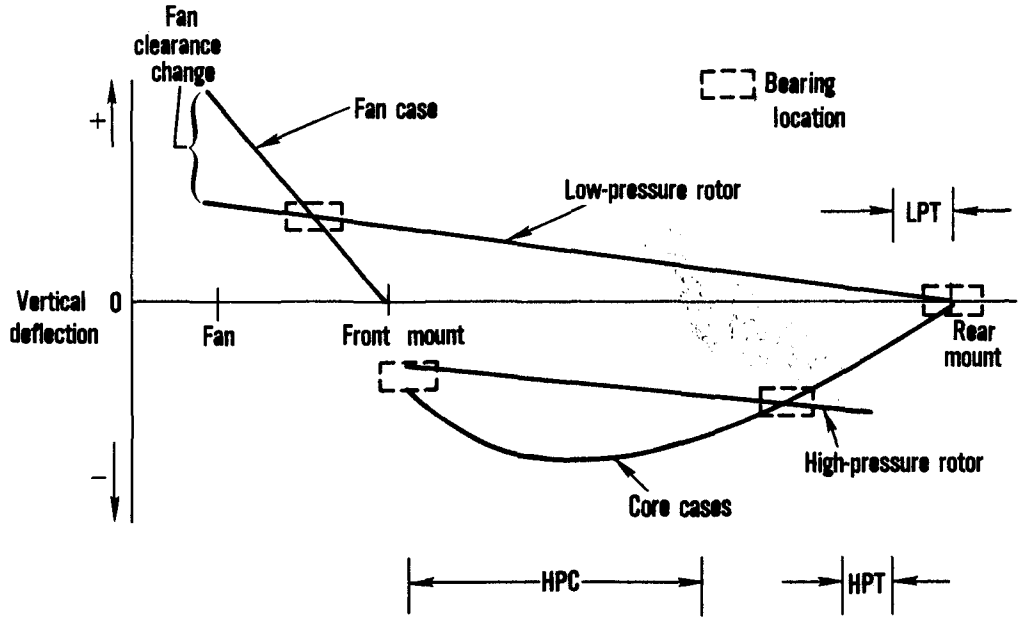

Figure 5-4 Typical Backbone Bending Plot for the JT9D Engine - A backbone bending moment resulting from the engine thrust reaction causes the front flange of the fan to deflect upward more than the front section of the low-pressure rotor. (J24318-1)

Table 5-I lists the fan maximum clearance closure and location of the pinch point for each of the test conditions as computed from the measured clearance values on position numbers 3 and 4 fans. The table also lists the axisymmetric closure and thrust-induced and flight loads-induced asymmetric closures for each condition. The axisymmetric closures are computed from the measured values and validated using the actual fan speed and Figure 5-3. The thrust and flight loads closures are computed using the NASTRAN finite element mathematical model of the JT9D/747 propulsion system which was validated using test data which isolated individual changes in thrust and aerodynamic loads.

In Table 5-I, the differences (in column 5) between the predicted (column 4) and the measured (column 6) total clearance closure values represent the sum of possible clearance measurement errors and limitations in the NASTRAN models.

The thrust load effect on JT9D fan running clearances were computed using previously developed analytical models which were validated by test data from this program.

The combined effects of power loads on fan running clearances are shown on Figure 5-5 which plots the running clearance measured at the four probe locations during a stabilized ground idle, run up to power, ground calibration, and the first test take-off. The probe locations are shown in the lower left hand corner of the figure. Engine power level is proportional to the plotted fan rotor speed (N_1). Reading from the left, the engine operated at stabilized ground idle for 6 minutes. The running clearance indicated by the lower probes is about 0.050 inch greater than at the top due to the offset grind in the fan outer air seal.

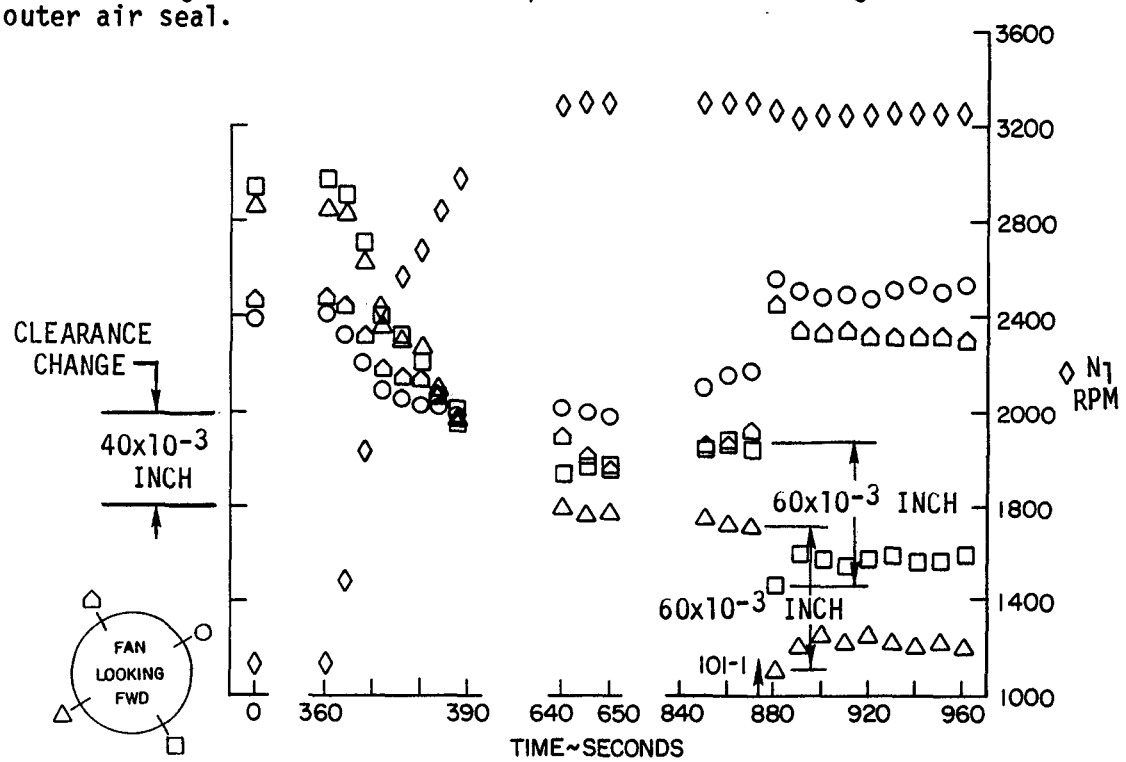

Figure 5-5 Change in Fan Running Clearance from Stabilized Ground Idle to the First Take-Off - Thrust and air loads are additive in closing clearances at the bottom of the position number 3 fan.

The engine was then accelerated to approximately 80 percent of take-off power. As engine speed increased, the centrifugal force effect axisymmetrically reduced the running clearance at all four probe locations. This effect can be seen in Figure 5-5 during the initial 10 seconds of the acceleration. As the static thrust increased, the

resulting backbone bending effect opened the clearance at the top and closed it further at the bottom of the engine. The net effect at the end of this acceleration was to close the clearances by 0.068 inch axisymmetrically plus an additional 0.023 inch asymmetrically at the lower probe locations. At the subsequent increase to full power (640 seconds) there were additional closures with the axisymmetric and asymmetric closures of about equal magnitude.

5.2.2.2 Flight Loads Effects

The flight load-induced clearance closures and the total clearance closures at each of the test conditions, at the minimum clearance position (approximately 190 degrees), are listed on Table 5-I, columns 3 and 4. As indicated on the table, the flight conditions which exhibit the greatest amount of closure are take-off, stall warning, airplane stall, and high g turns. All of these test points correspond to conditions of maximum fan airflow rate and high angles of attack. A time history plot of the fan clearance changes during take-off (Figure 5-5) clearly shows the effect of flight loads on fan clearance. As the airplane rolled down the runway (at 860 seconds), the thrust bending load decreased slightly; however, the clearances remained essentially constant. This apparent contradiction resulted from the generation of an aerodynamic load on the inlet cowl while the airplane was on the runway. At take-off rotation (flight condition 101-1), there was a large change in the inlet angle of attack which, combined with a high fan airflow, resulted in a large load on the inlet cowl. This load caused the engine to bend as a beam (Figure 5-4), resulting in a 0.060-inch decrease in fan clearance at the bottom and an increase in clearance at the top of the engine (Figure 5-5).

The maximum clearance closure during this typical revenue service take-off and the contributing effects are shown on Table 5-I for the 612,000-pound take-off with 20-degree flaps (Condition 101-1). The actual measured closure at the pinch location at Condition 101-1 relative to the ground idle condition was within 10 percent of the predicted closure based on NASTRAN structural analysis. The 0.221-inch fan clearance closure caused a rub (Figure 5-6) resulting in an average increase (Table 5-II) in fan clearance of 0.033 inch relative to build clearance. The effects of this rub on engine performance is discussed in Section 6.

TABLE 5-II

POSITION NUMBER 3 FAN OUTER AIR-SEAL WEAR

Test Flight Number	Incremental Wear (inch)	Cumulative Wear (inch)
1	0.033	0.033
2	0.013	0.046
3	0.005	0.051
4	0.003	0.054
5	0.001	0.055

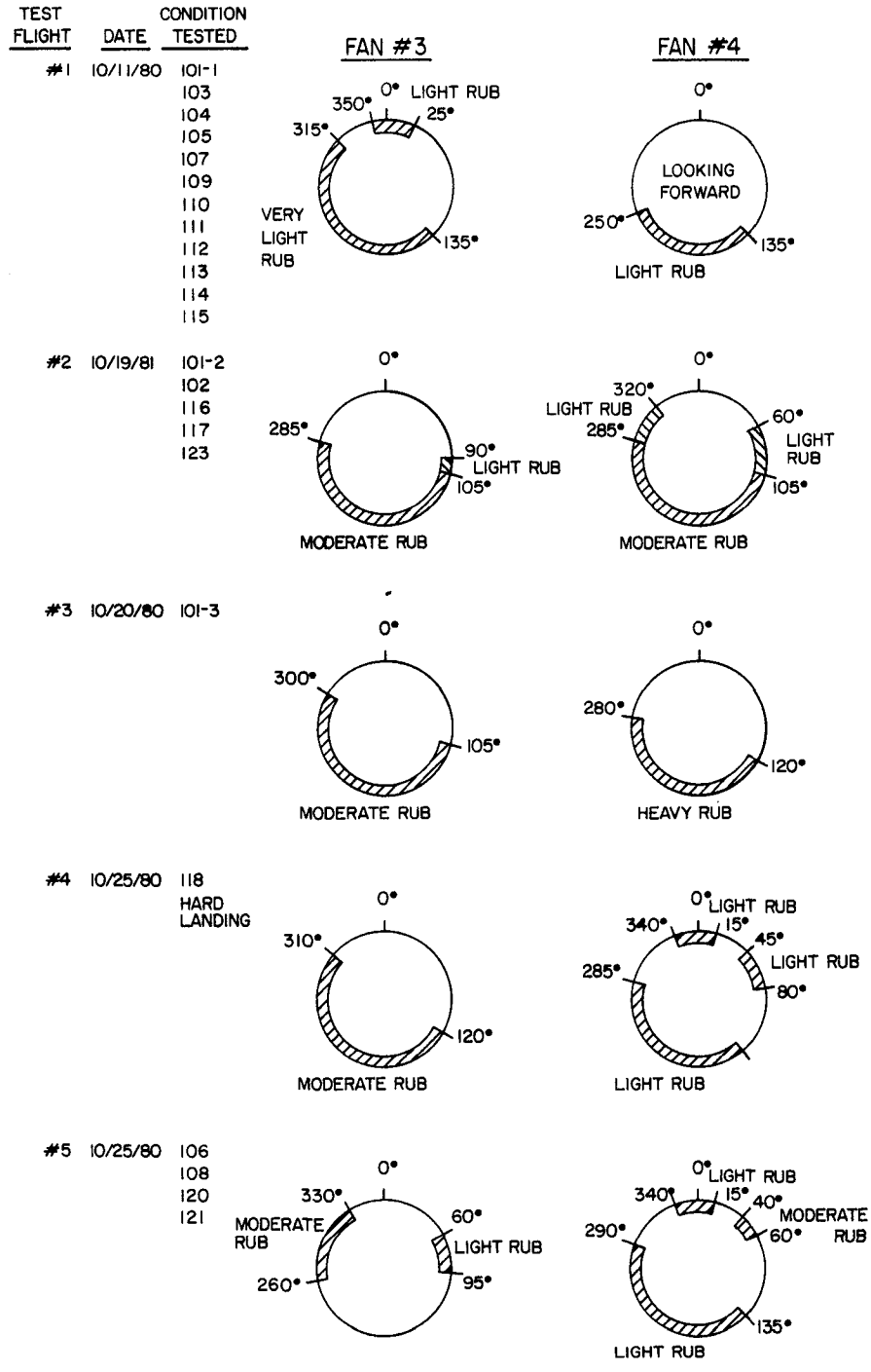

Figure 5-6 Post-Test Observation of Fan Rubs - Rub patterns for take-off tests are quite similar for the two test engines.

The second test take-off (Condition 101-2) was a full power take-off at 538,000 pounds with 10-degree flaps, which is representative of a production airplane acceptance flight take-off. The lift-off speed (Table 3-I) was slightly less than that for the first take-off, however the rotation angle was greater because of the lower flap setting. The 0.238-inch measured clearance closure (Table 5-I) was significantly greater for this lighter weight take-off as compared to that for Condition 101-1. The average fan rub depth was increased to 0.046 inch (Table 5-II) with resulting increased loss in fan performance.

The Third and fourth take-offs (Conditions 101-3 and 118) were also conducted at full power and with 10-degree flaps for both tests. However, gross weights were increased to establish the effect of weight on aerodynamic load and the resulting clearance closure. The rotation angles were about equal to that of Condition 101-2. However, the rotation speed (Table 3-I) increased with higher gross weight. The result was an increasing aerodynamic load and clearance closure (Table 5-I and Figure 5-7) with increasing take-off gross weight, at constant power and flap setting, due to the higher dynamic pressure (speed) at rotation. Figure 5-7 shows that change in flap setting has a greater effect than gross weight on fan clearance closure and rub depth.

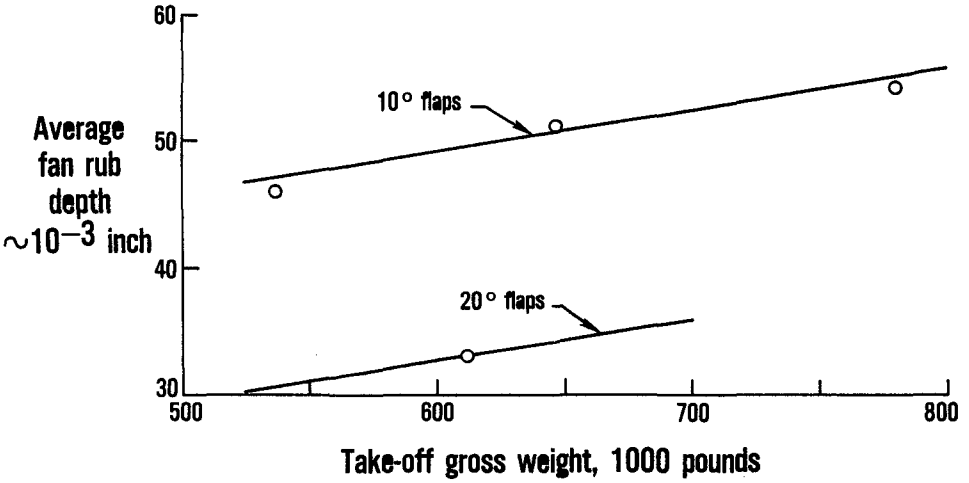

Figure 5-7 Effect of Take-Off Gross Weight and Flap Setting on Fan Clearance Closure at Take-Off - Change in flap setting has a greater effect than gross weight on fan clearance closure and rub depth.

Since all four take-off tests were conducted at full take-off power, the flap angle, and thus rotation angle, appears to be the prime difference between the first and second take-offs, and the rotation speed (V_R*) is the prime difference between the second, third, and fourth take-offs.

---

* V_R = airplane flight speed at take-off rotation.

The stall warning conditions (flight conditions 109, 110, and 111), which were part of airplane acceptance testing and the inadvertent airplane stall (condition 123), provided good examples of the combined effect of high angle of attack and high fan airflow rate. The stall warning condition 110, see Figure 5-8, establishes that both high fan airflow and high vane angle are required. As seen on the double plot in this figure, prior to the stall warning the vane angle is high (25 degrees) and the engine speed and, thus, airflow rate are low. The asymmetric clearance closure is small as shown by the close spread between probe readings.

At the stall warning signal, the pilot nosed over the airplane and accelerated the engine to prevent a stall. As engine speed increased, the pilot raised the airplane nose to a position slightly below that prior to the stall warning. Note that as engine speed, and thus fan airflow, increase there is a rapid increase in both the axisymmetric and asymmetric closures of the fan as indicated by the probe readings.

High G turn simulated avoidance maneuvers provided the other maximum clearance closure condition in the fan. The effect of increasing angle of attack (in the turn) while flying at a constant engine speed is shown in the measured clearance data plot of the 1.6-G turn, condition 121. This plot is shown in Figure 5-9.

The NASTRAN finite element mathematical model of the JT9D/747 propulsion system was used to provide an analytical interpretation of the closures measured during the flight events which caused the largest amount of fan rubs. The ability of the model to demonstrate the effect of flight loads on fan clearance was examined by comparing the measured change in fan clearance which occurred between two time points in a take-off rotation, where only an inlet cowl load is varying, with that which the model would predict given the change in load. The results presented in Table 5-III indicate that the clearance change trends can be predicted by the model with a reasonable degree of accuracy.

5.2.2.3 Effect of Engine Position

Fan running tip clearance changes were measured on both the inboard and outboard engines of a 747. The laser proximity probes were placed at the same circumferential locations in each fan case to ascertain the effect of engine position on both the magnitude and direction of fan closure. As illustrted on Table 5-III, there is slight difference in the maximum pinch clearance closure on the inboard and outboard engines under all test conditions. The actual location of the pinch point on the outboard engine would be expected to be closer to 180 degrees since the fuselage would have less influence on the direction of the inlet air stream.

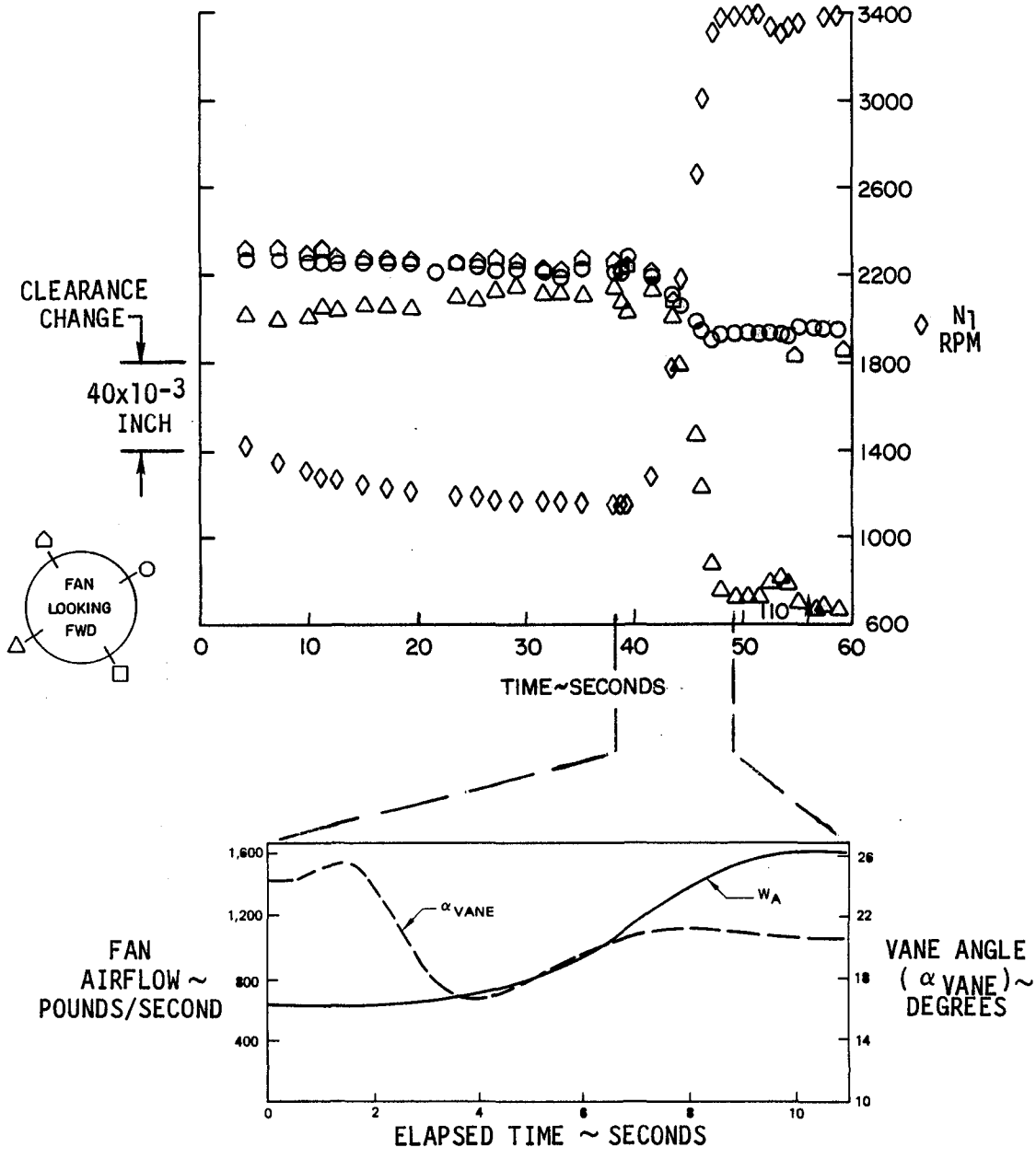

Figure 5-8 Change in Fan Running Clearance During the Stall Warning (Condition 110) - The stall avoidance maneuver and the accompanying increase in engine speed and fan airflow rate resulted in a rapid increase in both the axisymmetric and asymmetric closure.

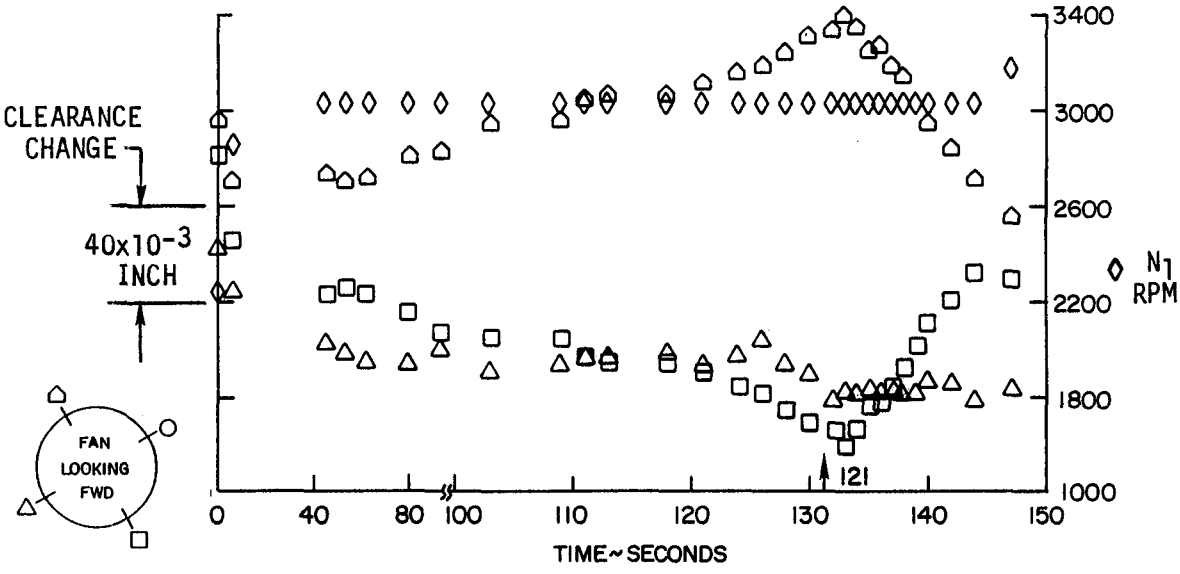

Figure 5-9 Change in Fan Running Clearance During a High G Turn Simulated Avoidance Maneuver (Condition 121) - The increasing angle of attack in the turn at constant engine speed resulted in an increased aerodynamic load-induced closure in the position number 3 fan.

Figure 5-10 presents a plot comparing fan clearance closure on the two engines during a ground run, take-off, and climb. Data are plotted for proximity probes at 60 and 240 degrees for each of the two test engines. With the engines at the same rotor speed, there is no difference in fan clearance closure as measured by the two probes in each of the two engines.

Figure 5-11 presents a similar comparison of seven additional test conditions. Clearance closures at the 60 and 240 degree probe positions are recorded. Fan speed is also recorded to identify similar power levels.

Based on these data, it is concluded that the influence of engine position on aerodynamic load-induced clearance closures or resulting seal rubs is negligible.

5.2.3 Inspection Results

Fan performance loss in airline service occurs due to rub-induced increase in fan running clearances, increased roughness of the fan blade surfaces, and blunting of the blade leading edges.

Assembled fan blade clearances were measured at the beginning and the end of the test program. Outer air-seal wear was measured during and at the end of the program. Fan blade surface condition and leading edge profile were measured at the beginning and end of the program.

TABLE 5-III

NASTRAN PREDICTED COMPARED TO MEASURED FAN ASYMMETRIC CLEARANCE CHANGE DUE TO FLIGHT LOADS

Flight Condition Description	Number	Mach number	Data Source	Clearance Change (inch) at Circumferential Location (degrees) 60	150	240	330
612,000 lb Take-Off with 20° Flaps	101-1	0.25	Engine No. 3	+0.045	-0.062	-0.058	+0.059
			Engine No. 4	+0.056	-0.059	-0.055	+0.052
			NASTRAN	+0.077	-0.070	-0.065	+0.056
647,000 lb Take-Off with 10° Flaps	101-3	0.25	Engine No. 3	--	-0.084	-0.085	+0.077
			Engine No. 4	+0.083	-0.080	-0.080	+0.071
			NASTRAN	+0.084	-0.081	-0.092	+0.087
780,000 lb Take-Off with 10° Flaps (Simulated)	118	0.30	Engine No. 3	--	-0.100	--	--
			Engine No. 4	--	-0.080	--	+0.080
			NASTRAN	+0.073	-0.089	-0.077	+0.095
2.0-G Left Turn with Flaps Up	116	0.49	Engine No. 3	--	-0.025	-0.020	+0.020
			Engine No. 4	+0.013	-0.016	-0.014	+0.011
			NASTRAN	+0.022	-0.020	-0.027	+0.021
2.0-G Right Turn with Flaps Up	120	0.48	Engine No. 3	--	-0.025	-0.009	+0.023
			Engine No. 4	+0.019	-0.028	--	+0.029
			MASTRAN	+0.027	-0.026	-0.033	+0.027

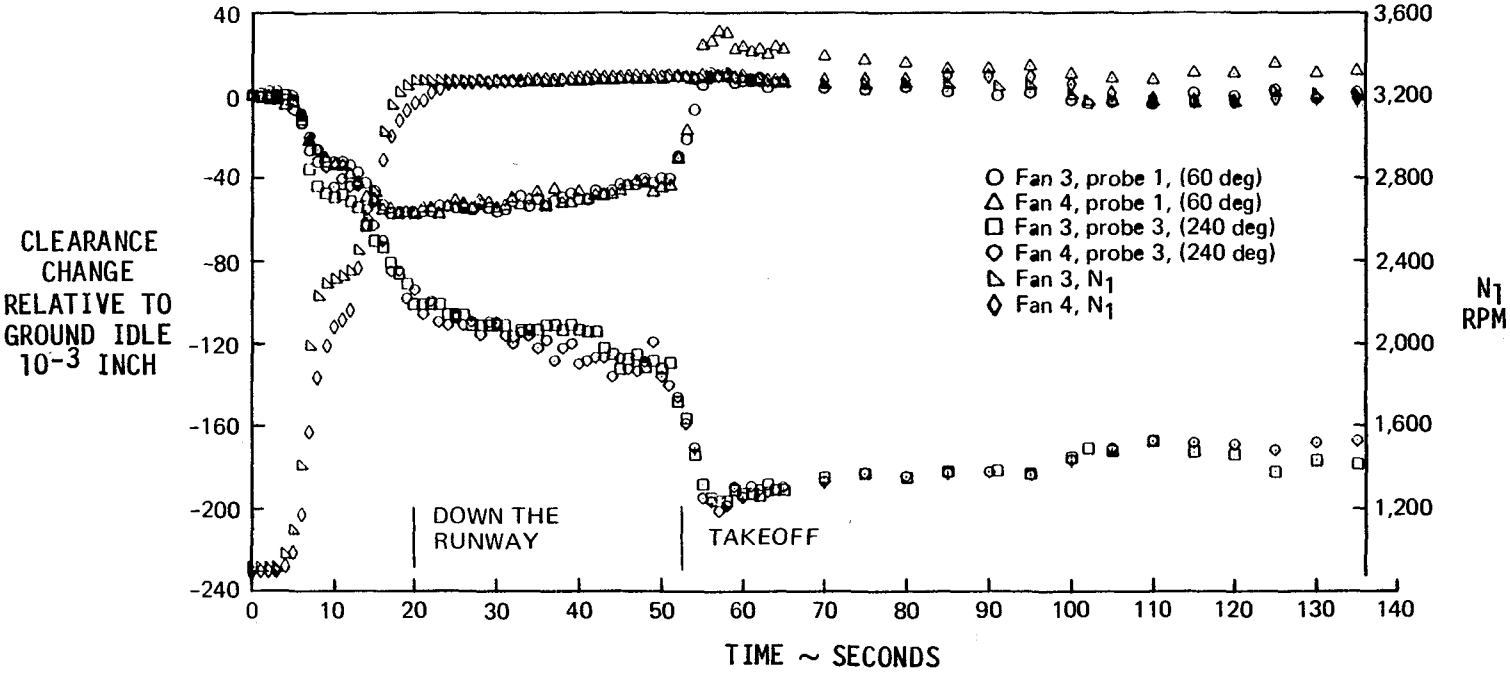

Figure 5-10 Comparison of Fan Clearance Change versus Engine Position Under Transient Conditions - The influence of engine position on fan clearance change during a typical ground run, take-off, and climb sequence is negligible.

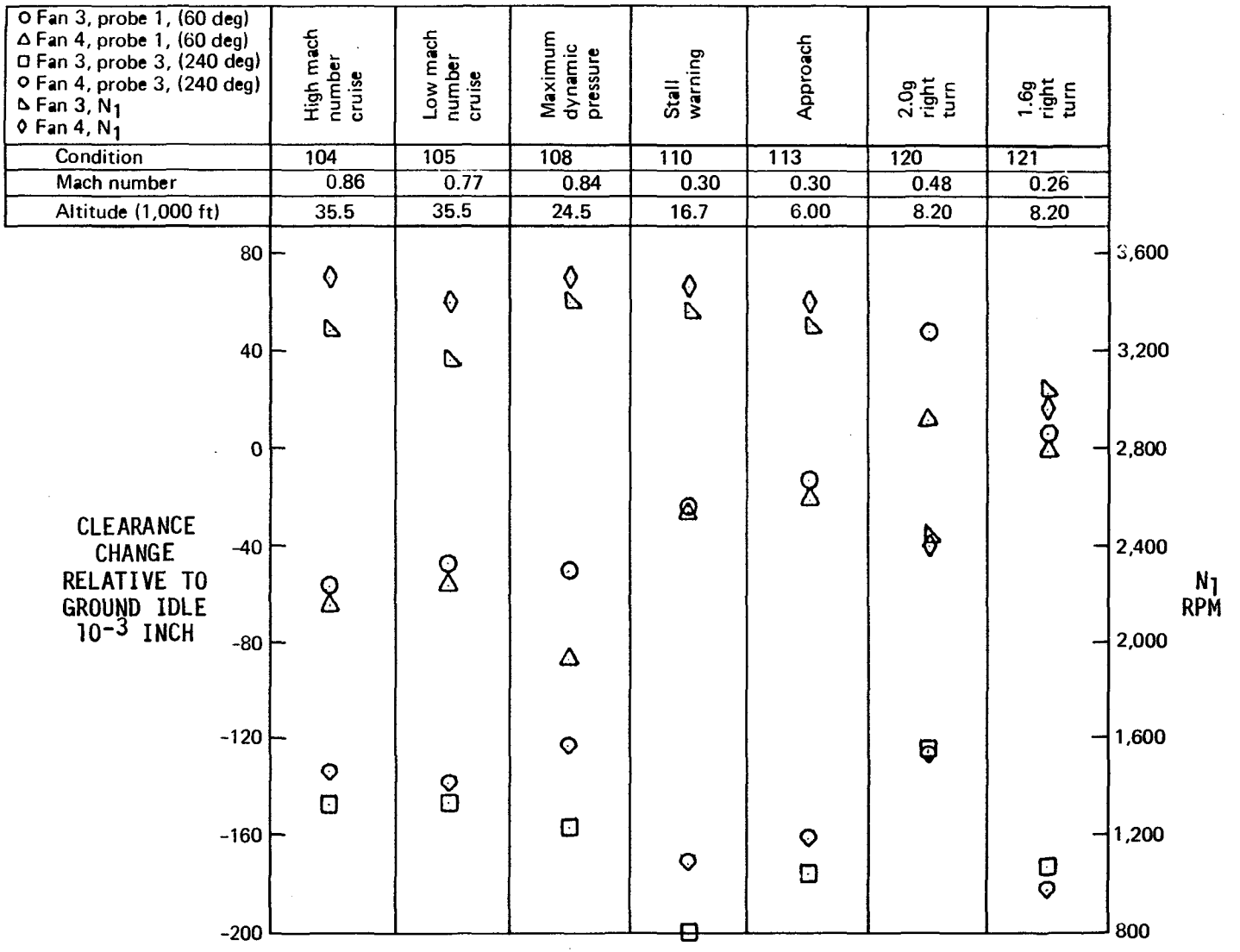

Figure 5-11 Comparison of Fan Clearance Change versus Engine Position Under Several Steady State Conditions - The influence of engine position on fan clearance change during a variety of flight conditions is negligible.

The change in static blade-to-seal clearance in the assembled fan of the position number 3 engine was 0.062 inch, based on feeler gage measurements around the circumference at the beginning and end of the program.

Outer air seal rubs were monitored throughout the program by two methods. With the first method, the outer air-seal rub shoes in the two test fans were sprayed with a red dye before each test flight. Rub patterns were then observed (Figure 5-12) after the flight to identify the location and depth of rubs. The rubs observed after each of the five test flights are summarized in Figure 5-6. Note that in test flights one through four, where the take-off is the dominant flight load condition, the rub patterns on the inboard (number 3) and outboard (number 4) engines are quite similar. In the fifth test flight, the rubs in the upper left hand quadrant validate the tighter clearances measured by the laser probe in that quadrant during the maximum dynamic pressure portion of the flight (condition 108).

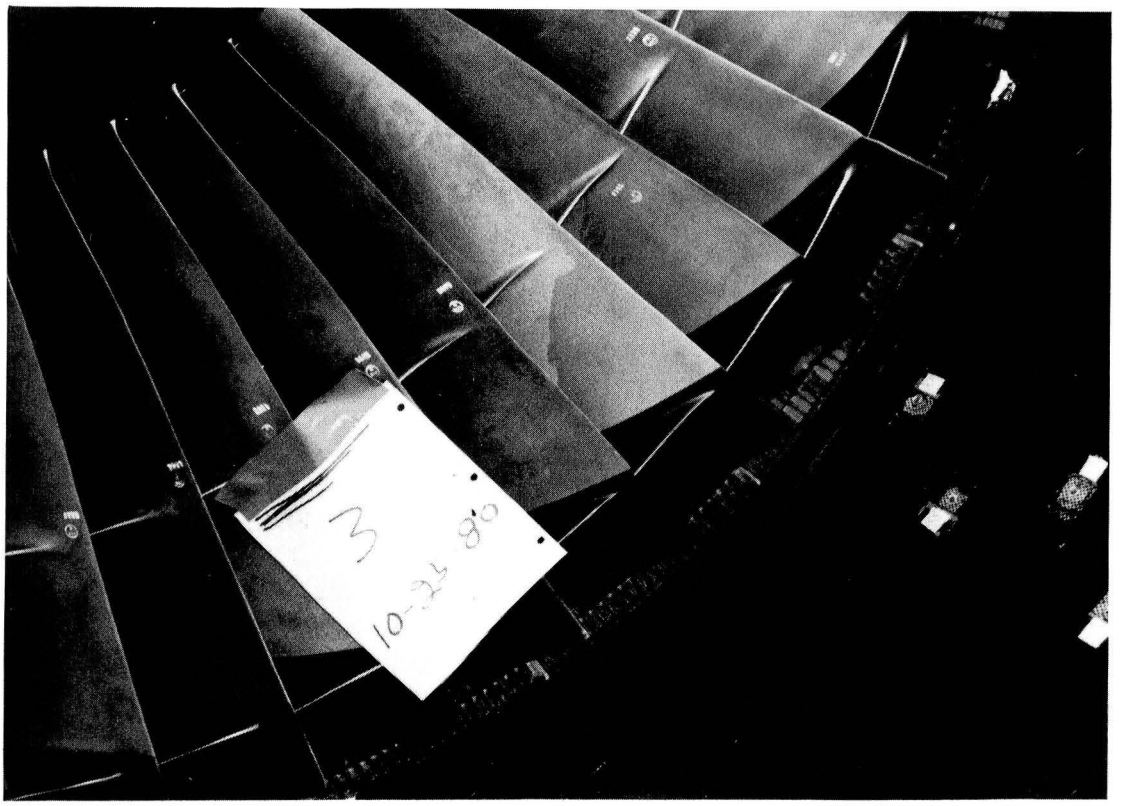

Figure 5-12 Visualization of Fan Rubs - Red dye sprayed on the fan outer air-seal shoes prior to each test flight permitted easy location of rubbed areas. (Boeing, FA-123468)

In addition, fan rub depth measurements were made after each test flight by recording the depth of eight equally-spaced predrilled holes in the rub shoes. With progressive wear, the depths of the holes decrease. The incremental and cumulative average outer air-seal wear after each test flight, as computed from these hole depth measurements, is listed on Table 5-II.

The average rub-strip wear based on post-test analytical teardown measurements was 0.057 inch at the center of the rub.

Comparison of pretest and post-test sample blade inspections showed no loss of blade length, leading edge shape, or surface roughness.

Using the above inspection results, an average blade-to-seal clearance increase of 0.057 inch was assumed, and the fan efficiency and flow capacity changes were computed. The results of this analysis are presented in Section 5.5

5.2.4 Comparison with Previous Test

Similar fan clearance closure patterns were seen in the Flight Loads Test and in the previous "Simulated Aerodynamic Loads Test", thus indicating that the direction and magnitude of the simulated loads were reasonable. This can be seen in Figure 5-13 on which is plotted the clearance closures of the four fan probe locations during a real and sumulated take-off sequence. Flight Condition 101-1 was used in this comparison. The close agreement between the simulated and actual fan clearance closures validates the use of the low- and high-pressure compressor clearance closure data in refining the analytical model.

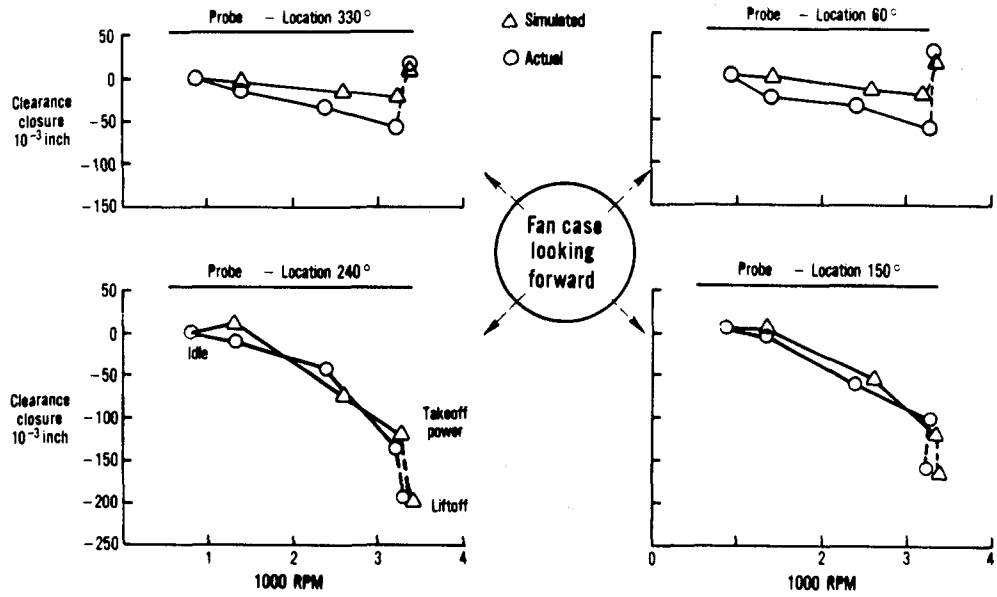

Figure 5-13 Comparison of Flight Loads Test Data with Simulated Aerodynamic Loads Test Data - The comparison of data taken under comparable loading conditions shows good agreement. (J24873-10)

5.3 HIGH-PRESSURE TURBINE EFFECTS

5.3.1 Summary of High-Pressure Turbine Effects

Tight running clearances and local rubs occurred in the high-pressure turbine during four test conditions. During simulated revenue service, minimum clearance occurred during climb. It also occurred during stall warning and high G simulated avoidance maneuvers. Both of these conditions combined moderate aerodynamic load and long time, high-power operation of the engine. However, the tightest high-pressure turbine running-clearance condition occurred during extended high power operation on the ground which was run prior to the flight test and is not representative of either production acceptance testing or revenue service. At all times in this program, the pinch occurred in the lower right quadrant as it did during the prior Simulated Aerodynamic Loads Test program.

High-pressure turbine clearance closures are the combined effect of axisymmetric closures and asymmetric closures, see Figure 5-2. Analysis of the data established that rotor speed-induced centrifugal force and thrust-induced "backbone" bending are nearly instantaneous clearance change effects following a power change. Thermal expansion of blades, seals, cases, and disks are time and power-level dependent contributors to clearance closure. Finally, inertia- and aerodynamic load-induced asymmetric closures will further pinch the turbine running clearances. Section 5.3.2 discusses the magnitude and timing of power-induced and flight load-induced closure and their combined effect on turbine running clearances.

5.3.2 Measured Clearance Closures

5.3.2.1 Power Effects

Power effects on turbine clearance include the centrifugal force induced rotor/blade assembly expansion due to rotor speed; thermal expansion effect of rotating and static parts due to gas temperature; and the backbone bending effect due to thrust load.

These various power effects on high-pressure turbine running clearances are seen in Figure 5-14 which is a plot of the measured clearance changes at four probe locations during a high power ground calibration starting at a stabilized ground idle condition. The plot shows the transient and steady state effects of power induced loads on running clearances in the high-pressure turbine.

Power level is represented by high-pressure rotor speed. From stabilized idle, the engine was accelerated in two steps, at 115 seconds and at 360 seconds. The symbols on Figure 5-14 show the measured changes in clearances at the four probe locations. The solid line represents the computed axisymmetric clearance change based on the four readings. Axisymmetric clearance change is caused by the centrifugal and thermal expansion of the rotating parts and the uniform thermal expansion of the case. The calculated thrust-induced

asymmetric closure effects on clearance at the top and the bottom of the engine are shown by the dashed lines. The difference between the dashed lines and the plotted symbols is the asymmetric case clearance change due to nonuniform thermal effects.

The magnitude and timing of these various effects is shown in Figure 5-14. The initial effect of the acceleration at 115 seconds is an axisymmetrical closure due to centrifugal forces. The net effect of thermal expansion of the blade and case then increases the axisymmetrical clearance. Concurrently, as thrust is increased, the backbone bending effect asymmetrically closes the clearance at the bottom of the engine and opens the clearance at the top as illustrated by the spread between symbols on the figure. The thermal expansion of the disk is seen next as it causes a slower axisymmetrical closure which was still in progress when the engine power level was increased again at 360 seconds. The immediate effects of this acceleration are additional closures induced by centrifugal load and backbone bending load. These closures are followed by additional disk expansion which continues out to the end of the test run when clearances have nearly stabilized.

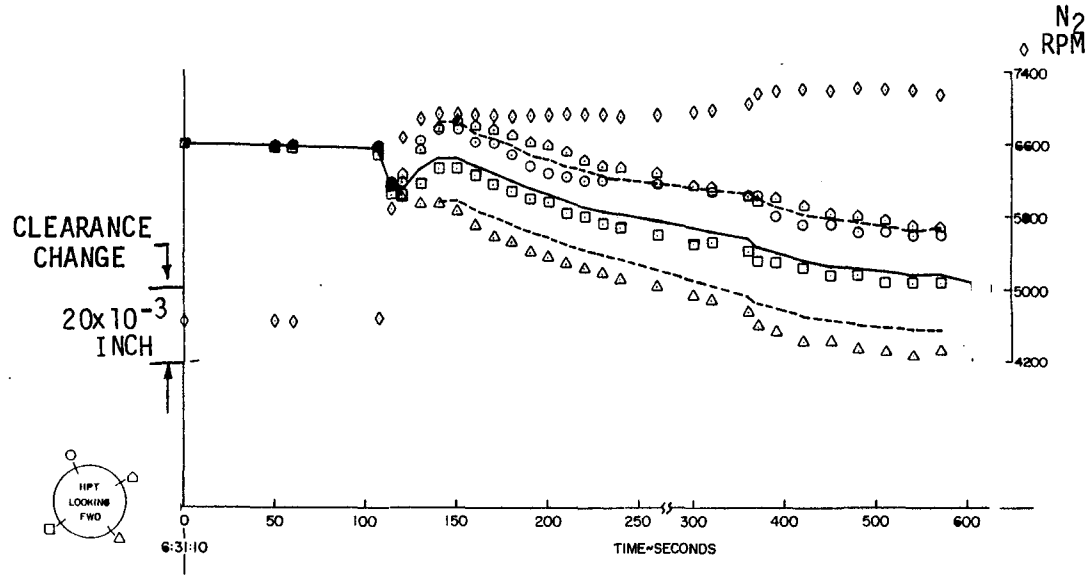

Figure 5-14 Effects on High-Pressure Turbine Clearance due to Power-Induced Take-Off Loads (Condition 101-1) - Both axisymmetric and asymmetric closures increased with increasing power setting.

As can be seen on the figure, the nonuniform thermal load-induced closure appears to increase with power level, with maximum closure occurring in the lower right hand quadrant of the engine.

This was an extreme case where the engine was stabilized at a power level greater than take-off power. The case was chosen because it best illustrates the various power-induced effects on the first-stage

high-pressure turbine clearance closure. It illustrates the risk of turbine rubs incurred by running at high power on the ground for an extended period and allowing the combination of maximum thermal and maximum thrust-induced closure to occur simultaneously.

The power-induced clearance closures typical of acceptance flight and other flight load test conditions are listed on Table 5-IV, relative to stabilized ground idle, for the 180-degree location (bottom center of the engine). The numbers presented in this table are a combination of measured and computed values. Column 1 lists the axisymmetric closures at each test condition and is the algebraic average of the four measured changes, relative to ground idle. Column 2 presents the asymmetric closure due to the thrust-induced backbone bending. This closure is a computed value that is proportional to estimated thrust. The previously developed analytical model used for predicting the effect of backbone bending on turbine closure was validated by measurements made in this program in those cases where the thrust effect could be isolated.

Column 6 presents the total clearance closure. This value was computed from the measured values at the 142-degree and 231-degree probe locations.

Column 5 lists the asymmetric closure due to flight loads. These values were computed with a previously developed analytical model which was validated by the measured values from this program.

Column 4 lists the estimated total power load-induced closures at each flight condition. Column 4 is the difference between Columns 5 and 6.

Column 3 lists the asymmetric thermal load-induced clearance change. It represents the net value of thermally induced, asymmetric dimensional changes in the case, shifts in the rotor centerline relative to the case, and errors in the other factors. It was computed as the difference between Column 4 and the sum of Columns 1 and 2.

The first take-off of the Flight Loads Test program (Condition 101-1) is not typical since it immediately followed the ground run shown on Figure 5-14 and resulted in the high initial thermal closure, hence a much higher than normal total closure. The second and third take-offs are more representative of normal conditions. The 780,000-pound take-off was simulated by a 1.3-G pull-up executed one minute after lift-off at 710,000 pounds; hence, the thermal conditions are between normal take-off and the low-climb condition.

Conditions 102 through 115 cover the flight acceptance test. Conditions 116 through 121 cover the simulated avoidance maneuvers. Note that the right turns were executed at lower power settings on the position number 3 engine and resulted in lower power-induced closures.

As can be seen on Table 5-IV, power-induced closure is a function of instantaneous power level (thrust load and speed effects) and the immediate past history of power levels (thermal expansion effects). Thus, in the normal revenue flight, climb and high Mach number cruise

TABLE 5-IV

POSITION NUMBER 3 HIGH-PRESSURE TURBINE CLEARANCE CLOSURES (INCH) RELATIVE TO GROUND IDLE AT 180-DEGREE CIRCUMFERENTIAL LOCATION

Flight Condition		Estimated Thrust	Power Induced Closure				Flight Loads	Measured Total
			Axisymmetric	Asymmetric		Estimated		
Description	Number	(pounds)	(Speed + Thermal)	(Thrust Load)	(Thermal Load)	Total	Closure	Closure
612,000 lb Take-Off with 20° Flaps	101-1	32,000	-0.036	-0.010	+0.002	-0.044	-0.007	-0.051
538,000 lb Take-Off with 10° Flaps	101-2	31,000	-0.004	-0.009	+0.002	-0.011	-0.008	-0.019
647,000 lb Take-Off with 10° Flaps	101-3	30,000	-0.005	-0.009	0.000	-0.014	-0.009	-0.025
780,000 lb Take-Off with 10° Flaps (Simulated)	118	31,000	-0.016	-0.009	+0.002	-0.023	-0.009	-0.032
Low-Climb	102	25,000	-0.026	-0.007	-0.004	-0.037	-0.004	-0.041
Pinch Point		20,000	-0.031	-0.006	-0.005	-0.042	-0.004	-0.046
Mid-Climb	103	18,000	-0.031	-0.005	-0.001	-0.037	-0.003	-0.040
High Mach Number Cruise	104	9,000	-0.030	-0.003	-0.001	-0.034	-0.001	-0.035
Low Mach Number Cruise	105	8,000	0.024	-0.002	-0.004	-0.030	-0.002	-0.032
Maximum Mach Number Flight	106	9,000	-0.026	-0.003	-0.003	-0.032	0.000	-0.032
In-Flight Relight	107	5,000	-0.039	-0.002	+0.001	-0.040	-0.002	-0.042
Maximum Dynamic Pressure Flight	108	14,000	-0.036	-0.004	-0.003	0.043	+0.002	-0.041
Stall Warning with Flaps Up	109	17,000	-0.028	-0.005	+0.004	-0.029	-0.005	-0.034
Stall Warning with 10° Flaps	110	20,000	-0.029	-0.006	+0.003	-0.032	-0.006	-0.038
Stall Warning with 30° Flaps	111	20,000	-0.037	-0.006	0.000	-0.043	-0.004	-0.047
Idle Descent	112	0	0.000	0.000	+0.004	+0.004	-0.002	+0.002
Approach	113	27,000	-0.022	-0.008	-0.001	-0.031	-0.004	-0.035
Touch and Go	114	34,000	-0.025	-0.010	+0.002	-0.033	-0.005	-0.038
Thrust Reverse	115	26,000	-0.034	-0.008	-0.001	-0.043	0.000	-0.043
2.0-G Left Turn with Flaps Up	116	22,000	-0.033	-0.007	-0.001	-0.041	-0.005	-0.046
1.6-G Left Turn with 30° Flaps	117	25,000	-0.031	-0.008	+0.002	-0.037	-0.006	-0.043
2.0-G Right Turn with Flaps Up	120	8,000	-0.019	-0.003	-0.002	-0.024	-0.005	-0.029
1.6-G Right Turn with 30° Flaps	121	21,000	-0.025	-0.006	+0.001	-0.030	-0.006	-0.036
Airplane Stall	123	26,000	-0.031	-0.008	+0.002	-0.037	-0.007	-0.044
Hard Landing		20,000	-0.024	-0.006	-0.004	-0.034	0.000	-0.020
Ground Calibration		48,000	-0.036	-0.014	+0.002	-0.048	0.000	-0.048

Note: Negative values of closure may be interpreted as reduced clearance and increased chance of rubs.

represent the conditions of maximum power-induced closure. The axisymmetric and asymmetric clearance closures typical of take-off and climb are shown on Figure 5-15. The minimum clearance pinch occurred about 200 seconds into the climb.

Conditions 107, 111, and 115 show the maximum power-induced closures of the flight test data. These three cases are examples of varying degrees of severity of the problem of hot-rotor deceleration followed by acceleration, which was identified as a severe problem in the report on Performance Deterioration Based on In-Service Engine Data (Reference 2). In these cases, after the engine has been running at high power level for some time, with all components thermally expanded, a rapid deceleration is executed to a low power or shutdown. This action results in thrust and centrifugal loads being removed immediately, causing clearances to open. Then, as the components cool, there is an initial closing of clearances due to the faster cooling rate of the case compared to the blade-and-disk assembly. If the engine is again accelerated to power before the disk cools sufficiently, the closing effect due to centrifugal and thrust forces will close the clearances to a value that is less than the steady state value prior to shutdown. This was the scenario during the in-flight relight (Condition 107, Figure 5-16), stall warning (Condition 111, Figure 5-17), and thrust reverse (Condition 115, Figure 5-18) where the clearances listed on Table 5-IV were measured after the engine acceleration.

5.3.2.2 Flight Loads Effects

Aerodynamic loads are the predominant flight loads. Aerodynamic loads are steady and quasi-steady loads applied to the engine inlet by the inlet air stream and, in turn, cause deflection of the fan, compressor, and turbine cases. During the flight test, the upward aerodynamic load on the fan inlet during take-off and other high angle of attack operation caused clearance closure at the bottom and clearance opening at the top of the high-pressure turbine, but to a lesser extent than in the fan.

The addition of this flight load-induced closure to the power-induced axisymmetric and asymmetric closures resulted in a large closure in the high-pressure turbine during initial climb from take-off. Thus, maximum clearance closure in a typical revenue flight occurs following take-off. This result is shown in Figure 5-15A on which is plotted the measured high-pressure turbine clearance closures during a take-off and climb (test Conditions 101-2 and 102).

On Figure 5-16A, the plot of data from the 231-degree probe location ([ ]) is an approximation since that probe was not functioning during this take-off (Condition 101-2). The axisymmetric closure during acceleration, take-off roll, and climb is shown as the upper bold line on Figure 5-15B. It includes centrifugal and thermal effects on the disk and blades plus uniform thermal expansion of the case.

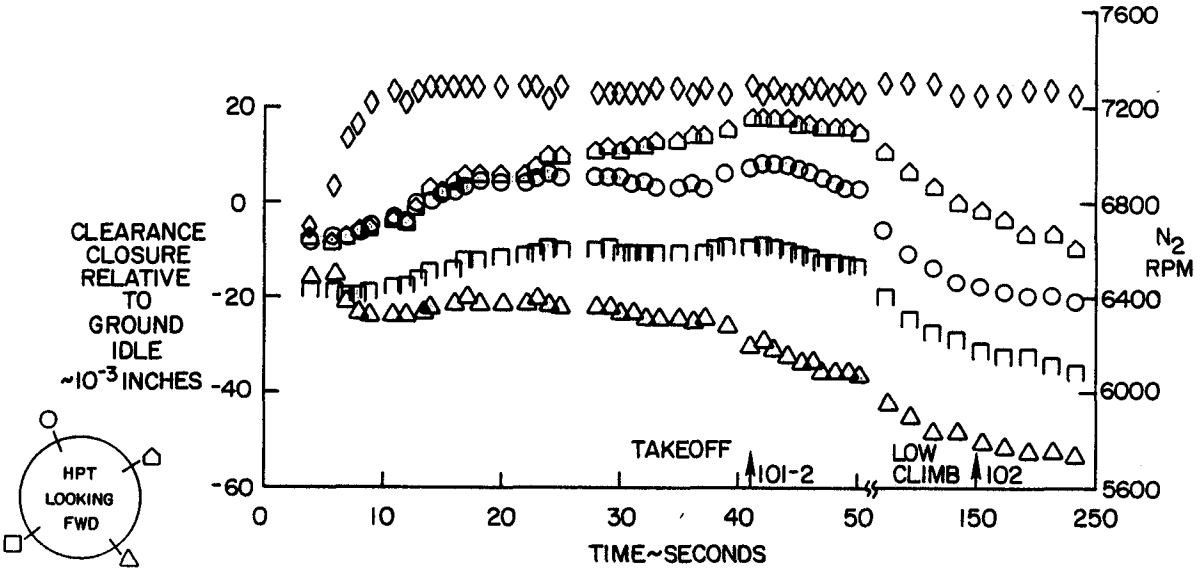

A

⊓ = ESTIMATED VALUES FOR □.

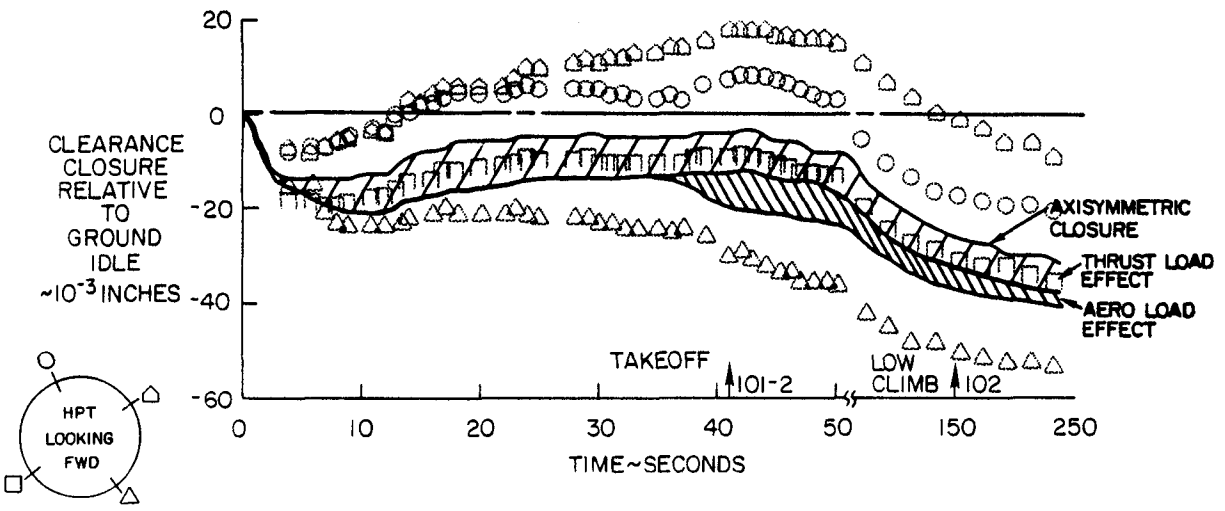

B

Figure 5-15 Axisymmetric and Asymmetric Clearance Closures During Typical Take-Off and Climb - The minimum clearance pinch occurred about 200 seconds into the climb.

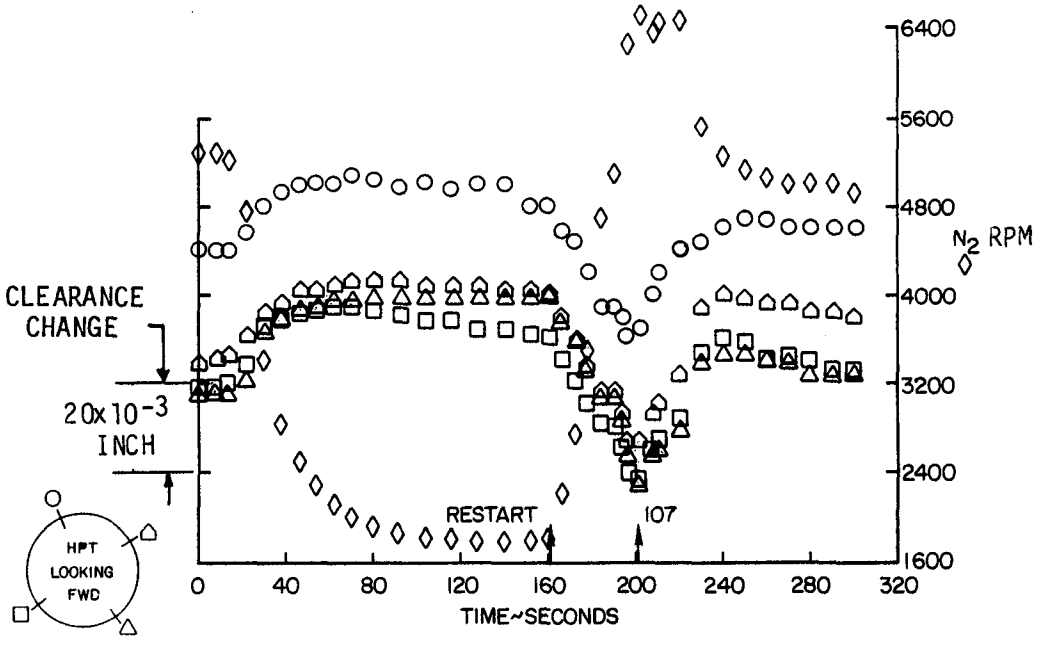

Figure 5-16 Change in High-Pressure Turbine Running Clearance During the In-Flight Shutdown and Restart (Condition 107) - Quick restart of an engine with a hot rotor can result in significant clearance closure.

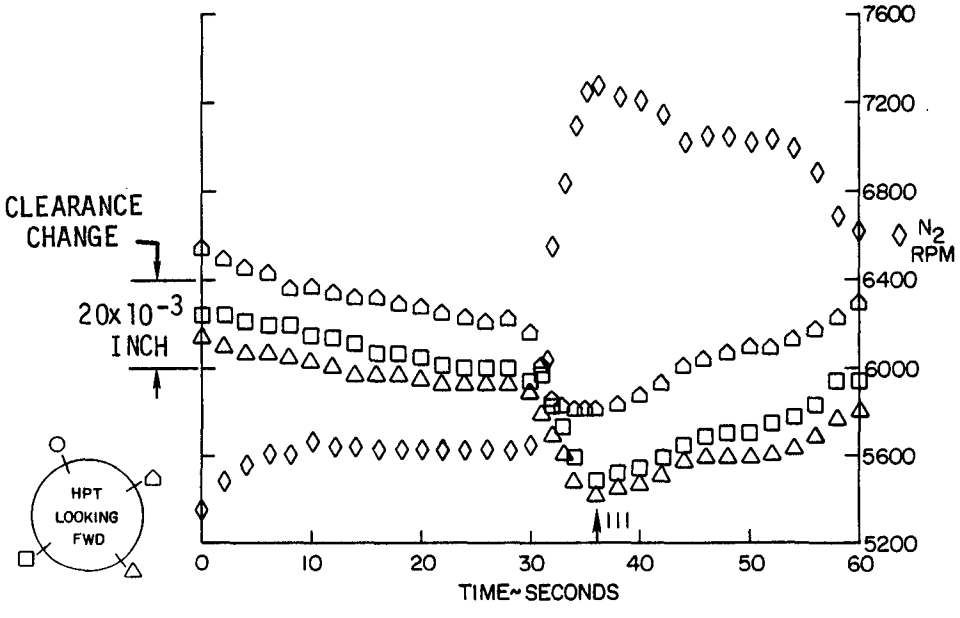

Figure 5-17 Change in High-Pressure Turbine Running Clearance During the Stall Warning (Condition 111) - Quick acceleration of an engine with a hot rotor can result in significant clearance closure.

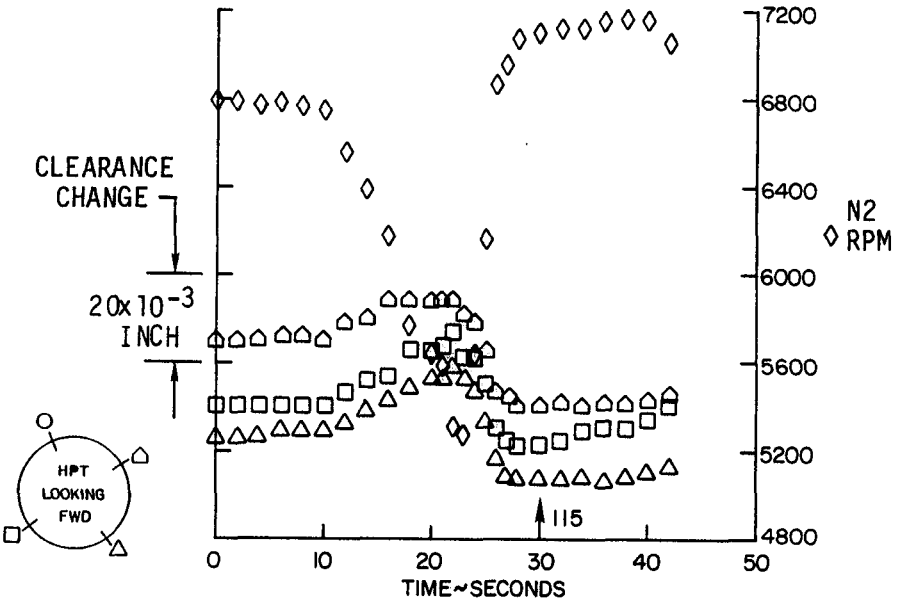

Figure 5-18 Change in High-Pressure Turbine Running Clearance During Thrust Reversal (Condition 115) - Quick acceleration of an engine with a hot rotor can result in significant clearance closure.

The additional asymmmetric closure (thrust load effect), based on NASTRAN analysis, is shown as the next band. Note that this effect decreases with increasing flight speed due to the thrust lapse rate. The lower shaded band on the figure represents the effect of aerodynamic load-induced closure at the bottom of the turbine case. This closure is a maximum at lift-off and decreases during climb due to the reduced angle of attack. The bottom of these bands represents the predicted clearance closure based on actual axisymmetric closure and NASTRAN calculated load effects with equilibrium occurring about four minutes after acceleration to take-off power. The difference between this closure and the measured probe readings (shown as data points) is due to a nonuniform thermal expansion in the high-pressure turbine case.

The net effect is small at take-off since the rapid thermal expansion of the case tends to open rather than close clearances as seen on Figure 5-15B. After 200 seconds of climb power, the disk has absorbed sufficient heat to complete its thermal expansion.

The asymmetric closure is caused by thrust-induced backbone bending, aerodynamic load-induced bending forces on the high-pressure turbine case, and nonuniform thermal expansion of that case. Thrust is a

maximum at the start of take-off roll and decreases continually as speed is increased; thus, the backbone bending force decreases with increasing airplane speed. Aerodynamic closure is a maximum at take-off rotation and decreases as the airplane climbs and the angle of attack is reduced. Finally, the nonuniform thermal expansion of the high-pressure turbine case is represented by the difference between the measured closures at the two lower proximity probes, Figure 5-15, and the sum of the computed axisymmetric and asymmetric closures. This time-temperature-dimensional change effect is being evaluated further in the Additional Ground Testing program.

The high-pressure turbine clearance closures measured at climb were such that they would have caused a rub of 0.004 to 0.005 inch had the turbine not rubbed during the prior ground run. This rub was considered in the performance deterioration modeling. High-pressure turbine closures during the remaining flight test conditions simulating revenue service were such that they would not have caused additional high-pressure turbine rubs.

During other flight conditions, as with the fan, the maximum flight load-induced closures in the high-pressure turbine occurred during conditions where the airplane was operating at a high angle of attack combined with a high level of power. These conditions included the stall warnings (Conditions 109, 110, and 111) where a high angle of attack and low power was used to induce the stall warning then, at the signal, power was applied rapidly and the airplane was nosed over slightly. As seen in Figure 5-17, the maximum closure occurs at the end of the acceleration when both power and angle of attack were high.

The high-G turn, avoidance maneuver (Conditions 116, 117, and 121) and the actual airplane stall (Condition 123) also combined high angle of attack, due to the maneuver and high power level. These maneuvers also combined with high power loads resulting in pinch point conditions.

The approach (Condition 113) and touch and go (Condition 114) test conditions show aerodynamic flight load effects also. These effects also are due to the combined effect of angle of attack and power level. Note that for the touch and go the data point was recorded following the rotation and, hence, was similar to take-off.

Data for the remaining test conditions were taken during level flight, and the flight load effects were insignificant.

5.3.3 Inspection Results

The estimated performance deterioration of the flight test engine (P-662204), based on the before and after measurements, is a -1.65 percent high-pressure turbine efficiency change, a -0.02 percent low-pressure turbine efficiency change and a 0.61 percent increase in the high-pressure turbine flow parameter. The increase in tip clearance on the first-stage blade accounts for most of the high-pressure turbine efficiency deterioration.

The high-pressure turbine rub-induced wear was much greater than that which is representative of acceptance testing and typical revenue service for two reasons: 1) the first-stage was assembled with outer air seal clearances that were 0.008 inch tighter than normal; 2) the preflight ground tests, the first of which was run for an extended time period, resulted in extensive thermal expansion-induced closure and, hence, blade/seal rubs.

First-Stage Blade Tip

The diametral tape measurements showed a nonuniform wear across the blade tip which averaged 0.022 inch.

First-Stage Outer Air Seal

A rub spanning a 70-degree arc, with a maximum depth of 0.020 inch, did occur in the lower right hand quardrant.

Second-Stage Blade Tip Knife Edge Wear

The diametral tape measurements show that the knife edge incurred an average radial wear of 0.002 inch.

Second-Stage Outer Air Seal

The groove depth measurements show an average wear depth of 0.025 inch and 0.026 inch on the front and rear seal lands, respectively.

Second-Stage Vane Inner Diameter Twisting

Vane inner diameter twisting was evaluated by measuring the change in the axial distance between the vane inner feet (see Figure 5-19). Based on the before and after measurements on 15 vanes, the axial distance increased an average of 0.0022 inch. The Simpson's rule measurement also showed the twisting of the inner-diameter portion of the vane (see Figure 5-20).

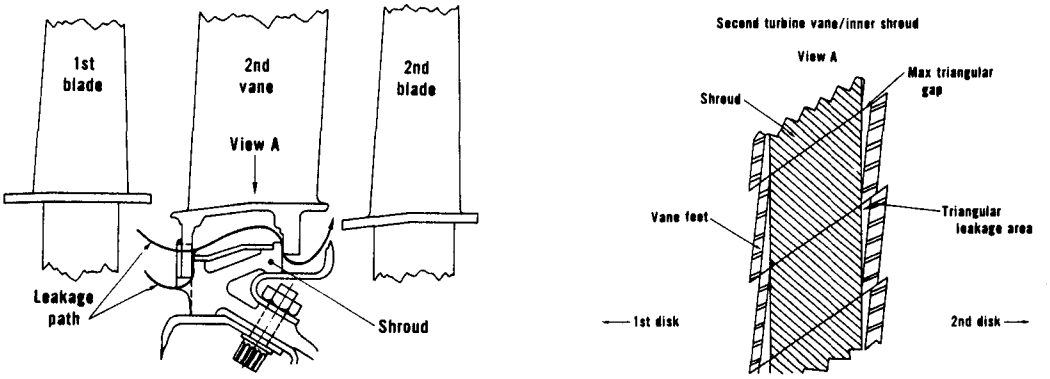

Figure 5-19 Configuration of High-Pressure Turbine Second-Stage Vane Assembly - Vane twisting causes leakage paths.

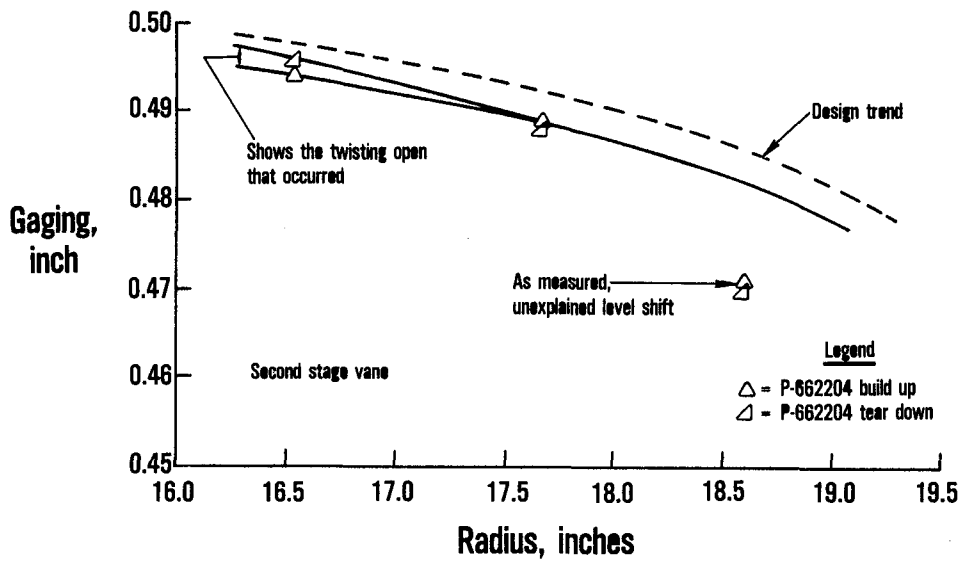

Figure 5-20 Comparison of Methods of Vane Twist Measurements - Simpson's Rule results is in good agreement with measurement of the change in axial distance between the vane inner feet.

Estimated Performance Deterioration

The calculated turbine performance changes that result from the hardware measurements are as follows:

Item	Efficiency Change (points) High-Pressure Turbine	Efficiency Change (points) Low-Pressure Turbine	Station 5 Flow Parameter Change (%)
First-Stage Blade to Outer Air Seal:			
ΔGap = 0.026 inch	-0.98	0	+0.57
Second-Stage Blade Knife Edge:			
ΔGap = 0.002 inch	-0.04	-0.02	0
Second-Stage Vane ID Twist:			
ΔGap = 0.0022 inch	-0.13	0	+0.04
Second-Stage Outer Air Seal Grooves:			
ΔGap = 0.025 inch	-0.50	-0.20	0
Total	-1.65	-0.22	+0.61

These efficiency and flow parameter changes are used in a performance evaluation (based on hardware inspection), and the results are presented in Section 5.5.

5.3.4 Comparison with Prior Test

Power load-induced turbine clearance closures measured during this program showed good agreement with the comparable closures measured during the Simulated Aerodynamic Loads Test program (Reference 6). Figure 5-21 compares the clearance closures at the four probes as measured in both programs. Note that clearance closure is plotted as a function of low-pressure rotor speed since it is more representative of thrust.

Wear patterns observed after disassembly of the turbines used in the two test programs also show similarity. Both engines showed the predominant rub in the first-stage outer air seal in the lower right quadrant with a kiss in the lower left quadrant (see Figure 5-22).

In the second-stage high-pressure turbine outer air seal, a 360-degree rub occurred on both lands on the flight test engine while the rub was limited to 270 degrees on th simulated flight test engine (see Figure 5-23).

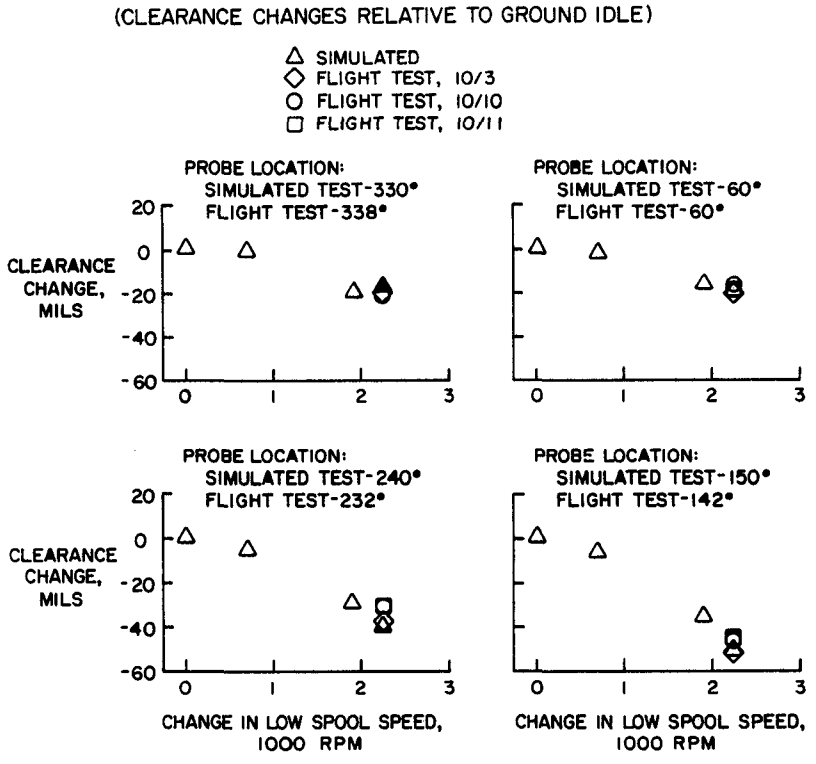

Figure 5-21 Comparison of Flight Loads Test Data with Simulated Aerodynamic Loads Test Data - The comparison of comparable closure data shows good agreement.

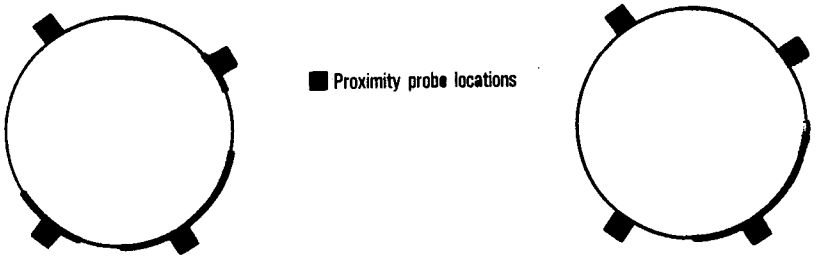

A. Simulated Aerodynamic Loads Test

Engine P-662211

B. Flight Loads Test

Engine P-662204

Figure 5-22 Comparison of Teardown Wear Patterns in the First-Stage High-Pressure Turbine Outer Air Seals (Rear View) - Both engines incurred rubs in the lower right quadrant.

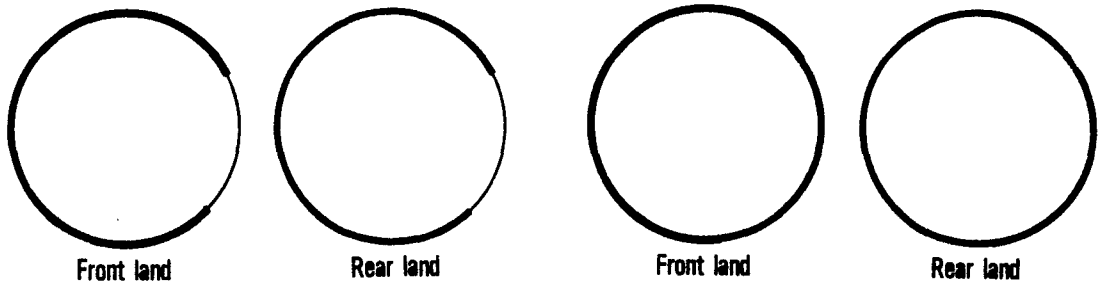

A. Simulated Aerodynamic Loads Test

Engine P-662211

B. Flight Loads Test

Engine P-662204

Figure 5-23 Comparison of Teardown Wear Patterns in the Second-Stage High-Pressure Turbine Outer Air Seals (Rear View) - The flight test engine incurred a full 360-degree rub while the rub was limited to 270 degrees on the simulated loads test engine.

A comparison of the high-pressure turbine blade tip/knife edge wear for the Flight Loads Test engine, P-662204, and the Simulated Aerodynamic Loads Test engine, P-662211, is given in the tabulation below.

Item	Simulated Aerodynamic Test Engine Value (inch)	Flight Test Engine Value (inch)
First-Stage Blade Tip Wear	0.010	0.022
First-Stage Outer Air Seal Wear	0.002	0.004
First-Stage Blade Build Clearance (Blueprint = 0.073 ± 0.006 inch	0.073	0.066
Second-Stage Blade Knife Edge Wear	0.004	0.002
Second-Stage Outer Air Seal Rub	0.036	0.025

5.4 DYNAMIC LOADS EVALUATION

During flight, the engine is subjected to three types of loads. Normal flight at constant thrust, altitude, and heading subjects the engine to steady state loads. During a thrust change or controlled maneuver, quasi-steady state (slowly changing) loads are imposed on the engine. Dynamic loads on the engine result during a sudden inertia load such as that caused by a significant vertical gust or a hard landing. The effects of such dynamic loading on the JT9D engine were investigated during an analytical study conducted as part of the third phase of the Engine Diagnostics Program. The results of this study, presented in Reference 5, included a prediction that an insignificant level of JT9D-7 engine performance deterioration would occur as a result of a vertical gust encounter. The hard landing case was more complex, and a firm quantitative estimate of the extent of rub damage could not be analytically determined. Therefore, the hard landing case was added to this Flight Loads Test program to experimentally measure the effect of a hard landing on fan and high-pressure turbine running clearances and engine performance.

The hard landing was conducted at the end of the fourth test flight at an estimated sink rate of 5 feet/second, which is about double the normal sink rate, and an airplane gross weight of 690,000 pounds. Both approach power level and airplane angle of attack were greater than normal due to the high gross weight. Hence, the resulting aerodynamic plus thrust load-induced fan clearance closure was much greater than normal for the landing approach. At touch down, fan clearance closed an additional 0.015 inch, then opened when the engines were throttled back prior to thrust reversal (see Figure 5-24). The tightest fan clearance was equal to that at maximum gross weight take-off. There were no sharp changes in laser-monitored fan blade tip clearance at the time of touch down. Neither were there any marks in the fan rub strip to indicate sudden impact with the fan blades.

High-pressure turbine laser measured running clearance, as shown in Figure 5-25, also indicated no sudden clearance closure at touch down. High-pressure turbine running clearance (see Figure 5-25) indicated no additional clearance closure at touch down. The net result was that the high sink rate landing had small effect on fan clearance and no effect on turbine clearance. The combined result of aerodynamic forces and impact force would be even less in a high sink rate landing of a revenue service airplane where landing gross weights would not exceed 600,000 pounds.

Since the measured clearance closures were small and Boeing-measured loads were small, no further dynamic analyses were conducted.

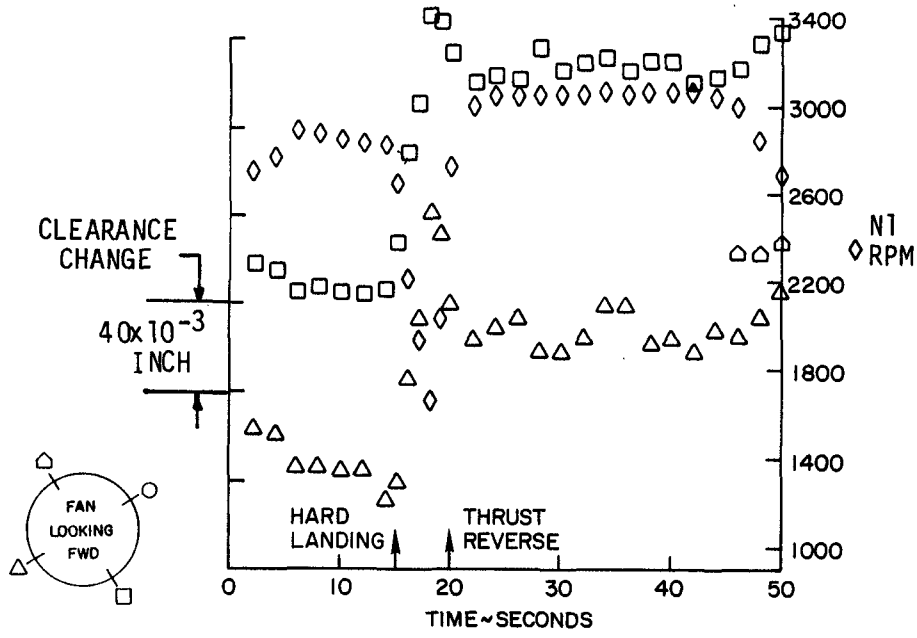

Figure 5-24 Effect of a Hard Landing on Fan Clearance - The landing at a 5 feet/second sink rate and 690,000-pound gross weight had only a small effect on clearance in the fan of the position number 3 engine.

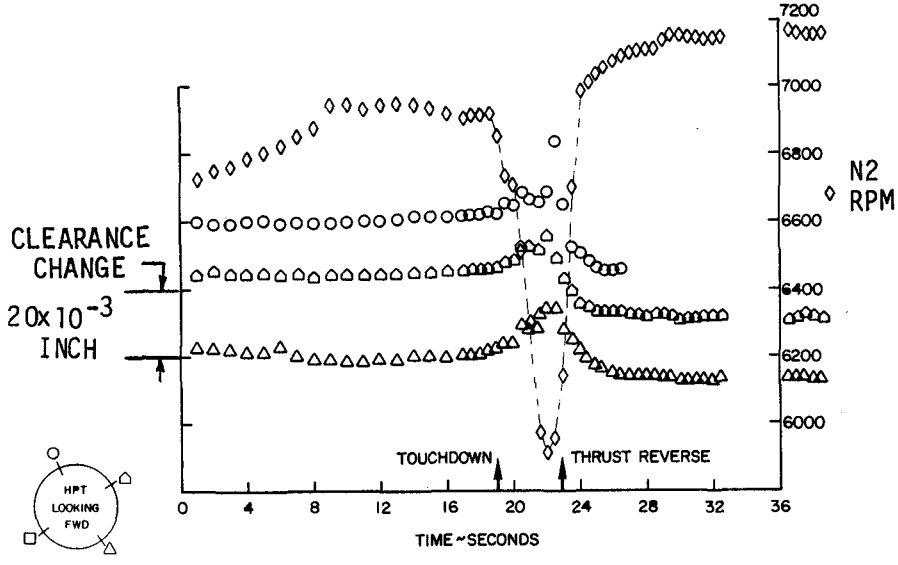

Figure 5-25 Effect of a Hard Landing on High-Pressure Turbine Clearance - The landing at a 5 feet/second sink rate and 690,000-pound gross weight had no effect on clearance in the high-pressure turbine of the position number 3 engine.

5.5 PERFORMANCE ANALYSIS RESULTS

The loss in engine performance was a 0.75 percent increase in thrust specific fuel consumption (TSFC) between the preflight-test base-line calibration and the postflight-test calibrations. This loss was primarily due to a decrease in high-pressure turbine efficiency with smaller losses in the fan efficiency and flow capacity. The performance deterioration appears to have occurred prior to the preflight-test installed calibration.

5.5.1 Summary of Performance Analysis

The test stand calibrations and the installed static calibrations of the engine are summarized in Table 5-V. The preflight-test calibration was run in June, 1980 in the Pratt & Whitney Aircraft test facility in Middletown, Connecticut, and the first installed calibration was run on October 3, 1980 at Boeing Field, Washington. After this calibration was run, it was learned that air was inadvertently being bled from the engine so that these data were of no use in deterioration analyses.

A successful initial installed calibration (1-2) was run at Glasgow, Montana following the ferry flight to that facility. The second calibration followed the acceptance test flight. The third calibration followed the third test flight which included a 647,000-pound take-off with 10-degree flaps and high-G avoidance turns. The fourth calibration followed the fifth test flight and the completion of the NASA Flight Test program. The fifth installed calibration was run at the completion of the companion flight test program to identify any additional performance loss and provide a better comparison with the post-test uninstalled calibrations. The aircraft was then ferried back to Boeing Field for engine removal in November, 1980. Postflight-test calibrations were made in Middletown in January, 1981. Calibration A was run with the engine as-received, while calibration B was run after an engine vane control (EVC) check and washing of the fan blades.

A summary of the test stand and installed calibration data (Figure 5-26) shows that most of the performance deterioration occurred between the preflight test-stand calibration and installed ground calibration 1-2. A 5°C increase in turbine exhaust gas temperature (EGT, TT7) at constant engine pressure ratio (EPR) is indicated for calibration 1-2 and for all the other installed calibrations, within experimental accuracy. The postflight test-stand calibrations agree with the installed data within about 1°C. Note that the test stand data were adjusted for the change from the test stand environment and hardware to the outdoor nacelle installation, based on previously established indoor/outdoor corrections.

TABLE 5-V

ENGINE TEST AND CALIBRATION SEQUENCE

Calibration No.	Type of Test	Location	Date
	Preliminary Uninstalled Calibration	Middletown, Conn. P-2 Test Stand	06-24-80
1-1	Installed Calibration (Voided due to inadvertent engine bleeds)	Boeing Field	10-03-80
	Functional Flight with Reduced Power on Test Engine	Seattle, Wash.	10-03-80
	Ferry Flight with Reduced Power on Test Engine	Seattle to Glasgow, Mont.	10-06-80
1-2	Installed Calibration	Glasgow, Mont.	10-10-80
	First Test Flight (Acceptance Test)	Glasgow, Mont.	10-11-80
2	Installed Calibration	Glasgow, Mont.	10-11-80
	Second Test Flight	Glasgow, Mont.	10-19-80
	Third Test Flight	Glasgow, Mont.	10-20-80
3	Installed Calibration	Glasgow, Mont.	10-20-80
	Fourth Test Flight	Glasgow, Mont.	10-25-80
	Fifth Test Flight	Glasgow, Mont.	10-25-80
4	Installed Calibration	Glasgow, Mont.	10-25-80
	Remaining JT9D-7R4 Flights	Glasgow, Mont.	11-05 to 11-07-80
5	Final Installed Calibration	Glasgow, Mont.	11-07-80
A	Postflight-Test Uninstalled As-Received Calibration	Middletown, Conn. P-5 Test Stand	01-09-81
B	Postflight-Test Uninstalled Calibration after Vane Trim	Middletown, Conn. P-5 Test Stand	01-12-81

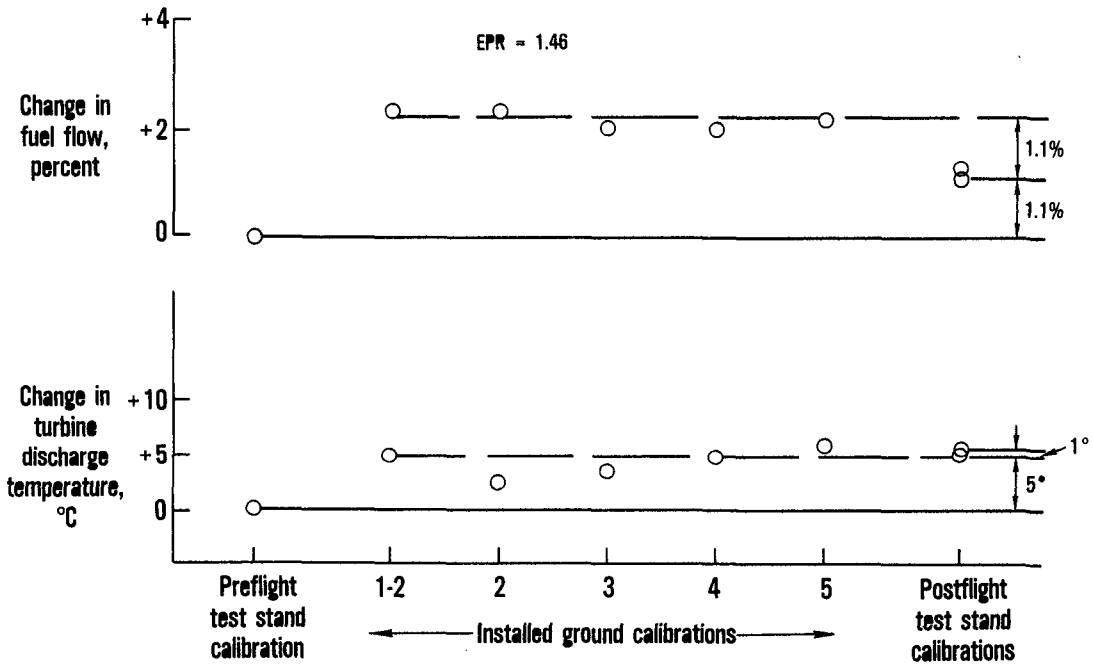

Figure 5-26 Summary of Engine Calibration Results - Most of the performance deterioration occurred between the preflight test stand calibration and the first installed ground calibration (1-2).

A fuel flow (Wf) increase at constant EPR of about 2.2 percent is indicated between the preflight test-stand calibration and installed calibration 1-2. That same fuel flow increase is apparent for all of the installed calibrations, within experimental accuracy, but a 1.1 percent decrease is indicated for the postflight test-stand calibration relative to the installed data. This 1.1 percent is attributed to instrumentation differences between the test stand and the airplane.

Because of space considerations, the test stand flow meters were not included in the airplane installation. It is concluded that only 1.1 percent of the fuel flow increase noted during the installed calibrations is due to engine deterioration.

The fuel flow and exhaust gas temperature data both indicate that most of the engine deterioration occurred between the preflight test-stand calibration and installed calibration 1-2. During this interval, calibration 1-1 (bleed open) and two reduced take-off power flights were made.

5.5.2 Preflight-Test and Postflight-Test Calibration Results

5.5.2.1 Deterioration by Module

A comparison of the postflight-test sea level calibrations with the preflight-test base-line calibration shows a deterioration of 0.75 percent in thrust specific fuel consumption at 46,000 pounds thrust (Figure 5-27). Engine data indicated a loss in overall turbine efficiency of 0.4 percentage point (Figure 5-28) which is equivalent to a 0.9 percentage point loss in high-pressure turbine efficiency when no loss is assumed for the low-pressure turbine; 0.1 percent increase in high-pressure turbine flow parameter (Figure 5-29); and a 0.3 percent loss in fan flow capacity (Figure 5-30). Changes in gas generator characteristics of the engine at high power are listed on Table 5-VI along with the estimated impacts of module deterioration on those characteristics. Only high-pressure turbine and fan deterioration were considered, since these were the only gas-path modules that were refurbished prior to this program. The other modules were high-time units and were less sensitive to rub-induced performance deterioration. Best agreement between the estimated gas generator changes and the measured changes was achieved with the 0.9 percentage point loss in high-pressure turbine efficiency, 0.1 percent increase in high-pressure turbine flow parameter, and 0.3 percent loss in fan flow capacity noted above combined with a 0.4 point loss in fan efficiency. Thus, the measured module changes, where available, and those implied by gas generator shifts are in agreement.

High-pressure turbine deterioration was responsible for most (0.5 percent) of the loss in thrust specific fuel consumption while the fan impact on thrust specific fuel consumption was smaller (0.25 percent), which is consistent with results of previous test programs as indicated in Section 5.6.2.2 below.

5.5.2.2 Comparison with Earlier Results

The comparison in Table 5-VII shows that during this program only about half of the deterioration of thrust specific fuel consumption occurred that was experienced in earlier programs. Only the fan and high-pressure turbine were refurbished prior to this Flight Loads Test program, whereas all modules were refurbished for the Simulated Aerodynamic Loads Test and the Short-Term Performance Deterioration (P-695743) Test. Since the low-pressure compressor, high-pressure compressor, and low-pressure turbine were not refurbished from their deteriorated state for this Flight Loads Test program, no further deterioration is attributed to these modules. The deterioration attributed to the fan and high-pressure turbine is approximately the same as in previous test programs.

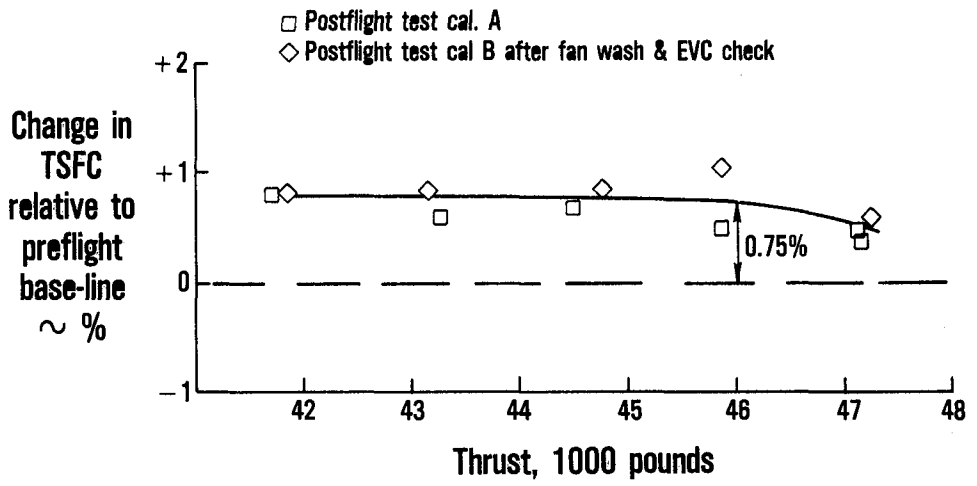

Figure 5-27 Overall Performance Deterioration at Sea Level from Preflight Test-Stand Base-Line Calibration to Postflight Test-Stand Calibrations - The data indicate a thrust specific fuel consumption loss of 0.75 percent at a thrust level of 46,000 pounds.

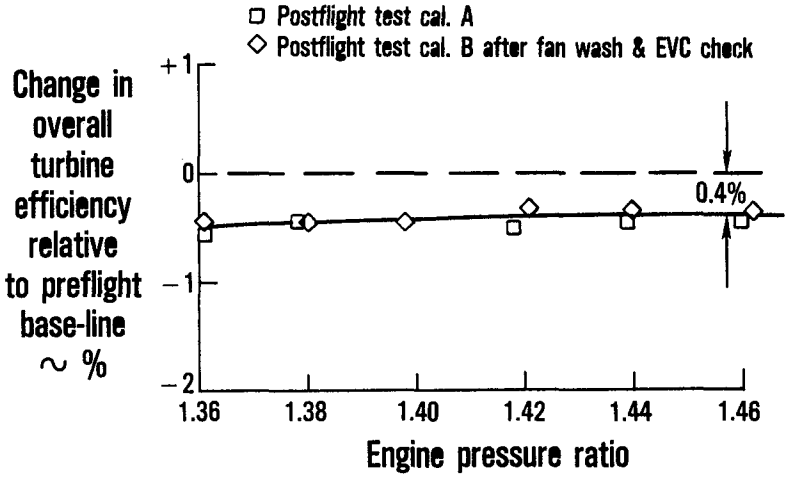

Figure 5-28 Turbine Efficiency Loss from Preflight Test-Stand Base-Line Calibration to Postflight Test-Stand Calibrations - The data indicate an overall turbine efficiency loss of 0.4 percentage point at an engine pressure ratio of 1.46.

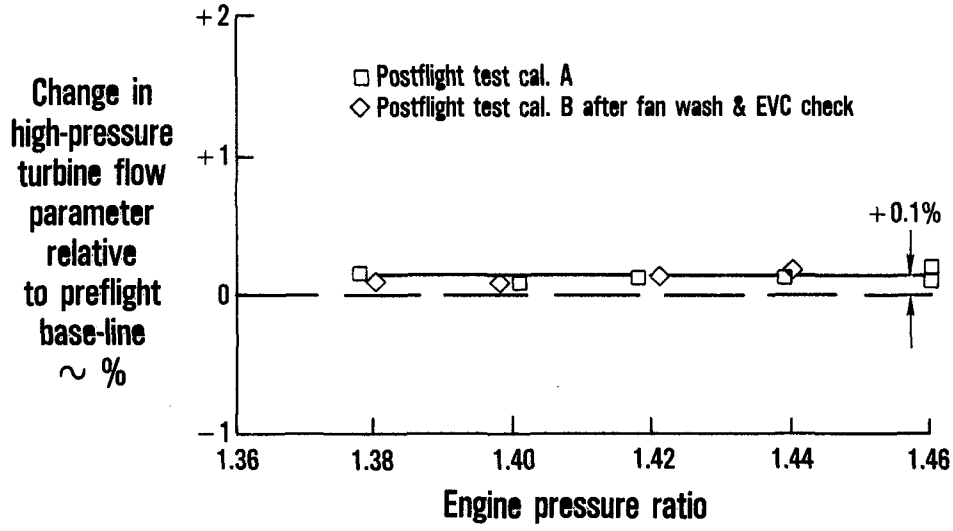

Figure 5-29 High-Pressure Turbine Flow Parameter Change from Preflight Test-Stand Base-Line to Postflight Test-Stand Calibrations - The data indicate a high-pressure turbine flow parameter increase of 0.1 percent at an engine pressure ratio of 1.46.

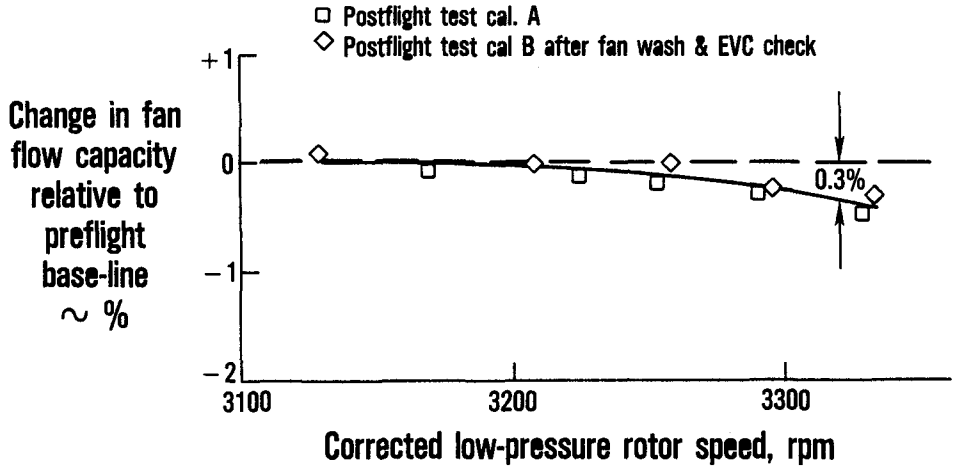

Figure 5-30 Fan Flow Capacity Loss from Preflight Test-Stand Base-Line to Postflight Test-Stand Calibrations - The data indicate a fan flow capacity loss of 0.3 percent at a corrected low-pressure rotor speed of 3320 rpm.

TABLE 5-VI

COMPARISON OF MEASURED PARAMETER SHIFTS
WITH SHIFTS DERIVED FROM MODULE CHANGES

Parameter	Measured Parameter Shifts (% or °F)	Estimated Module Characteristic Changes: High-Pressure Turbine Efficiency -0.9%	High-Pressure Turbine Flow Parameter +0.1%	Fan Flow Capacity -0.3%	Fan Efficiency -0.4%	Total Parameter Shift (% or °F)
		Corresponding Parameter Shifts (% or °F)				
TSFC @ FN=46000 *	+0.75	+0.5	0	-0.05	+0.3	+0.75
PS4/PT7 @ EPR=1.46	-0.1	-0.2	-0.1	0	0	-0.3
PT3/PT2 @ EPR=1.46	+1.2	+1.2	0	+0.5	-0.3	+1.5
PT2.4/PT2 @ EPR=1.46	+0.2	0	0	-0.1	0	-0.1
TT7 @ EPR=1.46	+10°F	+11°F	0	-3°F	+2°F	+10°F
FN @ EPR=1.46	+0.4	+0.1	0	-0.1	-0.2	-0.2
Wf @ EPR=1.46	+1.1	+0.6	0	-0.2	+0.2	+0.6
N1 @ EPR=1.46	+0.1	0	0	+0.2	-0.2	0
N2 @ EPR=1.46	+0.3	+0.2	0	0	0	+0.2
WA Fan @ N1C=3320	+0.3	0	0	-0.3	0	-0.3
LPC Opr. Line	+2.1	+1.4	+0.1	+0.5	-0.2	+1.8
Fan Opr. Line	+0.2	0	0	0	0	0

* at sea level conditions.

TABLE 5-VII

COMPARISON OF FLIGHT TEST PROGRAM MODULE DETERIORATION
WITH PREVIOUS PROGRAM RESULTS

Module	Historical Data Analysis (149 Cycles)	In-Service Engine Analysis (150 Cycles)	P&WA Testing of P-695743 (141 Cycles)	Simulated Aero Loads Test	Flight Test of P-662204
	Change in TSFC (%) at Sea Level Static Take-off Thrust				
Fan	+0.1	+0.2	+0.1	+0.2	+0.2
Low-Pressure Compressor	+0.2	+0.4	+0.4	+0.3	-
High-Pressure Compressor	+0.3	+0.2	+0.3	+0.2	-
High-Pressure Turbine	+0.4	+0.4	+0.6	+0.5	+0.5
Low-Pressure Turbine	+0.5	+0.1	+0.1	+0.1	-
Total	+1.5	+1.3	+1.5	+1.3	+0.7

5.5.3 Installed Engine Ground Test Results

Comparison of the five installed ground calibrations shows no measurable evidence of engine deterioration. Table 5-VIII indicates that measured fuel flow did not increase after calibration 1-2 and instead shows a small (0.3 percent) decrease for some calibrations. This decrease along with the changes in turbine exhaust temperature after calibration 1-2 are attributed to the nonrepeatability of data. Calibration 1-1 is not shown, since the inadvertent air bleed during that calibration had a significant impact on engine performance and made those data useless for deterioration evaluation.

TABLE 5-VIII

COMPARISON OF INSTALLED GROUND CALIBRATION PERFORMANCE CHANGES AT ENGINE PRESSURE RATIO = 1.46

Calibration No.	Time Period	Change in Fuel Flow (%)	Change in Exhaust Gas Temp. (°C)
1-2	After Functional Check and Ferry Flights	Base-Line	Base-Line
2	After Typical Acceptance Flight	0	-2.5
3	After Second and Third Test Flights	-0.3	-1.5
4	After Fourth and Fifth Test Flights	-0.3	0
5	After JT9D-7R4 Program Completion	-0.1	+1

In-flight calibrations were not planned for this program, but calibrations were made at an altitude of 15,000 feet at Mach 0.45 in conjunction with the JT9D-7R4 program during two flights. Those calibrations, like the ground calibrations, indicated no engine performance deterioration during flight testing.

SECTION 6.0

MODEL REFINEMENTS

6.1 INTRODUCTION

An assessment of the performance deterioration resulting from rubs due to flight loads was accomplished using the structural model developed as part of the Simulated Aerodynamic Loads Test program. The basis for the structural model is the NASTRAN finite element model of the JT9D-7, as described in Reference 6 and Section 4.1 of this document. Base-line engine axisymmetric clearances, which include the combined effects of average case thermal growth and rotor centrifugal/thermal growth, are input into the NASTRAN model as a function of flight condition and power setting. The NASTRAN model predicts the deflections due to the input flight loads and, when these are combined with the base-line axisymmetric clearances and abradability factors, computes depth and location of rubs at each flight condition/power setting. A final step involves use of influence coefficients, which relate tip clearance changes to engine performance, to compute performance losses due to rubs.

6.2 ANALYTICAL STRUCTURAL MODEL REVISIONS AND REASSESSMENT OF FLIGHT LOADS

The following changes were made in the structural model analysis, relative to that performed following the Simulated Aerodynamic Loads Test program:

- Input loads were updated based on actual loads computed from static pressure measurements during flight loads testing. The loads obtained from flight loads testing were higher than the estimated loads used previously.

- Base-line axisymmetric clearances were revised for the high-pressure turbine to reflect more rapid case thermal response than had previously been estimated. This new information was a direct result of proximity probe clearance measurements obtained during flight loads testing.

- Load exceedance factors, which represent the degree by which first-flight load levels are exceeded as a function of number of flights, were revised by Boeing as follows:

    - Initial predelivery (acceptance test) rub-induced performance loss is based on loads which correspond to a 550,000-pound gross weight full-power take-off with 10-degree flaps followed by the acceptance test flight profile and maneuvers.

- Additional rub-induced deterioration during early revenue service was based on the assumption that the rubs resulting from heavy gross weight (780,000 pounds with 10-degree flaps) full-power take-off and climb would occur in the first 50 revenue flights.

- Longer term rub-induced deterioration is now assumed to be caused by random incidences of gust, avoidance maneuver, and stall-induced clearance closures occurring during high power operation such as at climb and cruise conditions. The load exceedance factor curves previously provided by Boeing present the statistical probability of load levels corresponding to these random occurrences, as a function of number of flights. Thus, the additional clearance closures induced during these occurrences were applied to the climb and cruise conditions using the exceedance curves provided by Boeing. The resulting rubs were used to establish the long-term rub-induced performance deterioration.

- Tip clearance influence coefficients on engine performance were updated to reflect results of the latest in-house testing and analysis of the JT9D components.

It should be noted that the NASTRAN-based structural analysis does not account for rubs induced by thermal mismatch during power transients or as a result of local temperature gradients in turbine cases. In the case of the high-pressure turbine, these effects have been simulated in the analysis through modification of the base-line clearance since the proximity probe test data permits quantification of the base-line clearance. For the low-pressure turbine, these effects are as yet unaccounted for in the structural analysis. However, since the module and engine performance deterioration models reflect a variety of data sources, the models reflect these losses.

6.3 REVISED PERFORMANCE DETERIORATION MODELS

Engine and module performance deterioration models were developed and refined as new data became available from the various tasks under the JT9D Engine Diagnostics Program. These models relate the engine performance losses (increases in thrust specific fuel consumption and exhaust gas temperature) since new-engine condition as well as module performance losses (efficiency and flow capacity) to engine flight cycles from first flight through 3000 flights. All of the models assume no engine repair. All of the known contributors to performance loss are included in the deterioration models. These contributors are: 1) clearance increases resulting from rubs due to flight loads, thrust bending loads, and centrifugal/thermal effects; 2) changes in airfoil geometry, blade-to-seal clearance increases, and surface roughness changes resulting from erosion; and 3) thermal distortion of hot section parts.

The engine and module performance deterioration models were progressively updated and refined during earlier phases of the JT9D Engine Diagnostics Program as new data became available. The most recent revisions of the models were completed following the Flight Loads Test program and are referred to as "final" models.

A comparison of these models with earlier data used during the development and refinement process (References 1, 2, and 6) as well as module contributions to performance loss by damage mechanisms are shown on figures presented later, starting in Section 6.3.4. Finally, the final model is adjusted to altitude flight conditions and compared to in-flight engine condition monitoring data.

6.3.1 Application of Flight Loads Test Results to Deterioration Models

Module performance deterioration results from the Flight Loads Test were obtained from the average of two approaches. The first approach (test data analysis) involved calculation of module changes through analysis of actual engine data obtained on the test stand and has been previously discussed in Section 5.5. The second approach (teardown analysis) consisted of comparing measured clearance and thermal distortion changes, following the completion of testing, with measured build clearances. The measured physical changes were then converted to efficiency and flow capacity changes for each module. The results of the two approaches were then averaged.

In order to obtain the first-flight module losses for the models, the fan and high-pressure turbine module loss levels were further adjusted to remove additional losses which were encountered as a result of testing which was not representative of the first-flight (acceptance test) profile.

6.3.2 Comparison of Flight Loads Engine Test Results with Teardown Results

Since the test engine was not subjected to the typical Pratt & Whitney Aircraft JT9D-7A production "green run", teardown clearance changes were compared to build clearances, rather than clearances after the green run. These clearance changes must be adjusted to remove the effect of green-run wear so that the results from the Flight Loads Test program can be incorporated into the performance deterioration models, which utilize green run performance losses as a base line. Typical production green run module losses for the JT9D-7A have been documented previously in Reference 3, "Short-Term Performance Deterioration in JT9D-7A(SP) Engine P-695743". Since only the fan and high-pressure turbine were built and torn down analytically and all other modules in the test engine had varying levels of deterioration prior to flight loads testing, only the fan and high-pressure turbine modules can be compared in this manner. Also, the first-stage high-pressure turbine build clearance was 0.008 inch tighter than the normal production clearance (0.066 inch versus 0.074 inch nominal), so that the estimated green run damage for this module must be increased from that typically encountered during production running to account for the tighter build

of the flight test engine. Table 6-I shows this adjustment process which results in reductions in efficiency loss and flow capacity increase for this turbine module from teardown analysis levels. Fan losses are unadjusted, since typically there is no green run damage in the fan module.

TABLE 6-I

REDUCTION OF TEARDOWN LOSSES BY ESTIMATED PRODUCTION RUN DAMAGE

Change in:	Losses per Teardown Analysis	Estimated Production Run Damage	Adjusted Losses
Fan Efficiency (points)	-0.59	--	-0.59
Fan Flow Capacity (%)	-0.77	--	-0.77
High-Pressure Turbine Efficiency (points)	-1.65	-0.52*	-1.13
High-Pressure Turbine Flow Capacity (%)	+0.61	+0.27*	+0.34

* Estimated 0.013-inch Rub

Table 6-II compares the adjusted module losses derived from the teardown analysis with the module losses from the test data analysis. In general, the results are similar, but the teardown analysis shows somewhat higher fan losses. Reasons for the differences are uncertain but may be related to the instrumentation or associated with limitations of the design system techniques to accurately analyze teardown losses. The method selected to resolve the differences was to average the two results as shown in the last column of Table 6-II.

TABLE 6-II

MODULE LOSSES AS AVERAGE OF TEARDOWN RESULTS AND TEST DATA ANALYSIS

Change in:	Teardown Results Adjusted for Production Run Damage	Module Loss by Test Data Analysis	Module Loss as Average
Fan Efficiency (points)	-0.59	-0.4	-0.5
Fan Flow Capacity (%)	-0.77	-0.3	-0.5
High-Pressure Turbine Efficiency (points)	-1.13	-0.9	-1.0
High-Pressure Turbine Flow Capacity (%)	+0.34	+0.1	+0.2

6.3.3 Adjustment of Flight Loads Results to Represent the First Flight

A final adjustment step is required to obtain first (acceptance) flight module losses. This adjustment involves removing those portions of the module losses which resulted from testing that was not representative of the acceptance test flight profile, load levels, or engine operation. In the case of the fan, measured increase in fan clearance over and above that which was incurred on the 538,000-pound gross weight take-off with 10-degree flaps (typical acceptance test configuration and flight profile) was obtained. This clearance increase resulted from operation at heavier gross weight, during wind-up turns, and during a hard landing and resulted in a cumulative increase in fan clearance of about 0.009 inch. The increased fan clearance was converted into equivalent efficiency and flow capacity, and the results in adjusted fan loss levels are shown in Table 6-III.

TABLE 6-III

FAN LOSSES ADJUSTED TO REMOVE DAMAGE BEYOND FIRST FLIGHT

	Fan Losses; Average of Teardown & Test Data	Portion due to Additional Rub	Fan Losses due to First Flight
Change in:			
Fan Efficiency (points)	-0.5	-0.09	-0.41
Fan Flow Capacity (%)	-0.5	-0.12	-0.38

A final adjustment step is also required for the high-pressure turbine. Analysis of flight test data (Section 5.5) and proximity probe data shows that first-stage high-pressure turbine rub occurred during ground calibrations prior to actual flight testing, and the rub which occurred on the ground was sufficiently large that no additional turbine rub or deterioration occurred during the flight test. This turbine rub was a result of ground operation at take-off power for an extended time period (25 minutes) with the customer bleeds inadvertently open, which caused a thermal/centrifugal high-pressure turbine "pinch" and rub. Such operation is not representative of acceptance testing, where ground operation is conducted only to check out systems and trim the engine. Using first-stage high-pressure turbine build and teardown clearances plus proximity probe minimum measured clearance during the typical acceptance test flight, it is possible to estimate the turbine tip rub that would have occurred for a nominal build-clearance turbine with no ground run damage prior to flight test.

This estimated first-stage turbine rub for a nominal build-clearance turbine module is 0.004 inch and is in good agreement with the NASTRAN analysis results. Table 6-IV compares the high-pressure turbine losses from the flight test program (average of the two approaches) with the first-flight losses predicted, as discussed above, for a nominal build-clearance turbine module.

TABLE 6-IV

HIGH-PRESSURE TURBINE LOSSES ADJUSTED TO REMOVE GROUND RUN DAMAGE PRIOR TO FIRST FLIGHT

Change in:	Turbine Losses; Average of Tear-down & Test Data	Predicted Turbine Losses due to First Flight
High-Pressure Turbine Efficiency (points)	-1.0	-0.55
High-Pressure Turbine Flow Capacity (%)	+0.2	+0.1

6.3.4 Updating of Deterioration Models

After the module losses from the two approaches (engine test versus engine teardown) have been averaged and adjusted to remove losses that were not representative of first flight, the remaining module losses can be added to the module deterioration models. As previously mentioned, this procedure can be used only for the fan and high-pressure turbine, because there were no build or teardown measurements for the other modules. These other modules were high time parts before the test, and analysis of the engine test data shows that no additional losses occurred in those modules as a result of flight loads testing. Accordingly, module losses for the low- and high-pressure compressors and the low-pressure turbine remain as previously defined following the Simulated Aerodynamic Loads Test. As pointed out in Section 5.2.4, the good agreement between measured fan clearance closures in the Flight Loads Test with those of the Simulated Aerodynamic Loads Test confirms this approach.

Figures 6-1 through 6-5 present the results of the flight loads analysis, together with the historical data module losses, and the module losses from JT9D-7A prerepair and Plug-In Console (PIC) data. The final model resulting from application of Flight Loads Test results is shown as a dashed line. The effects of predelivery airplane acceptance testing by the airplane manufacturer are identified.

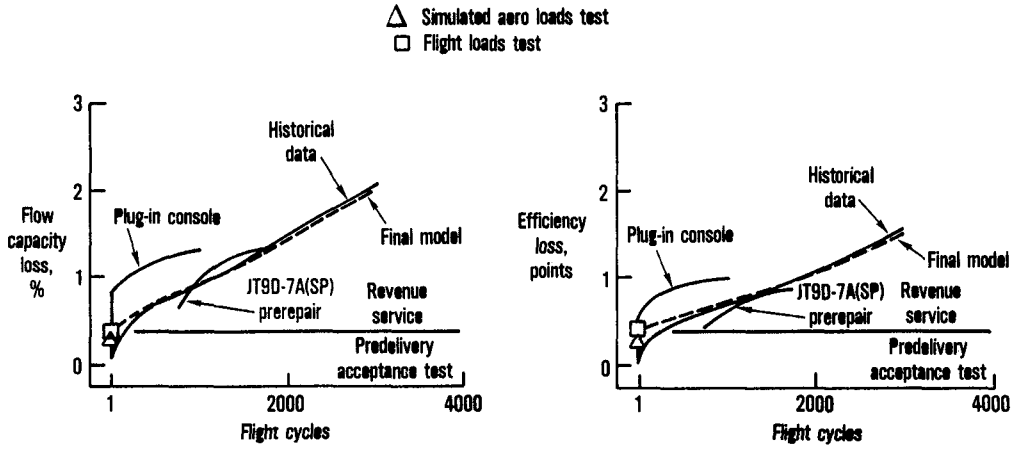

Figure 6-1 Estimated Fan Deterioration with Usage. (J26090-12)

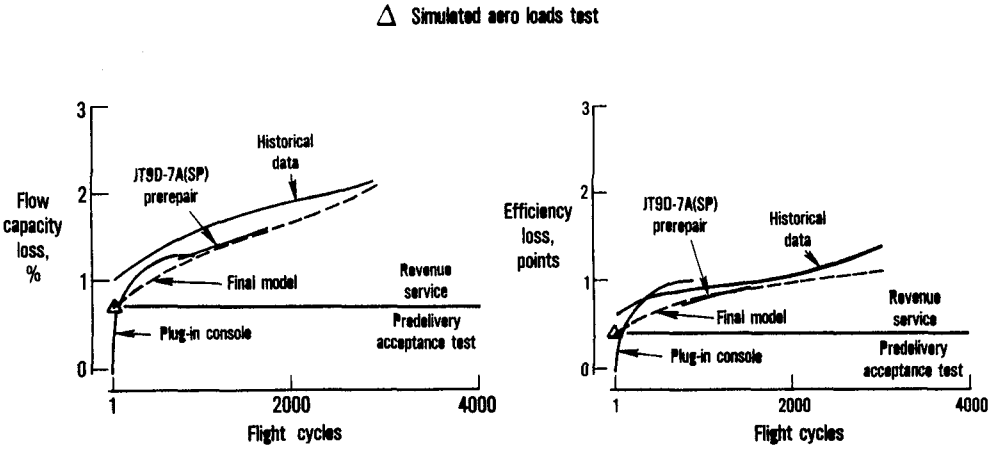

Figure 6-2 Estimated Low-Pressure Compressor Deterioration with Usage. (J26090-13)

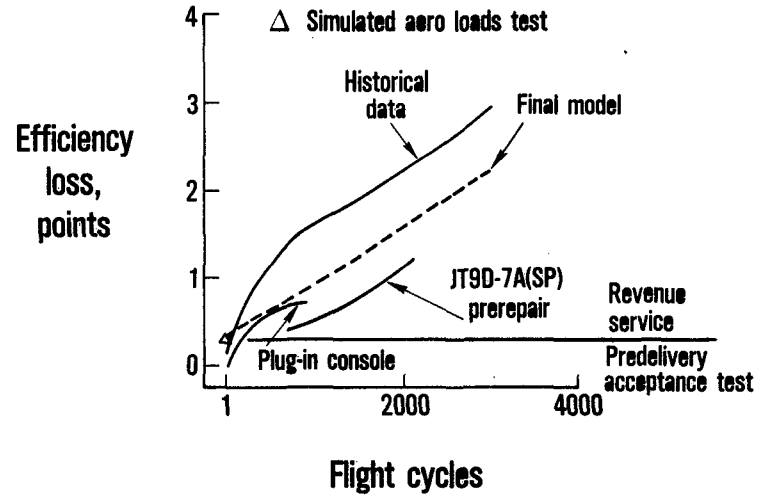

Figure 6-3 Estimated High-Pressure Compressor Deterioration with Usage. (J26090-10)

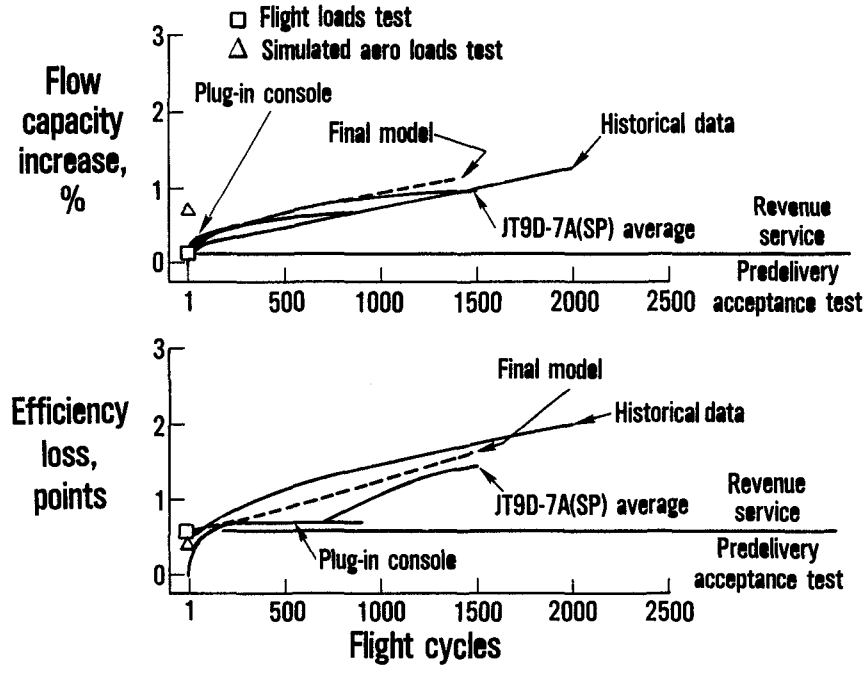

Figure 6-4 Estimated High-Pressure Turbine Deterioration with Usage. (J26090-11)

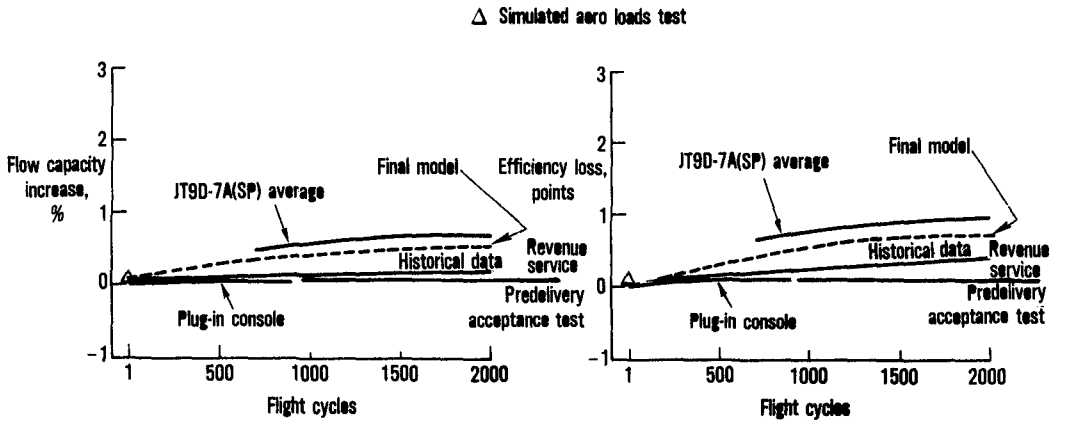

Figure 6-5 Estimated Low-Pressure Turbine Deterioration with Usage. (J26090-9)

Results of the final model, in terms of sea level take-off thrust specific fuel consumption loss by module and major cause, are shown in Figure 6-6. The losses due to clearance increases resulting from rubs is derived primarily from the NASTRAN analysis results. However, as previously mentioned, the NASTRAN analysis does not currently account for losses due to power transient-induced rubs or for rubs caused by local temperature gradients in the turbine cases. For this reason, total engine thrust specific fuel consumption increases due to rubs, shown in Figure 6-6, are greater for increased flight cycles than the NASTRAN analysis indicates. Previous work under the JT9D Engine Diagnostics Program, documented in References 1 and 2, identified losses due to thermal distortion and erosion. Total first-flight thrust specific fuel consumption loss is 1.15 percent, while the 1000 and 2000 flight loss levels are 2.9 and 3.8 percent, respectively. Figure 6-7 shows total engine thrust specific fuel consumption loss at take-off, in terms of major causes, versus flight cycles. Note that the performance change on Figure 6-7 is normalized to the start of revenue service.

6.3.5 Performance Deterioration Model Verification at Sea Level

Thrust specific fuel consumption loss predicted by the model at take-off compared with actual measured thrust specific fuel consumption data is shown in Figure 6-8. The model agrees well with the average of the data sources. Note that the performance deterioration model includes the effects of rubs, plus the effects of erosion and thermal distortion.

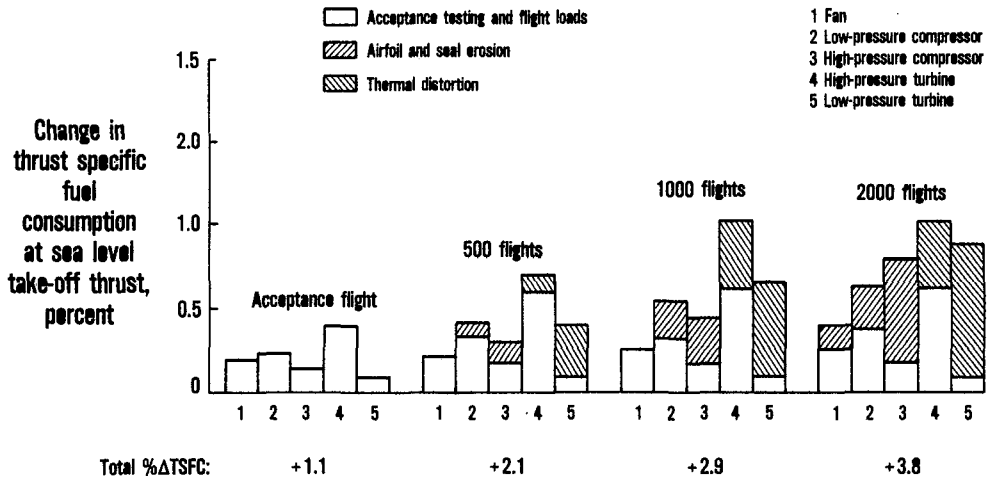

Figure 6-6 Module Performance Deterioration Relative to Production, at Sea Level, as Predicted by the Final Model. (J26090-15)

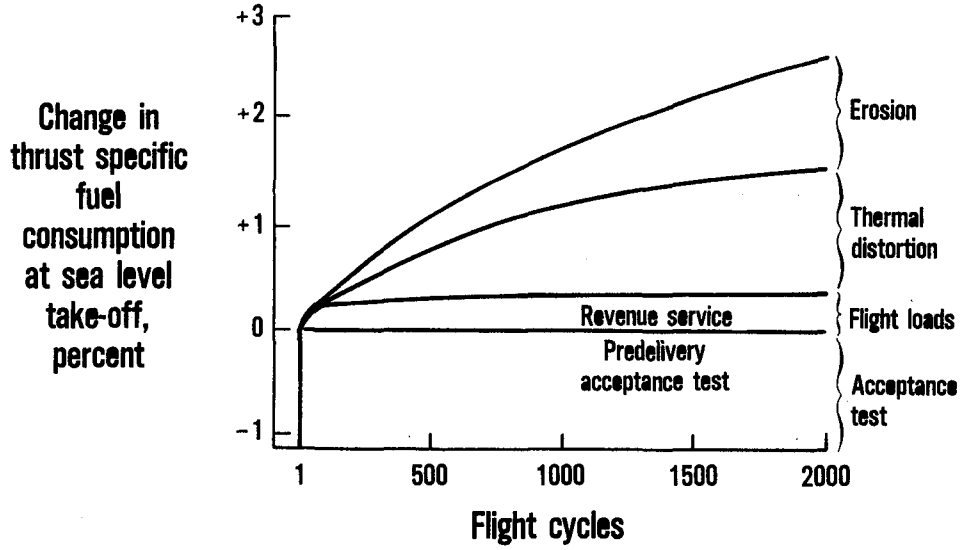

Figure 6-7 JT9D-7 Engine Performance Deterioration Relative to the Start of Revenue Service, at Sea Level Take-Off, by Major Causes. (J26090-14)

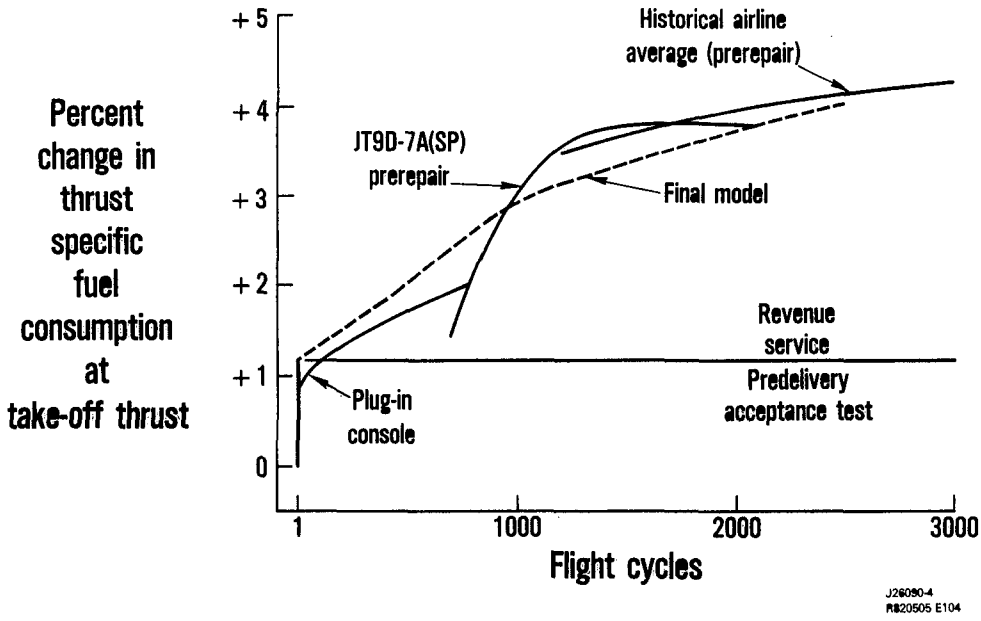

Figure 6-8 Model Compares Favorably with Sea Level Thrust Specific Fuel Consumption Data, Relative to Production. (J26090-4)

Increases in exhaust gas temperature (EGT) predicted by the model is compared to the measured increases from the various data sources in Figure 6-9. The model agrees well with the average of the data sources, although the initial exhaust gas temperature increase predicted by the model is somewhat greater than Plug-In Console data. Both the Simulated Aerodynamic Loads Test engine and the Flight Loads Test engine data support the higher level.

6.3.6 Measured In-Flight Deterioration

To validate the model at cruise conditions, it is first necessary to obtain actual in-flight average performance measurements. The source for this performance data was the Engine Condition Monitoring (ECM) data for the 747SP/JT9D-7A(SP) fleet collected as part of the in-service engine phase of the JT9D Engine Diagnostics Program. First installation data for 28 of these engines were analyzed, and the computer regression fits of the data are shown in Figures 6-10 and 6-11. Percentage change in fuel flow and change in exhaust gas temperature at constant engine pressure ratio, both relative to the Flight Manual base line, are shown in the figures which include nearly 1400 points. The analyses of the data revealed a wide range of results and significant variability for individual engines. However, with this quantity of data plotted and trend fitted, the results will be representative of the average engine.

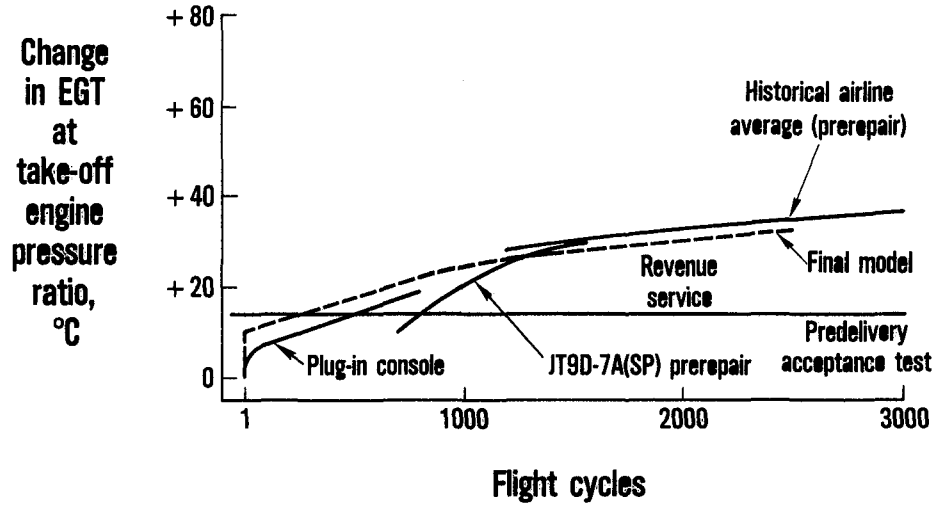

Figure 6-9 Model Compares Favorably with Sea Level Exhaust Gas Temperature Data, Relative to Production. (J26090-5)

SOURCE: INITIAL INSTALLATION JT9D-7A(SP) ENGINES
BASELINE: BOEING COMMERCIAL AIRPLANE COMPANY FLIGHT MANUAL

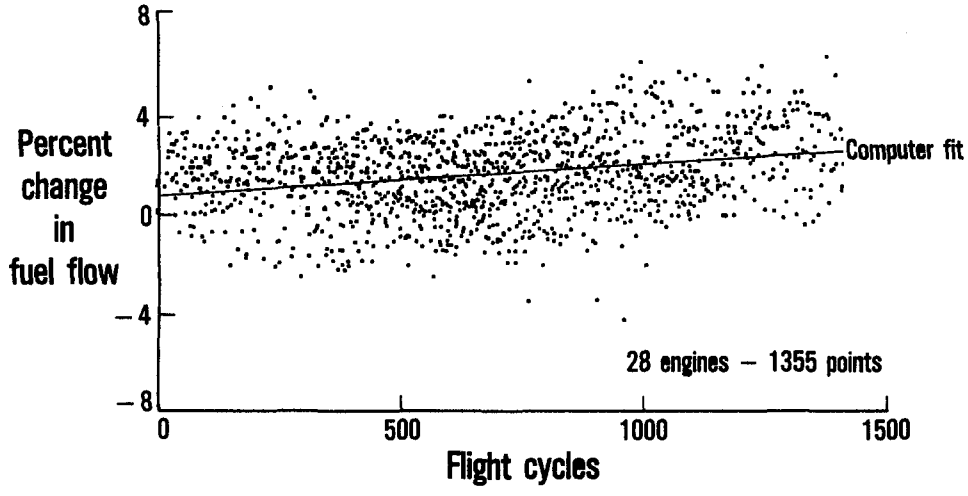

Figure 6-10 Cruise Monitoring Fuel Flow Data Trend Fit. (J24173-1)

SOURCE: INITIAL INSTALLATION JT9D-7A(SP) ENGINES
BASELINE: BOEING COMMERCIAL AIRPLANE COMPANY FLIGHT MANUAL

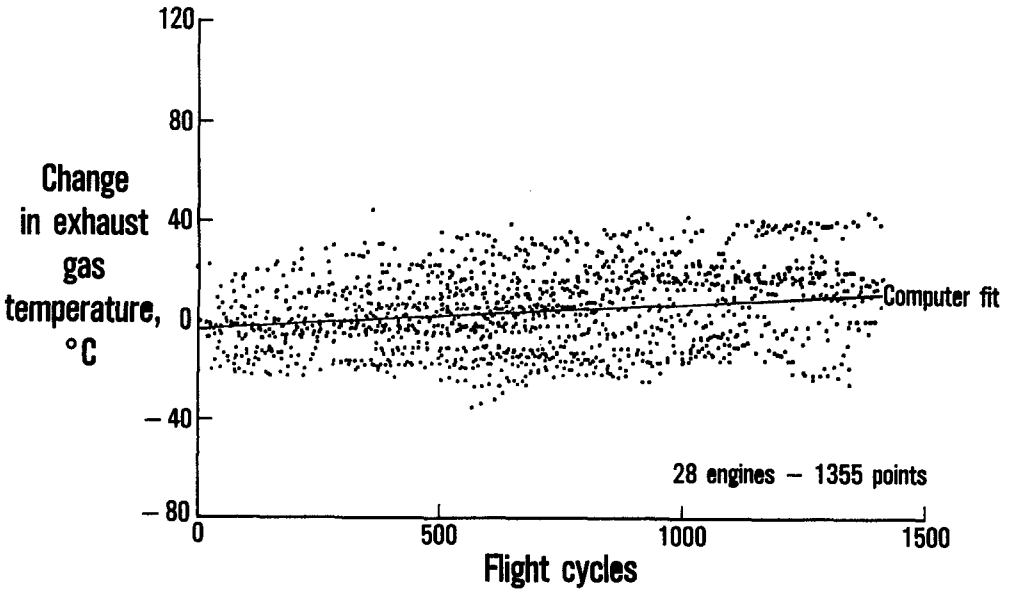

Figure 6-11 Cruise Monitoring Exhaust Gas Temperature Data Trend.
(J24173-2)

6.3.7 Model Verification at Cruise Conditions

Module performance loss levels from the performance deterioration model can be built into the engine computer simulation and "flown" at typical cruise conditions. Changes in fuel flow and exhaust gas temperature at constant engine pressure ratio can be evaluated and compared to engine condition monitoring data trends, as shown on Figures 6-12 and 6-13. The fuel flow trend, Figure 6-12, is good, except that the model shows a smaller rate of increase beyond 1000 flight cycles. This variation occurs because the model assesses a maximum loss level in the high-pressure turbine, which is typical of a maximum prerepair level. Since the measured data all represent initial installations, there is no corresponding stabilized level. Comparison of exhaust gas temperature increase for the model and the measured data, Figure 6-13, is good. The in-flight data thus confirms the accuracy of the model when applied to typical cruise flight conditions and power settings.

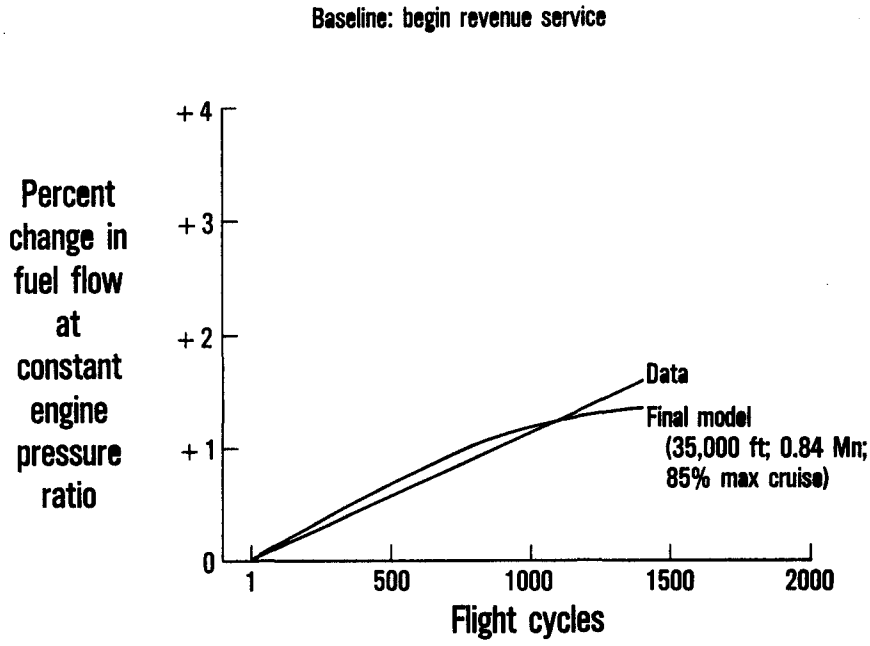

Figure 6-12 Model Trend Agrees Well with Cruise Fuel Flow Data.
(J26090-6)

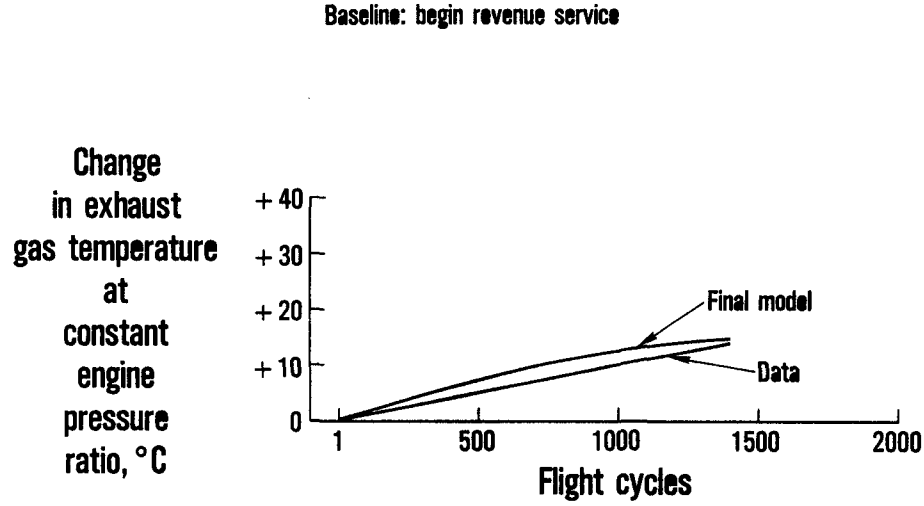

Figure 6-13 Model Trend Agrees Well with Cruise Exhaust Gas Temperature Data.
(J26090-7)

It should be noted that in-flight data can not accurately define actual loss of thrust specific fuel consumption because of the lack of thrust measurement. Also, the limited number of measured parameters provide little insight into individual module contributions to performance losses. To accurately model in-flight thrust specific fuel consumption deterioration, it is necessary to start with sea level test stand data where both thrust and fuel flow are measured, as well as sufficient parameters to make reasonable assessments of individual component contributions to deterioration. Detailed part assessment and loads testing or structural simulation are necessary to further establish deterioration causes (such as clearance, erosion, etc.) by component. The model can then be confirmed at sea level against a variety of test data. The model then has sufficient validity to be exercised at cruise conditions and compared with cruise data. This is the approach established in the JT9D Engine Diagnostics Program.

6.3.8 Cruise versus Take-Off Performance Deterioration

Thrust specific fuel consumption deterioration at cruise conditions differs from that evaluated at sea level in two significant ways. First, the engine is generally less sensitive to component loss at cruise conditions (less thrust specific fuel consumption increase for the same losses). Secondly, sea level thrust specific fuel consumption is commonly compared with a production test base line and, thus, does not include acceptance testing losses.

The reduced sensitivity of the engine to component losses at cruise conditions can be demonstrated with the computer engine simulation. The reduced sensitivity results from the fact that the ram pressure ratio increases the effective cycle pressure ratio at cruise and thus makes the performance less sensitive to the gas generator compression ratio. Table 6-V shows typical JT9D-7 computer simulation results for assumed 1-point component efficiency losses at sea level take-off and cruise conditions. Sensitivity is uniformly less at cruise.

TABLE 6-V

COMPARISON OF MODULE SENSITIVITY AT CRUISE AND SEA LEVEL
EFFECT ON TSFC OF 1 POINT LOSS IN EFFICIENCY

	Sea Level Static Take-Off Thrust	35,000 feet, Mach 0.84 85% Maximum Cruise
	Change in TSFC (%) at Constant Thrust	
Fan	+0.78	+0.5
Low-Pressure Compressor	+0.35	+0.28
High-Pressure Compressor	+0.54	+0.49
High-Pressure Turbine	+0.62	+0.58
Low-Pressure Turbine	+1.03	+0.77

Reduced sensitivity of the engine to component losses at cruise has been demonstrated in the Pratt & Whitney Aircraft altitude test facility (Willgoos Turbine Laboratory). Figure 6-14 presents results for a limited number of engines, where both sea level and altitude tests were performed. Some of the data represent production engine variations and some are tests after certification. Comparison of altitude with sea level thrust specific fuel consumption increase reveals a relationship of about 0.75 to 1, that is, altitude thrust specific fuel consumption increase is about 75 percent of the sea level increase.

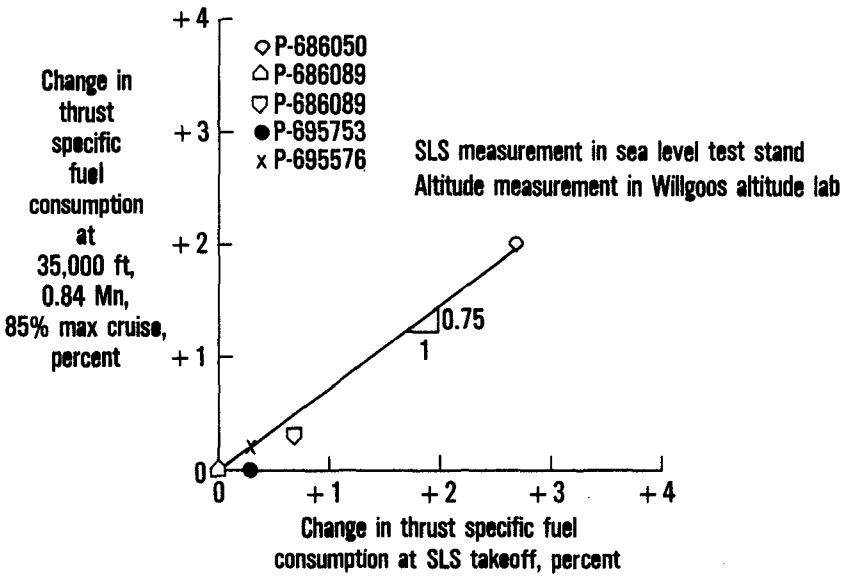

Figure 6-14 Reduced Module Sensitivity at Cruise Verified by Altitude Laboratory Testing. (J26090-8)

SECTION 7.0

CONCLUDING REMARKS

The performance deterioration analysis and deterioration prediction modeling conducted in the earlier phases of the JT9D Engine Diagnostics Program achieved the following:

- Established engine and module performance deterioration with usage;
- Defined and quantified the three primary causes of deterioration, namely: rub-induced opening of running clearances, erosion of airfoils and seals, and thermal distortion of hot section airfoils;
- Established deterioration as primarily a flight cyclic phenomenon;
- Established the relation between sea level and cruise altitude performance deterioration; and
- Identified predelivery airplane acceptance testing as the period of principle seal-to-blade rub-induced performance deterioration.

The Flight Loads Test program, as the final phase of the JT9D Engine Diagnostics Program, expanded our understanding of short-term performance deterioration and permitted a final refinement of the performance deterioration model. Specifically, the program achieved the following:

- Established the causes of aerodynamic loads and their magnitude as a function of flight condition;
- Verified that aerodynamic loads are the primary cause of blade-to-seal rubs on the fan and, it is assumed, in the low-pressure compressor;
- Established that the combination of flight load-induced and thrust bending load-induced closures, when added to the thermal closure effects, causes rubs in the turbine;
- Verified that hot-engine deceleration immediately followed by acceleration is a potential cause of rubs in the high-pressure turbine and, hence, performance loss; and
- Provided a final refinement of the JT9D performance deterioration prediction model.

None of the flight conditions created any significant dynamic vibration-induced load conditions, further supporting the prior conclusion that dynamic loads do not contribute to performance deterioration.

7.1 RUB CAUSES

Clearance closures and the resulting rubs are caused by the sum of power effects and flight load effects as shown on Figure 7-1. The axisymmetric closures are due to thermal and mechanical loads applied either to the rotating segments or uniformly around the static segments. The asymmetric closures are due to nonsymmetric mechanical and thermal loads applied to the static structure and not necessarily in the plane of the closure.

The test results on the two fans validate prior results and confirm that the aerodynamic load at lift-off is the dominant fan closure effect. When the aerodynamic load is combined with the centrifugal and thrust backbone-bending effect at take-off, maximum closure and rub is caused in the lower inboard quadrant of the fan air seal.

The 10-degree flap setting at take-off in the acceptance test flight required a greater rotational angle than that for take-off with a 20-degree flap setting. This increased angle of rotation resulted in increased fan closure and rub. Similarly, but to a lesser degree, fan clearance closure at take-off increased with gross weight due to the increased speed at lift-off. During the maximum gross weight, 10-degree flap setting take-off (flight condition 118), the asymmetric closures due to thrust and aerodynamic load-induced case bending exceeded 0.180 inch as shown on Figure 7-2A.

The flight test program identified midclimb as the maximum clearance closure condition in the first-stage high-pressure turbine during normal revenue service. Differential thermal expansion of rotating and static components plus the sum of the aerodynamic, centrifugal, and thrust bending effects combined to close the running clearance with the pinch occurring three to four minutes into climb and located in the lower outboard quadrant, see Figure 7-2B. Maximum closure occurs at this point due to the slow thermal expansion of the turbine disks which continued to close down the running clearances after the aerodynamic and thrust loads had peaked and started to decrease. Note that this Flight Loads Test was conducted using a JT9D-7A engine installed in a 747-200 nacelle; thus, the clearance closure values are not necessarily representative of those in later engine models.

Similar maximum clearance closures also occurred in two other flight conditions. The stall warning with 30-degree flaps (condition 111), which is part of the airplane acceptance flight, involved an engine deceleration followed a few minutes later by an acceleration while the airplane was oriented at a relatively high angle of attack. The acceleration following the deceleration induced an axisymmetric closure. The acceleration with a high angle of attack increased the aerodynamic load and caused asymmetric closure.

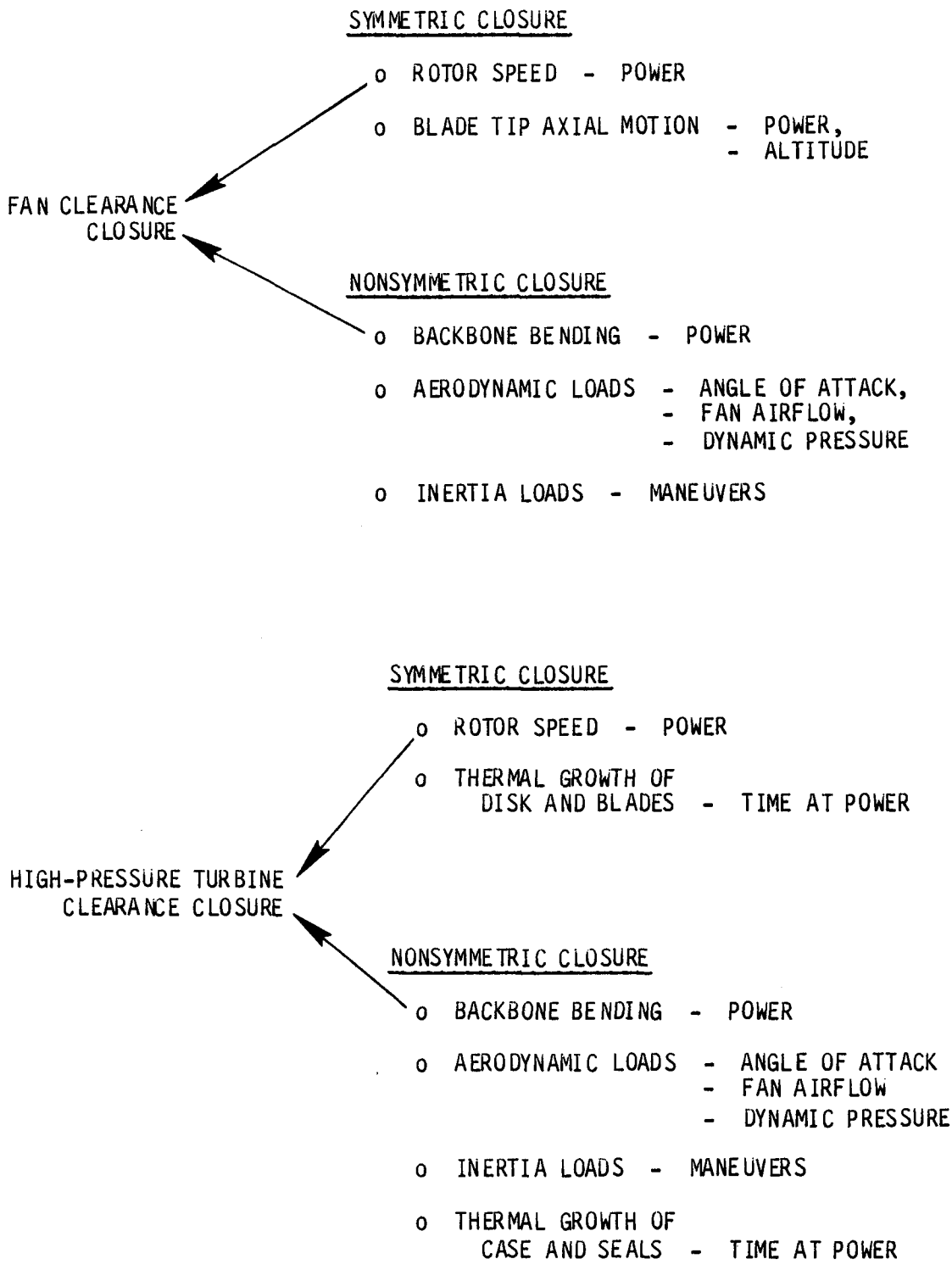

Figure 7-1 Fan and High-Pressure Turbine Clearance Closures - Closures in these components are caused by the sum of power effects and flight load effects.

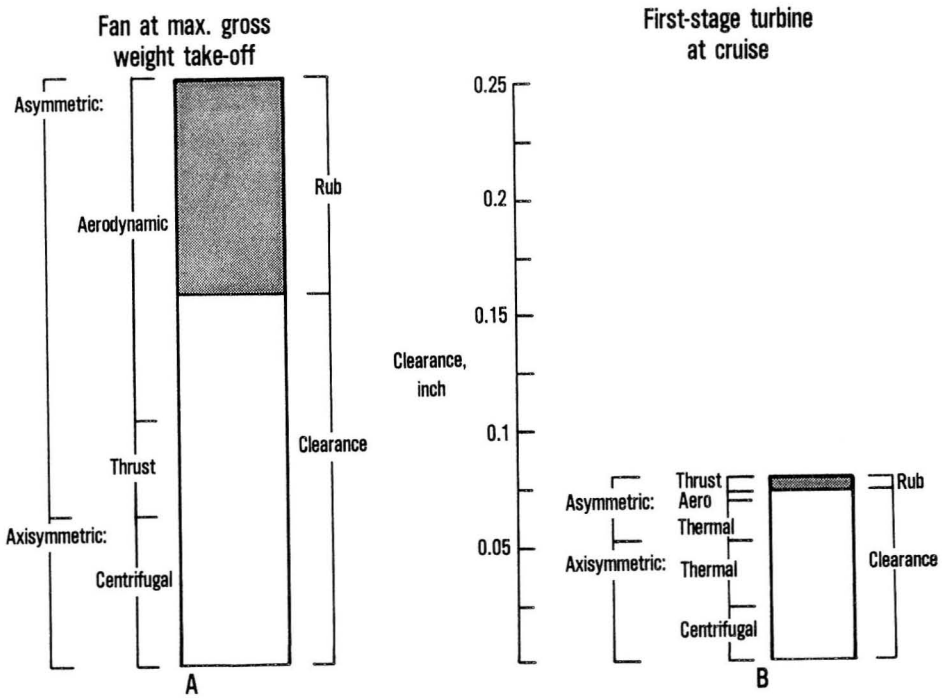

Figure 7-2 Maximum Clearance Closures - Maximum closure in the fan occurs during maximum gross weight take-off (A) and in the first-stage high-pressure turbine during midclimb (B). (J26090-2)

The high-G turn simulated avoidance maneuver (condition 116), which included high power and high angle of attack, caused a similar combination of high axisymmetric and asymmetric closures.

These three flight conditions demonstrate that maximum clearance closure in the high-pressure turbine is caused by a combination of axisymmetric closure, resulting from either extended high power operation or deceleration/acceleration operation, and asymmetric closure due to a combination of high power and moderately high angle of attack.

The heavy gross weight, hard landing (condition 124) provided no significant indication of closure in the fan or first-stage high-pressure turbine running clearance.

7.2 PERFORMANCE DETERIORATION

The analysis of the measured clearance closure, performance, build clearances, and measured rub data provided the basis for the final refinement of the JT9D performance prediction model, see Figure 7-3.

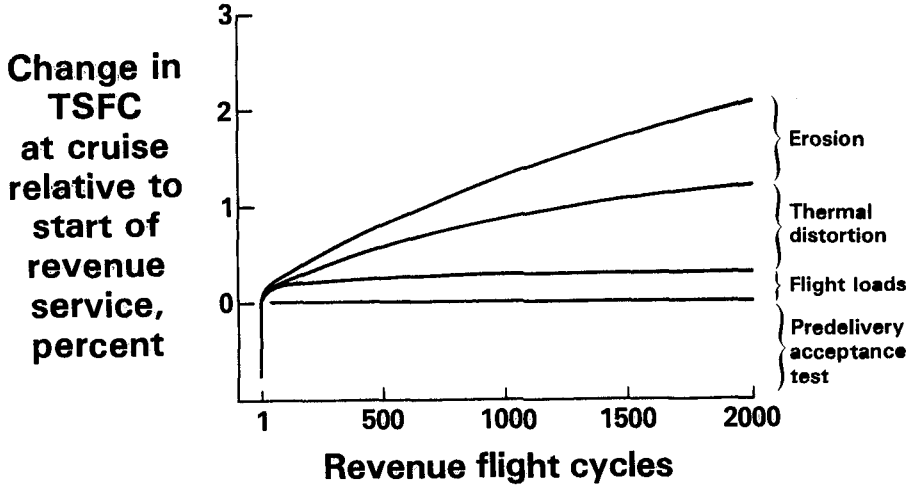

Figure 7-3 JT9D-7 Engine Performance Deterioration at Cruise - Predicted performance deterioration indicates a 2.1 percent increase in cruise thrust specific fuel consumption at 2000 revenue flights of an unrepaired engine. (J26216-21)

The current Boeing 747 production aircraft acceptance test procedure, assuming a nominal engine build, is estimated to cause an initial increase of 0.8 percent in engine cruise thrust specific fuel consumption prior to aircraft delivery. Up to 0.2 percent additional cruise thrust specific fuel consumption increase can be expected in the first 50 revenue flight cycles depending on the airplane gross weight in that service. Finally, additional gust- and maneuver-induced aerodynamic loads can be expected to increase the rub-induced JT9D performance loss during revenue service to 0.3 percent in 2000 flight cycles.

It should be noted that all phases of the NASA JT9D Engine Diagnostics Program, including in-service data gathering, special tests, analysis, and performance deterioration modeling, utilized JT9D-7A enines. Thus, the performance deterioration predictions, conclusions, and recommendations apply to engine models with that level of technology. Knowledge gained from this program has been and is continually being applied to improve the performance retention characteristics of later model engines.

SECTION 8.0

RECOMMENDATIONS

In this section, the recommendations presented first are those derived from the results of the JT9D Flight Loads Test program. These are then followed by a review and update of those recommendations presented following the earlier phases of the JT9D Engine Diagnostics Program, see References 1 through 6.

8.1 SUMMARY OF RECOMMENDATIONS

The new recommendations following the Flight Loads Test are as follows:

- o Investigate methods of structurally integrating the engine and nacelle to reduce the asymmetric closure due to aerodynamic and thrust loads.

- o Investigate further the extent and cause of thermally-induced closures in the high-pressure turbine with goal of minimizing nonsymmetric closures.

- o Continue development of gas-path clearance control systems and abradable rub strips to provide closer running clearances.

Previous studies in the JT9D Engine Diagnostics Program have also resulted in design criteria and recommendations which are repeated here, where still applicable, for the sake of completeness:

- o Develop improved erosion resistant coatings and materials for cold section airfoils and rub strips.

- o Develop designs to reduce ingestion of erosive materials into the compressor section of the engine.

- o Develop designs to reduce hot section temperature profile shifts and the resultant thermal distortion of gas-path parts.

- o Include clearance monitoring in the development testing of new engines.

- o Improve maintenance procedures.

A complete discussion of these recommendations is presented in Section 8.2, and maintenance recommendations by engine module are discussed in Section 8.3.

8.2 DETAILED RECOMMENDATIONS

The results of the analysis of the historical data, Reference 1, the Pan American 747SP in-service engine data, Reference 2, and the Flight Loads Test program provided the detailed information from which recommendations can be made for specific design and development actions. These recommendations are presented in this section and are grouped according to the operations-related major causes of performance deterioration. These causes are rub-induced increases in blade-to-seal running clearances, foreign object-induced erosion of airfoils and seals, and thermal distortion of turbine vanes.

8.2.1 Rub-Induced Blade and Seal Wear

Rub-induced wear and the resulting opening of running clearance occurs throughout the engine and is the primary cause of short-term engine deterioration. Rub occurs in each stage when the sum of the clearance closures caused by centrifugal force, thrust bending, differential thermal expansion, and flight loads exceeds the build clearance of that stage. The initial rub occurs during the take-off and climb phase of the airplane production acceptance test. The resultant performance loss is about 0.8 percent in cruise thrust specific fuel consumption and is a function of initial build clearances. Slight further performance loss will occur in revenue service when flight conditions cause slightly greater combinations of clearance closure.

This performance loss and the initial build performance can both be improved upon if the total clearance closures under the various critical flight conditions can be reduced.

The first recommendation is to investigate approaches to reduce the case bending-induced clearance closures throughout the engine through structurally integrated designs. The present engine thrust mount causes a bending moment in the cases which in turn causes a nonsymmetric clearance closure in the fan and turbine. Similarly, the aerodynamic flight load on the inlet is transmitted to the fan case, causing bending moments and case deflections which are additive to the thrust-induced deflections. Integrated engine case/nacelle wrap designs which stiffen the engine cases and provide alternate load paths through the nacelle to the pylon should be evaluated.

From Figure 7-2 it may be noted that if the thrust- and aerodynamic-induced closures can be halved, the fan and turbine running clearances during revenue service can be significantly reduced.

The second recommendation is for an investigation of the extent and cause of differential thermally-induced closures in the high-pressure turbine. Axisymmetric plus nonsymmetric differential thermally-induced closure appears to be the dominant closure effect in the high-pressure

turbine (Figure 7-2). Reduction in these closures will permit tighter running clearance, reduced case cooling-air requirements, and reduced susceptability to turbine rotor rubs induced by snap accelerations.

The follow-on Additional Ground Test program will establish basic transient and steady state, symmetric and nonsymmetric closure characteristics in a JT9D-7R4 bare engine at sea level. Further investigation as to the effects of case cooling, altitude operation, and ancillary equipment packaging around the turbine case is also required. This investigation should include analytical and experimental evaluations of turbine case temperature in assembled propulsion systems early in development programs to eliminate possible thermally-induced distortion.

The third recommendation is for continued refinement of turbine clearance control systems and abradable rub strip materials. Since the axisymmetric closure due to the cummulative effect of centrifugal load effects and differential expansion can not be reduced to zero, an advanced design case cooling system is required to match the running clearances at each stage over the various flight conditions. Similarly, the asymmetric closures due to mechanical loads and thermal expansion can not be practically eliminated; thus, abradable rub seals should be developed to ensure localized seal wear rather than blade wear which uniformly opens running clearances. Both of these efforts are underway.

Finally, relative to flight operations, the following recommendations are made:

- Use a derated power take-off when conditions permit to reduce hot section thermal distortion.
- Minimize high power operation immediately prior to start of take-off to prevent the combination of an increased thermal expansion-induced closure and the maximum load-induced closures at take-off, thereby reducing the possibility of turbine rub.
- Minimize the possibility of turbine rubs due to snap accelerations with a hot rotor and cooler case.

8.2.2 Performance Loss Due to Erosion

Erosion is the wearing away of airfoil and seal surfaces by the impingement of foreign matter in the gas path and, thus, occurs primarily during ground and near-ground operation. The extent of erosion damage is, therefore, a function of the number of take-offs to which the engine is subjected and the conditions at the airports served. Erosion reduces engine performance in two ways. It blunts and wears down airfoils, thereby reducing their performance, and it wears away blade ends and seal surfaces, resulting in increased gas-path clearances.

The documented effects of erosion on compressor airfoils and seals supported the need to improve the erosion resistance of these parts. The possibility of replacing rubber outer air seals with a more erosion resistant material, such as nickel graphite, nickel-chrome, or sintered metal materials, should be assessed. Erosion resistant coatings for application to compressor vanes have been developed, tested, and approved, or are about to be approved, by Pratt & Whitney Aircraft for the JT3D, JT8D, and JT9D engines. These coatings are particularly effective in reducing corrosion and dirt build-up and, during vane refurbishment, in recovering the performance loss associated with roughness.

The selection and testing of candidate coatings for compressor blades is underway under the NASA Materials Technology (MATE) Program at Pratt & Whitney Aircraft. The program calls for cyclic endurance testing of titanium, steel, and nickel alloy compressor blade coatings, to be completed in 1982. The potential improvement from coatings and new seal materials is at least a 50 percent increase in the performance life of these parts with a 100 percent increase or greater being the goal.

The control of the quantity of erosive material that enters the compressor through the use of passage shaping is a possibility for foreign object damage control; however, the size of the particles that cause the bulk of the erosion damage are estimated to be such that passage shaping may have little effect. Boundary layer bleeds located at positions where the erosive material tends to concentrate have a high probability of success. These methods of erosive material control are being investigated. The designs of future engines include bleeds designed to remove a large percentage of the dirt ingested into the engine during taxi and thrust reverser operations.

8.2.3 Thermal Distortion Effects

Thermal distortion effects are primarily twisting, bowing, and soldiering of turbine vanes which result from the basic temperature and stress environment of the turbines and changes to that environment. These turbine environmental changes are caused by compressor performance changes, combustor dimensional changes, and fuel nozzle coking with usage which alter combustor exit temperature levels and profiles. The resulting increase in turbine airfoil losses and increased leakages reduce high- and low-pressure turbine efficiencies.

Recent data from sources other than this program indicate that a part of the high- and low-pressure turbine long-term performance losses may be due to thermal distortion of turbine and exhaust cases which, in turn, contribute to further blade-to-seal rubs.

The designs of future engines will incorporate features to decrease the potential for adverse temperature profiles which result from all of the factors described above. Further, the NASA Hot Section Technology (HOST) program is progressing toward establishing the technology requirements of higher temperature engines of the future.

8.3 MAINTENANCE PRACTICES

This section presents recommendations for the retention of engine performance. To encourage such restoration, a cost/benefit analysis of cold section refurbishment was presented in Reference 6.

8.3.1 Fan

Fan performance deterioration is caused by the increased tip clearances which result from flight loads and which appear to stabilize after 1000 flights. Surface roughness at first increases with usage but then appears to stabilize. Fan blade leading edge bluntness, however, continues to increase and the performance penalty grows.

Based on these damage mechanisms, periodic hand cleaning of the fan blades and stator vanes when the engine is in the shop and restoration of leading edges of both blades and vanes are the two recommended maintenance actions. As long as the fan rub strip is mechanically sound and the tip clearances are within the Overhaul Manual limits, no restoration of fan blade clearance is recommended due to the short-term rub-out from the effect of flight loads. Continued monitoring and attention to fan blade and stator vane aerodynamic quality is essential for good altitude performance.

8.3.2 Low-Pressure Compressor

The mechanisms that reduce performance in the low-pressure compressor are tip clearance, roughness, and airfoil leading edge shape. Surface roughness increases and then appears to stabilize. Tip clearances, however, continue to increase from the effects of erosion on the rubber outer air seals. Airfoil leading edge shape or bluntness is not judged to be significant up to 4000 to 5000 cycles.

The low-pressure compressor should be cleaned and the rub strips replaced when the engine is in the shop. The effects of airflow losses, particularly on exhaust gas temperature, as well as thrust specific fuel consumption, suggest that more attention should be placed on the low-pressure compressor module. The second-stage blades inspected from samples with 5000 cycles usage showed signs of thinning. Continued monitoring of all low-pressure compressor airfoils should be undertaken. As the cost of fuel increases, the benefits favor earlier refurbishment.

8.3.3 High-Pressure Compressor

High-pressure compressor performance losses caused by erosion are due to blade length reduction, loss of outer air-seal material, and increased roughness. The effects of blade camber change, based on analysis, become more important at blade usage levels beyond 3000 cycles.

The performance losses in the high-pressure compressor suggest that the module should be refurbished between 2500 and 3500 cycles with long blades and new/refurbished rub strips in all stages. The stators should also be cleaned and coated (or recoated) at this time. Because of stator thinning, the stators, as well as the blades, and outer air seals may need to be replaced at the next interval or 5000 to 7000 total cycles.

The correlation of compressor blade length to exhaust gas temperature improvement is strong. The measured exhaust gas temperature improvement due to reduced clearance between the blade and the outer air seal appears greater than the predicted average exhaust gas temperature improvement. Thus, it appears that reductions in compressor blade clearances improve combustor temperature profile and, hence, the exhaust gas temperature profiles and measured values.

8.3.4 Combustion System

The direct effect of combustor deterioration on performance is insignificant since its efficiency stays at essentially 100 percent, even after repeated repair; however, the indirect effects are of major significance. Changes in radial and circumferential temperature patterns in the combustor exit gas affect turbine clearances and durability.

When the combustor is repaired, the dimensions, particularly the cone angle and hood concentricity, should be restored. The fuel nozzles should be removed and cleaned.

8.3.5 High-Pressure Turbine

The performance deterioration of the high-pressure turbine appears to be dominated by tip clearance changes and second-stage vane inner shroud leakage.

Blade tip wear of first-stage turbine blades correlates with initial blade clearances and build standards with respect to blade length. Control of first-stage blade length by hand selection or drum grinding to a constant diameter is recommended. The outer air seals should be offset ground to the requirement set forth in the Overhaul Manual. The second-stage blade clearances should be set to the nominal dimension, and the second-stage vane inner foot dimensions should be set to the tight side of the tolerance band.

8.3.6 Low-Pressure Turbine

Blade tip clearances are a major cause of low-pressure turbine deterioration. Rebuild standards which allow larger tip clearances cause an increase in postrepair performance deterioration. The ring seals of the low-pressure turbine are very responsive to temperature changes. Hot shutdowns will cause rubbing and performance loss due to the rapid contraction of these seals.

The performance penalties for increased tip clearance are larger in the front stage than in the rear stages of the low-pressure turbine. The tip clearances should be kept to nominal dimensions, particularly in the third and forth stages during rebuild, and platform soldiering should be eliminated by vane repair when the low-pressure turbine is opened for other reasons.

8.3.7 Engine Case Dimensional Control

Engine case roundness and flange flatness should be monitored and restored as required if clearances are to be maintained and excessive rub outs avoided. As significantly out-of-round cases and particularly out-of-flat flanges are assembled, the blade-to-seal clearances will be changed, and deeper rubs as well as different rub patterns will be caused in the engine, leading to confusion as to the causes of localized rubbing.

ADDENDUM

ADDITIONAL GROUND TESTING

ADDENDUM

ADDITIONAL GROUND TESTING

1.0 SUMMARY

An Additional Ground Test was conducted subsequent to the NASA JT9D Flight Loads Test to resolve some of the questions on power-induced high-pressure turbine clearance closures which were identified by the Flight Loads Test. This ground test, which was run at Pratt & Whitney Aircraft, utilized an available JT9D-7R4 test engine which was instrumented for monitoring high-pressure turbine running clearances.

The results confirmed the significance of thermal-induced effects on high-pressure turbine running clearances and the potential for tighter running clearances with reduction of asymmetric clearance closures.

The test also showed the JT9D-7R4 engine to have improved turbine clearance closure characteristics compared to the JT9D-7A engine. The thermal expansion characteristics of the turbine rotor and case are better matched in this later model engine, thus reducing the clearance closure at maximum power.

2.0 INTRODUCTION

The JT9D Flight Loads Test results generally validated prior information on blade-to-seal rubs caused by flight loads. However, the analysis of the measured clearance closures in the high-pressure turbine indicated two unexpected results. First, the maximum clearance closure in a normal flight cycle occurred about 4 minutes into climb rather than at take-off rotation as expected. This later closure appeared to be due to differential thermal expansion between rotating and static components. Second, the magnitude and direction of the asymmetric closure changes were more than could be accounted for by thrust backbone bending and aerodynamic loads. The change and rate of change of these asymmetric closures with changes in power level suggest that they also may be caused by differential thermal expansion originating outside of the first-stage high-pressure turbine.

These results identified the need for additional turbine clearance closure measurements to better understand the effects of power transients and sustained high power on the axisymmetric and asymmetric clearance closure. Specifically, it was desired to measure: 1) the effect of sustained high power operation as occurs during a performance calibration; 2) the effects of a typical full power take-off and climb to cruise altitude; and, 3) the effects of rapid snap accelerations and decelerations with subsequent thermal stabilization. This would cover the full range of transient and steady state power conditions.

After the Flight Loads Test was completed, a JT9D-7R4 development engine (X-568, build 4) was being assembled with special instrumentation. The special instrumentation systems, including laser clearance monitoring probes in the first-stage turbine and turbine case thermocouples, were of the same type as those used in the Flight Loads Test engine. The Additional Ground Test program, which included performance calibrations at the program start and completion, provisions for the measurements defined in the paragraph above, and clearance calibrations to identify any clearance rubs, was integrated into the start of the previously established development test program on X-568-4 engine. This Additional Ground Test was conducted in December, 1981 in a Pratt & Whitney Aircraft experimental, sea level, test facility.

The results of this Additional Ground Test are presented in this Addendum to the JT9D Flight Loads Test report.

3.0 TEST PROGRAM

3.1 Test Installation

The JT9D-7R4 development engine (X-568) included a rebuilt high-pressure turbine with new blades and outer air seals. The rotor/blade assembly was similar to that used in the Flight Loads Test engine. Thus, the mechanical and thermal properties were expected to be the same. The outer air-seal rub shoe design was also similar. However, the high-pressure turbine case, rub shoe support, and seal cooling designs differed slightly, thus, permitting the possibility of different case thermal characteristics than those in the Flight Test Engine (see Figure A-1).

The test engine was mounted in an experimental test stand and installed with a test fan cowl, core cowl, and nozzles which are aerodynamically similar to flight nacelles but mechanically stiffer. The test stand environment plus the lack of airplane-installed subsystems inside the core cowl presented a possibility for a slightly different thermal environment than that of the wing-mounted flight test engine.

3.2 Test Instrumentation

The turbine first-stage was fitted with four helium-neon laser clearance monitoring probes of a design similar to that used in the Flight Loads Test. The probes were mounted to the outer air-seal rub shoes and calibrated to measure blade-to-seal clearance from motoring clearance to a possible rub. The circumferential position of the probes as defined by Figure A-2 was determined by the available access through the air manifold of the "turbine case cooling" system. Nitrogen purging was used to cool the probe and prevent any soiling of the probe optics.

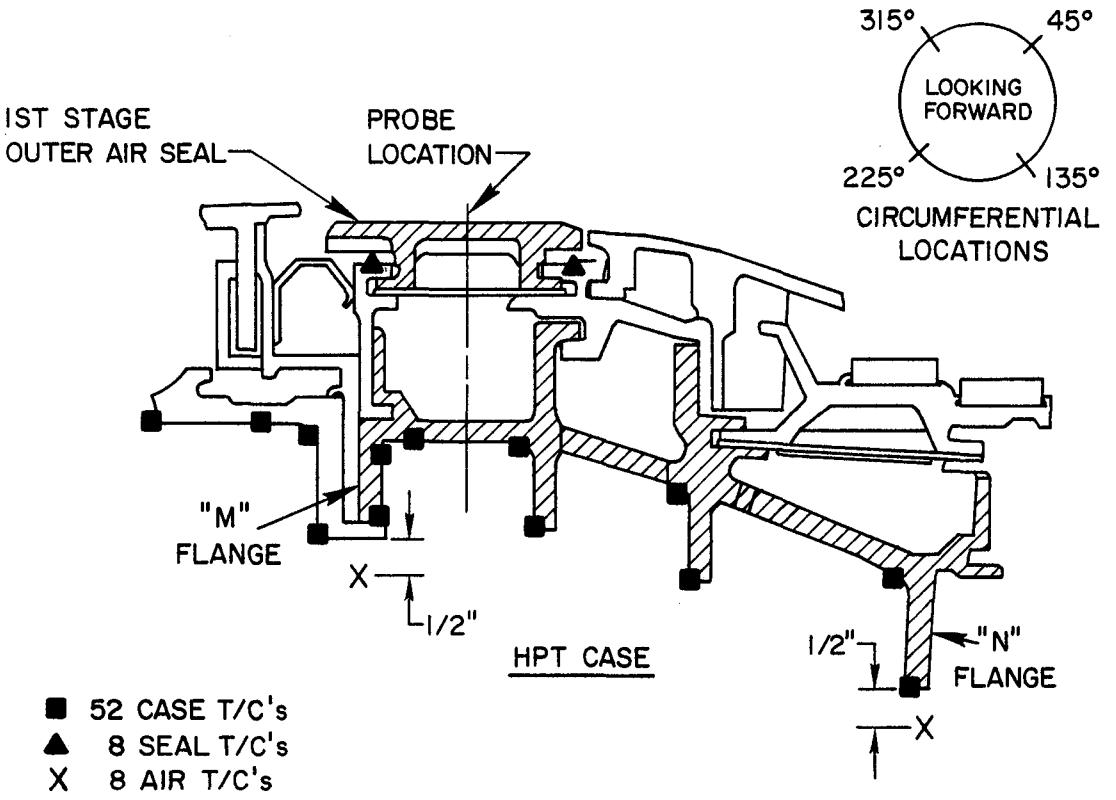

Figure A-1 High-Pressure Turbine Case, Seal, and Air Space Temperature Instrumentation.

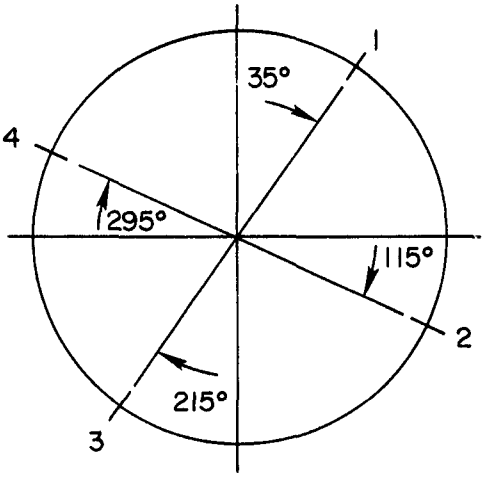

Figure A-2 Angular Location of High-Pressure Turbine Blade Laser Proximity Probes.

The four laser output signals were digitized and recorded continuously on a videotape along with high-pressure rotor speed and time to the nearest 0.1 second for subsequent analysis.

High-pressure turbine case thermal expansion response under transient and steady state conditions was measured by 68 case, seal, and air thermocouples and recorded an a portable data system which recorded these signals once per second.

Simultaneously, the engine performance parameters listed on Table A-I along with a time value were recorded to provide the same data base as in the Flight Loads Test.

TABLE A-I

ENGINE PERFORMANCE INSTRUMENTATION

Parameter	No. Probes	No. Measurements
$P_{ambient}$	1	1
Pt_2/Ps_2	8	8
Pt_{3c}/Ps_{3c}	3	1
Pt_3	4	4
Pt_4	4	4
Pt_7	6	7
$T_{ambient}$	1	1
Tt_{3c}	1	1
T_{t3}	4	4
T_{t4}	4	4
Tt_7	6	7
Thrust	1	1
Wf		1
N_1		1
N_2		1
Vane angle (β)		1
Bleed valve positions		1

3.3 Test Sequence

The engine test sequence was as follows with the laser system recording during all transients and all steady state calibration points:

- o Starter motoring of cold engine;
- o Light-off;
- o Stabilized ground idle;
- o 15-point up-down calibration with 5 minute stabilization at each point;

- o Snap acceleration to full power [1.48 engine pressure ratio (EPR)] and hold until laser measured clearances stabilize;
- o Snap deceleration to ground idle and hold until laser measured clearances stabilize;
- o Simulated full power take-off and climb to cruise altitude with EPR values set such that high-pressure compressor discharge total temperature (T_{T4}) matches actual take-off and climb values for 25 minutes following snap to take-off power;
- o Stabilized ground idle;
- o Eight-point down calibration with 5-minute stabilization at each point; and
- o Subsequent starter motoring of cold engine

The cold motoring prior to the test provided a reference for the axisymmetric and asymmetric clearance closures. The stabilized idle condition between each test condition provided a check for possible rubs during the prior test and for instrumentation drift.

The initial ground calibration provided a performance reference at the start of the test. It also defined turbine clearance closure during extended high power ground operation.

The take-off and climb closure, when adjusted to include the aerodynamic load-induced closures at rotation, lift-off, and climb, defines what is believed to be the most rub sensitive flight conditions in the high-pressure turbine.

3.4 Data Analysis Methodology

High-pressure turbine clearance closure is caused by the factors listed on Figure A-3. The approximate axisymmetric closures are defined by averaging the clearance changes immediately after a power change and after slower thermal effects have occurred. Similarly, the approximate asymmetric closures are determined by taking the vector sums of the differentials between the measured closures and axisymmetric closures immediately after power changes and after thermal effects have taken place. Aerodynamic effects determined in the Flight Loads Test can be added to these power effects to estimate totals.

Case and rub-shoe support ring temperatures were recorded at each transient and steady state test condition. These values were analyzed to establish thermal response characteristics of the case and to identify any nonuniformity in case thermal growth.

Performance data recorded in the initial and final calibrations were analyzed to identify any change in performance associated with the test program. Any performance change in the high-pressure turbine can be matched against any rub-induced increase in blade-to-seal clearances.

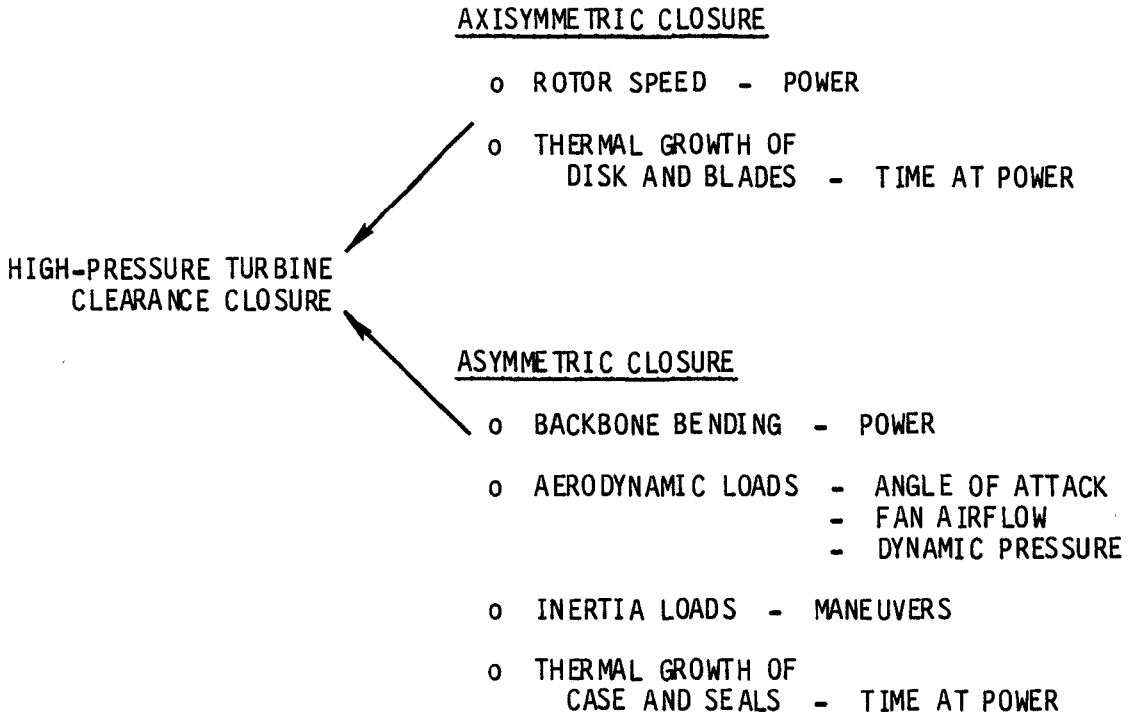

Figure A-3 High-Pressure Turbine Clearance Closure - Closure in the turbine results from engine power, time at power, angle of attack, fan airflow, dynamic pressure, and maneuvers.

4.0 RESULTS

4.1 Overview

The NASA test program was run as the initial test after assembly and installation of engine X-568-4; thus, there was no prior deterioration. The test program was completed during one shift. Three of the four laser probes operated flawlessly throughout the program and indicated no drift in measured clearance. The number 4 probe at 295 degrees was of questionable value after the initial calibration run.

The maximum clearance closure during extended ground running and during simulated take-off and climb to cruise altitude were both less than the closures measured on the JT9D-7A engine in the Flight Loads Test. Also of interest during the simulated take-off and climb, the clearance closure pinch occurred 60 to 70 seconds after acceleration to take-off power rather than 4 to 5 minutes later, as in the JT9D-7A Flight Loads Test engine. The laser probe data indicated no first-stage turbine blade-to-seal rubs during this testing.

Comparison of the pretest and post-test calibration runs indicated essentially no loss in high-pressure turbine performance due to this representative ground testing.

4.2 Measured Clearance Closures

The first test was the up-down calibration. The test was started from a stabilized idle condition. Table A-II lists the power settings, cumulative time at power above idle, N_2 speed, axisymmetric (four-probe average) clearance closure relative to idle condition and max measured closure (probe number 3) relative to idle. The total test time indicates that it was a conservative test when considering the effect of extended high power running on high-pressure turbine clearance closures.

TABLE A-II

HIGH-PRESSURE TURBINE CLEARANCE CLOSURES DURING INITIAL UP CALIBRATION

Time Since Idle Power (minutes)	Percent of Maximum Power	N_2 (rpm)	Clearance Closure, Relative to Idle (inch)	
			Average Closure (Axisymmetric)	Maximum Closure
18	62	6730	-0.013	-0.020
25	70	6880	-0.0155	-0.024
41	78	6990	-0.018	-0.026
48	87	7110	-0.021	-0.029
60	95	7220	-0.024	-0.034
25*	100	7250	-0.025	-0.034

* There was a test interruption with a return to idle power prior to running this point.

In comparison, axisymmetric and maximum closure values for the flight test JT9D-7A engine were 0.036 and 0.058 inch, respectively, when stabilized at maximum power less than 10 minutes after acceleration from stabilized idle (see Figure 5-14, Section 5.3.2 of this document).

The second test was the snap acceleration from stabilized idle to maximum power followed by a snap deceleration after the turbine clearance closures had stabilized at the maximum power condition. Figure A-4 presents a plot of the axisymmetric and maximum clearance closures relative to clearances at stabilized idle plotted versus time from start of the acceleration. High-pressure rotor speed (N_2) values are also plotted.

Figure A-4 First-Stage Turbine Blade-to-Seal Clearance Changes During Snap Acceleration from Stabilized Idle.

Note that the high-pressure rotor is nearly up to speed within 15 seconds. The tightest closure condition, both axisymmetric and maximum (axisymmetric plus asymmetric), occurs in slightly more than 1 minute with closure values of -0.026 and -0.033 inch, respectively. While power is maintained at constant value, the turbine blade-to-seal clearance slowly opens until, at 4 minutes after the acceleration, it appears to stabilize at -0.022 inch axisymmetric and -0.030 inch maximum closure relative to stabilized idle.

The engine was then snapped back to ground idle power and held at that level until the turbine blade-to-seal clearances again appeared to stabilize. A plot of these clearance changes versus time is shown on Figure A-5 with both average and maximum clearances normalized to their stabilized values at maximum power.

The engine speed drops to the idle level in 10 to 12 seconds. This transient resulted in the average clearance opening 0.024 inch in 20 seconds and the minimum clearance (at the 215-degree location) opening 0.029 inch. As rotor assembly and static structure subsequently cool, the clearance first closes, then opens, and appears to stabilize about 0.003 inch tighter than the idle clearance prior to the acceleration. This clearance indicates that the disk temperature still is above its initial idle temperature.

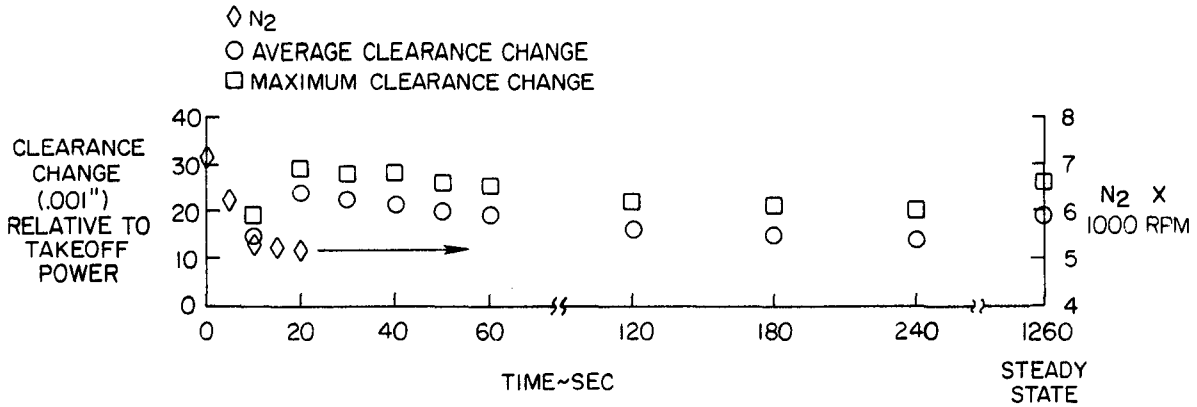

Figure A-5 First-Stage Turbine Blade-to-Seal Clearance Changes During a Snap Deceleration from Maximum Power to Ground Idle.

The third test was the simulated full power take-off and climb to the initial cruise altitude. The engine was accelerated from stabilized idle and followed the EPR versus time schedule shown on Figure A-6. This schedule, run at sea level, best simulated turbine temperature conditions of a normal take-off and climb.

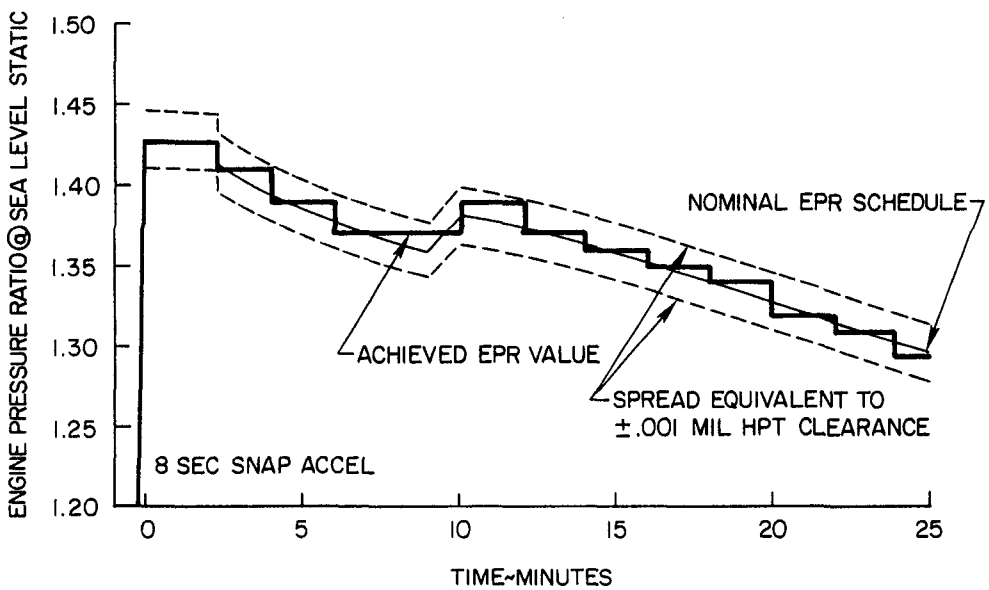

Figure A-6 Engine Pressure Ratio versus Time for the Simulated Full Power Take-Off and Climb.

Figure A-7 presents a plot of axisymmetric and maximum clearance closure relative to stabilized idle clearances. Note that, as would be expected, the response due to the initial acceleration duplicates that of the prior snap acceleration. After the first minute, the clearances start to open due to thermal growth effects. This clearance opening effect is greater than that following the snap acceleration (Figure A-4) due to the lowering gas temperatures during simulated climb as compared to constant gas temperature during the constant power ground run.

Note that in both acceleration cases, the asymmetric clearance closure (that is, maximum minus average) increases with time following the step change in power with the peak occurring 60 to 70 seconds after the snap acceleration. This same effect was seen in the Flight Loads Test results (see Figure 5-14, Section 5.3.2 of this document).

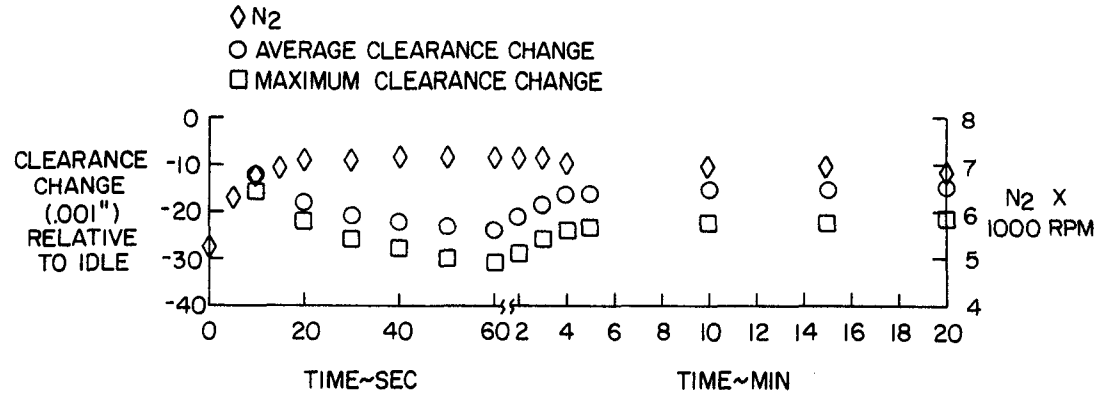

Figure A-7 First-Stage Turbine Clearance Change During Simulated Full Power Take-Off and Climb.

Following this test program, the faulty number 4 laser probe (295-degree location) was removed, recalibrated, and reinstalled. The cold engine motoring run was then repeated. The change in measured readings relative to the pretest readings were as follows:

Probe No.	1	2	3	4	Avg.
Circumferential Location (degrees)	35	115	215	295	
Change (0.001 inch)	-4	-1	-1	+4	-0.5

These differences, which are within the instrumentation system measurement accuracy, indicate no change in clearance; hence, no rub-induced blade loss occurred. This conclusion agrees with test clearance data which indicated no rubs.

4.3 Turbine Case Temperatures

The turbine case thermocouples, located as shown on Figure A-1, were recorded through each transient condition and at steady state test conditions. The data were used to determine case thermal response and aid in the analysis of clearance changes.

Figures A-8 and A-9 present plots of "M" flange root and tip (inner and outer radius) location temperature readings for a snap acceleration transient from stabilized idle to take-off power. Note the uniform temperature increase at the four circumferential positions.

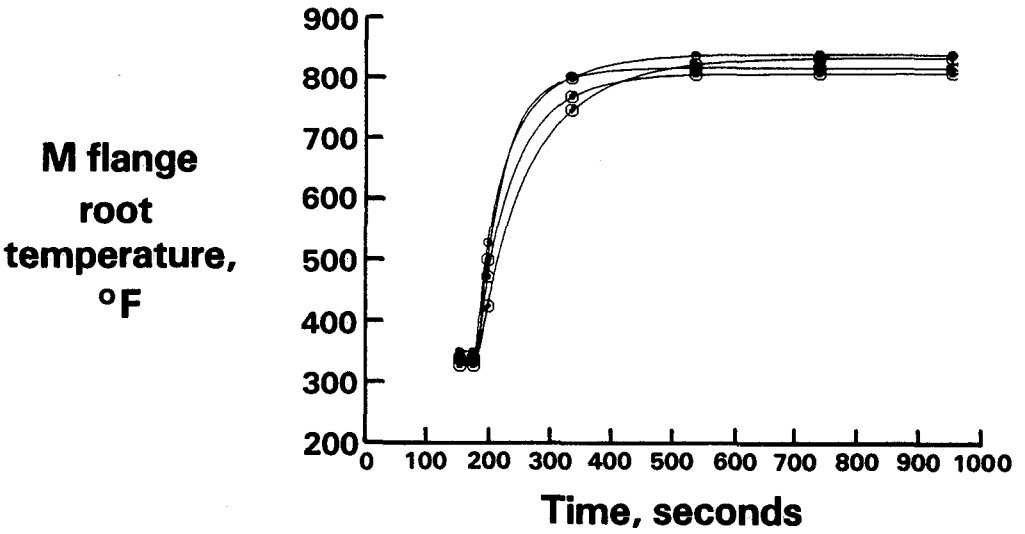

Figure A-8 M Flange Root Temperature Change due to Snap Acceleration. (J26355-1)

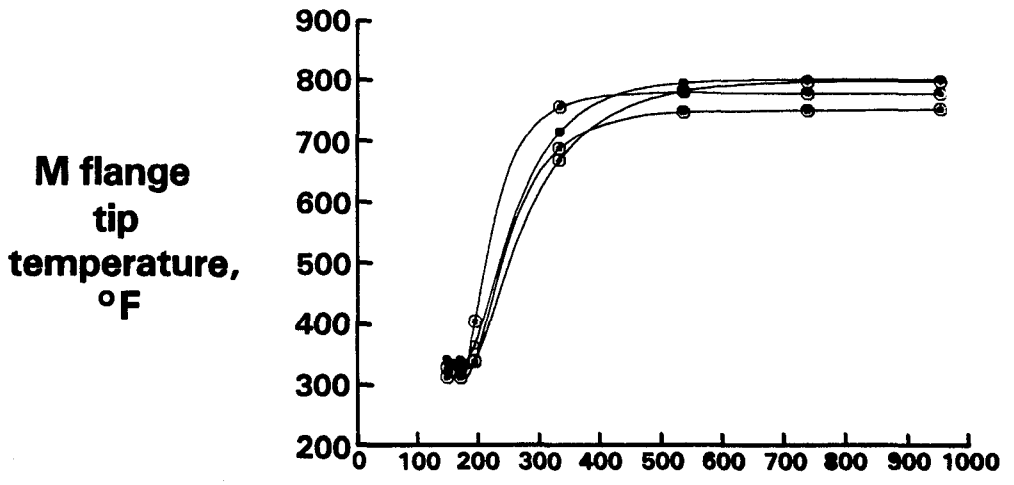

Figure A-9 M Flange Tip Temperature Change due to Snap Acceleration. (J26355-2)

Figure A-10 presents a typical tabulation of all the turbine case, inner support temperatures and air temperatures at steady state, full power operation following the snap acceleration.

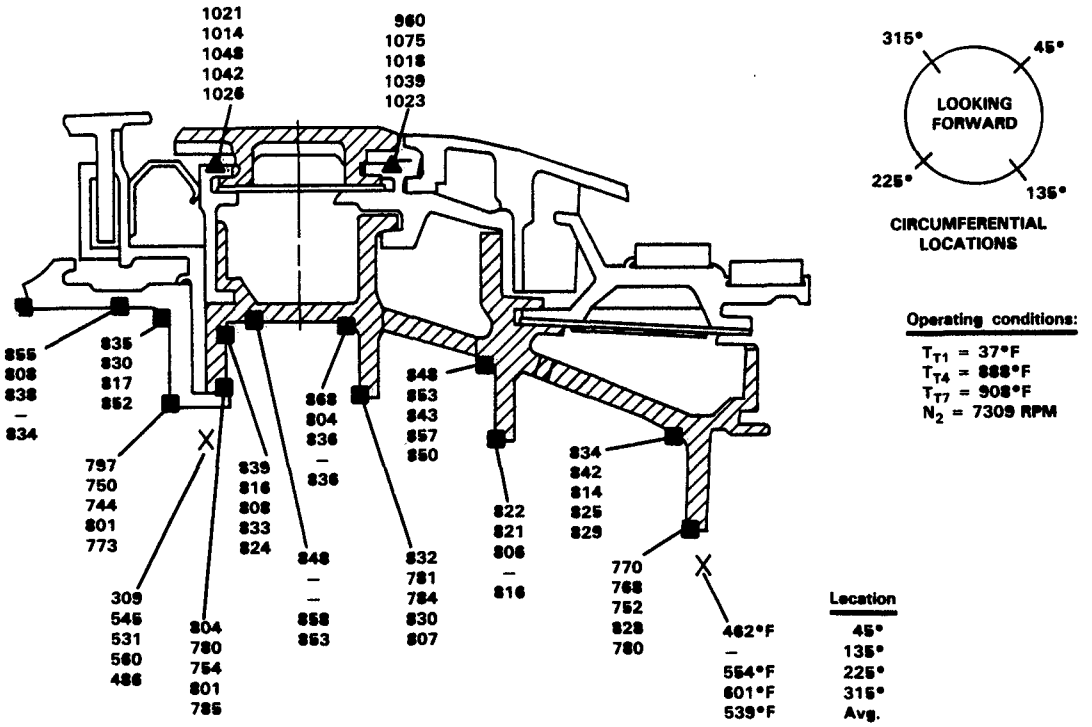

Figure A-10 High-Pressure Turbine Case Steady State Temperatures at Maximum Power. (J26355-3)

4.4 Clearance Closure Analysis

4.4.1 Steady State Response

The steady state clearance closures measured at high power levels during the ground calibration (Table A-II) were slightly tighter than the apparent steady state clearances 13 minutes after the snap to maximum power (Figure A-4). This clearance difference is due to the slight difference in thrust settings in two test runs plus measurement accuracy.

A comparison of these steady state measured clearance closures, both axisymmetric and maximum, with the comparable high power, steady state power-induced closures in the Flight Loads Test shows a reduction in clearance closure of about 0.010 inch (see Table A-III) for the JT9D-7R4 engine model.

TABLE A-III

COMPARISON OF STEADY STATE POWER-INDUCED CLEARANCE CLOSURES

Test	Engine	Condition	Closure (inch) Axisymmetric	Maximum
Flight Loads	JT9D-7A	Ground calibration	0.036	0.058
Flight Loads	JT9D-7A	Max Q (Condition 108)	0.036	0.043
Additional Ground Test	JT9D-7R4	Ground Calibration (48,000-lb thrust)	0.025	0.034
Additional Ground Test	JT9D-7R4	Stabilized after Snap Acceleration (46,000-lb thrust)	0.022	0.030

This comparison shows the JT9D-7R4 engine to be less sensitive to rubs from extended high power operation on the ground.

4.4.2 Transient Response

The transient response of first-stage turbine clearance closures, as measured in this test on JT9D-7R4 engine X-568, was somewhat different from that measured in the Flight Loads Test. Figure A-11 compares the change in axisymmetric clearance relative to stabilized idle during actual and simulated take-off cycles starting at stabilized idle. In the 538,000-pound gross weight, full power take-off (Test No. 101-2 in the Flight Loads Test), there was an initial 0.012-inch pinch at 10 seconds. The clearance then opened and after 40 seconds started to close again. The maximum 0.031-inch pinch occurred about 5 minutes after the acceleration. The clearance then increased. In the simulated full power take-off with the JT9D-7R4 engine X-568, there was a slower, greater initial pinch of 0.024 inch at approximately 70 seconds. With the engine still at take-off power, the axisymmetric clearance then opened. A similar effect was seen in the test with snap acceleration and hold at take-off power.

These different responses result from differences in transient and steady state thermal characteristics of the high-pressure turbine case/outer air seal support assemblies in the two engines since the rotor thermal characteristics are similar.

The maximum axisymmetric closure was less in the JT9D-7R4 engine. This advantage is reduced slightly when the combined asymmetric closure effects due to thrust backbone bending and aerodynamic loads are added, since they are both greater at 70 seconds than at 300 seconds after completion of the acceleration.

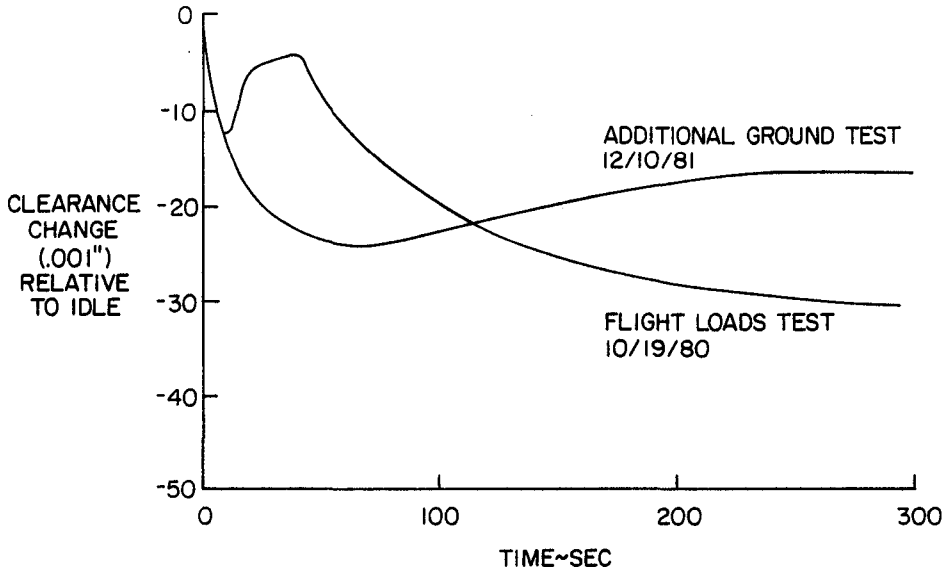

Figure A-11 Comparison of First-Stage Turbine Axisymmetric Clearance Change During Take-Off and Climb.

4.5 Performance Retention

A 15-point up-down engine calibration was conducted at the start of the test sequence to establish initial performance level. A seven-point down calibration was conducted at the end of the test sequence to identify any changes in engine and module performance. Stabilization times of 5 to 7 minutes between each data point were provided during these calibrations.

Comparison of the two calibrations indicated a performance change of less than 0.1 percent in thrust specific fuel consumption, which is within the instrumentation measurement accuracy. The absence of a performance change supports the laser probe measurement results which indicated no first-stage turbine rubs.

5.0 CONCLUSIONS

The Additional Ground Test validated the Flight Loads Test results on the JT9D-7A engine. It also identified the following improved turbine clearance closure characteristics in the JT9D-7R4 engine.

- The power (thermal) induced turbine clearance closure consists of both axisymmetric and asymmetric components in both engine tests. Further reduction of these closure components will permit tighter running clearances and achievement of the resulting increased turbine efficiency.

- The JT9D-7R4 high-pressure turbine showed a smaller power-induced clearance closure during the critical take-off mode, however, the pinch occurred earlier when the aerodynamic load-induced closure would be highest; hence, the maximum total closure effect is expected to be similar for both engines during take-off.

- The lesser thermally-induced clearance closure in the JT9D-7R4 engine following extended high power operation makes it less sensitive to blade-to-seal rubs resulting from extended ground runs and the combined effects of flight loads during high power operation (such as gusts during climb, etc.).

- Finally, the early occurrence of the clearance closure pinch in the JT9D-7R4 engine take-off cycle makes it more amenable to the use of active clearance control during climb.

APPENDICES

APPENDIX A

ENGINE TEARDOWN PHOTOGRAPHS

Engine Model JT9D-7A

Serial Number P-662204
(in Airplane Position No. 3)

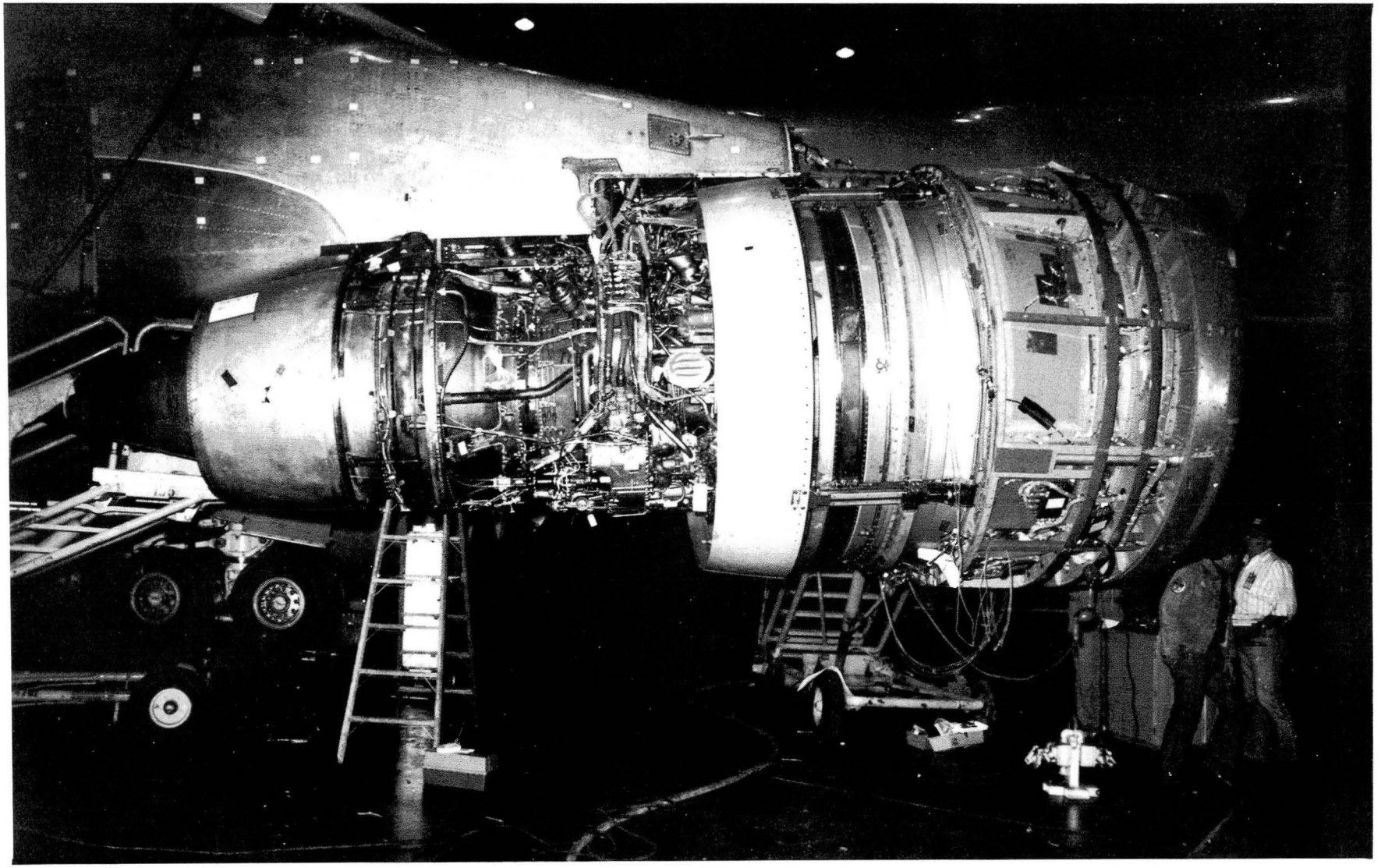

JT9D-7A Engine, Serial No. P-662204, Installed on Boeing 747 Test Airplane, RA001, in Position 3. (Boeing, FA 122279)

JT9D-7A Engines During Flight Testing over Montana; Serial No. P-662201 in Position 4 and Serial No. P-662204 in Position 3. (Boeing, FA 123616)

Blade Clearance Measurement During Disassembly of First-Stage High-Pressure Turbine. (81C-114-4)

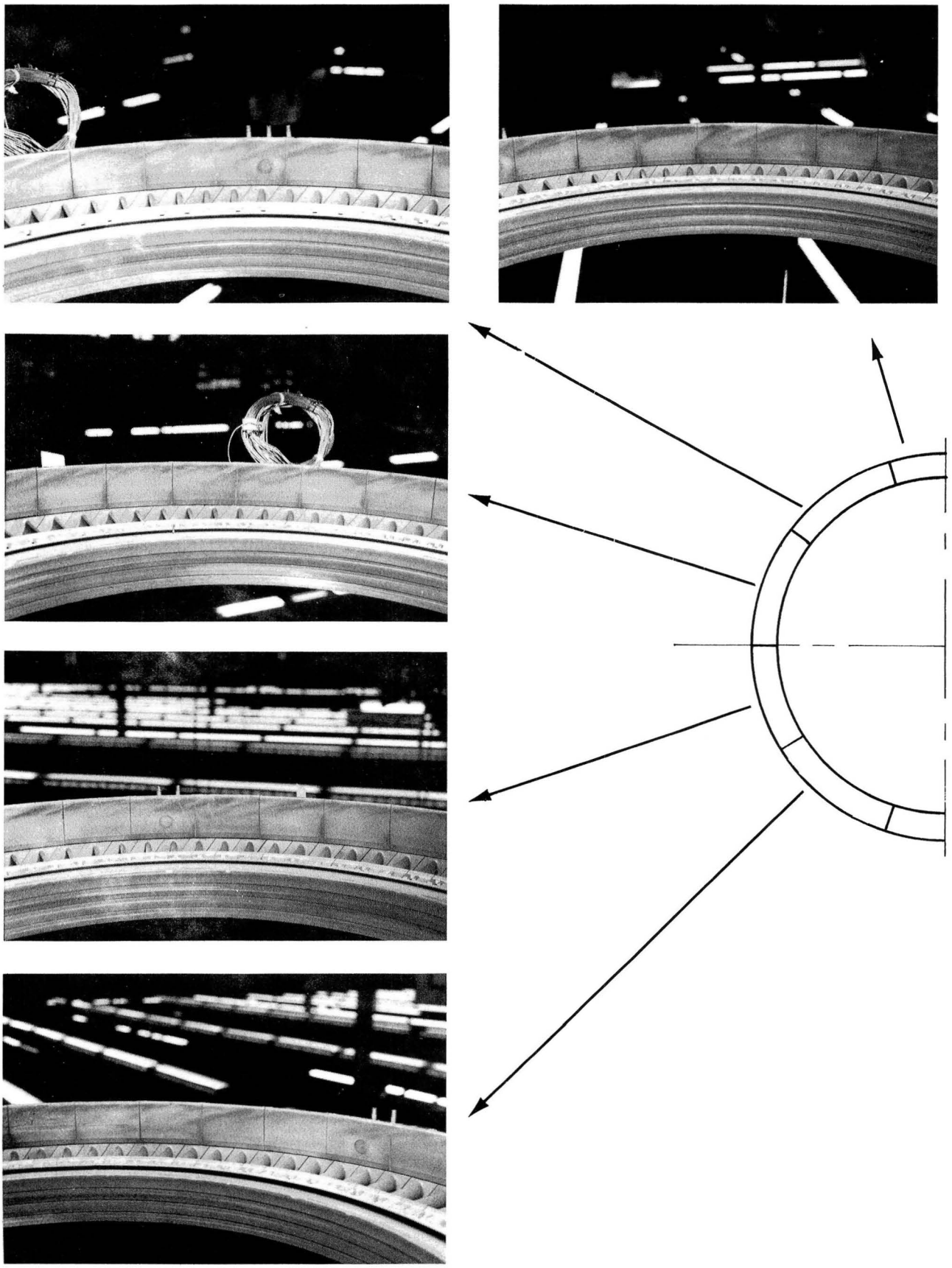

First-Stage High-Pressure Turbine Outer Air Seal Assembly After Test Program; Upper and Left-Hand Portions. (81C-153-23 and 81C-153-14 through -17)

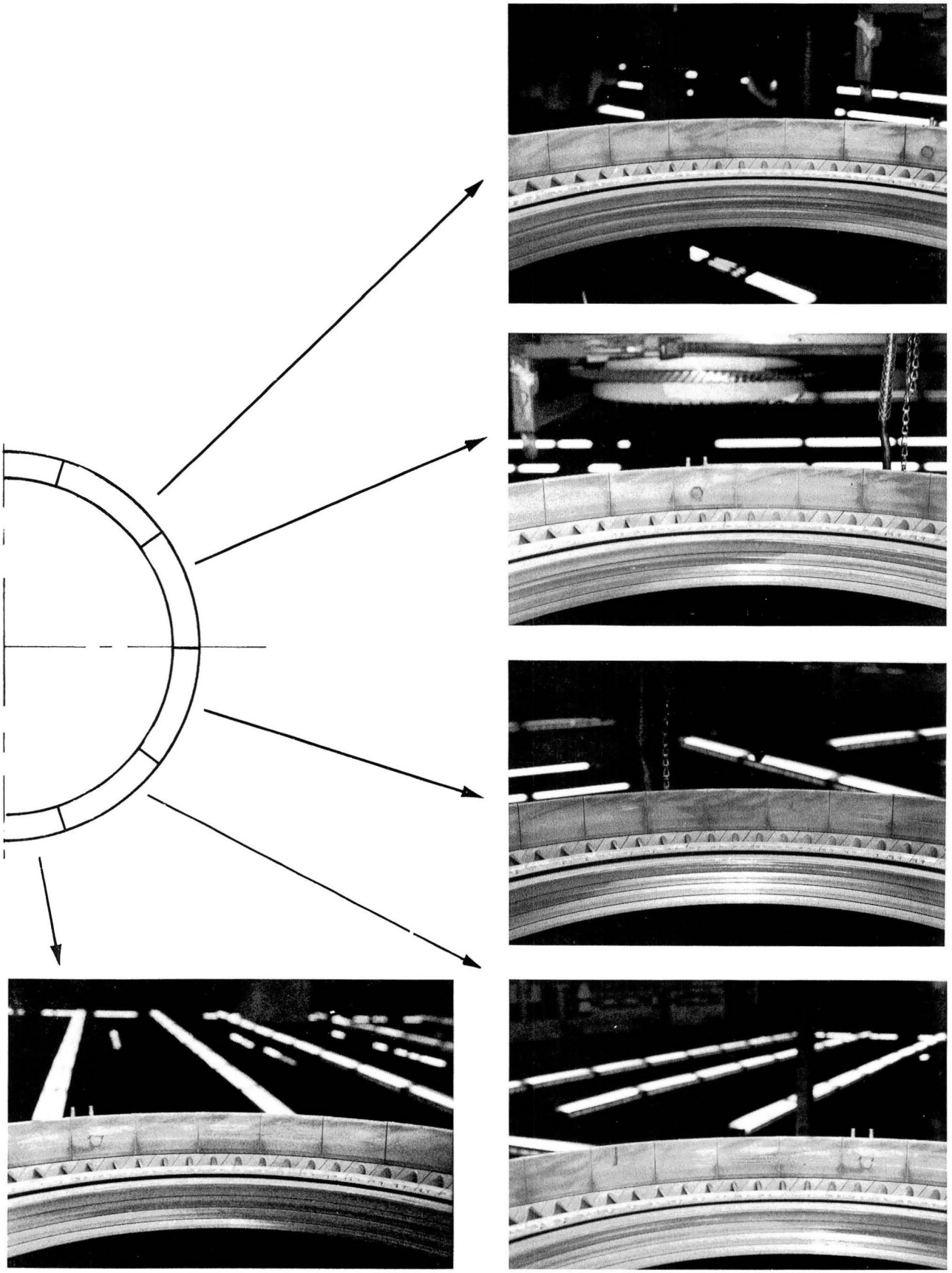

First-Stage High-Pressure Turbine Outer Air Seal Assembly After Test Program; Lower and Right-Hand Portions. (81C-153-18 through -22)

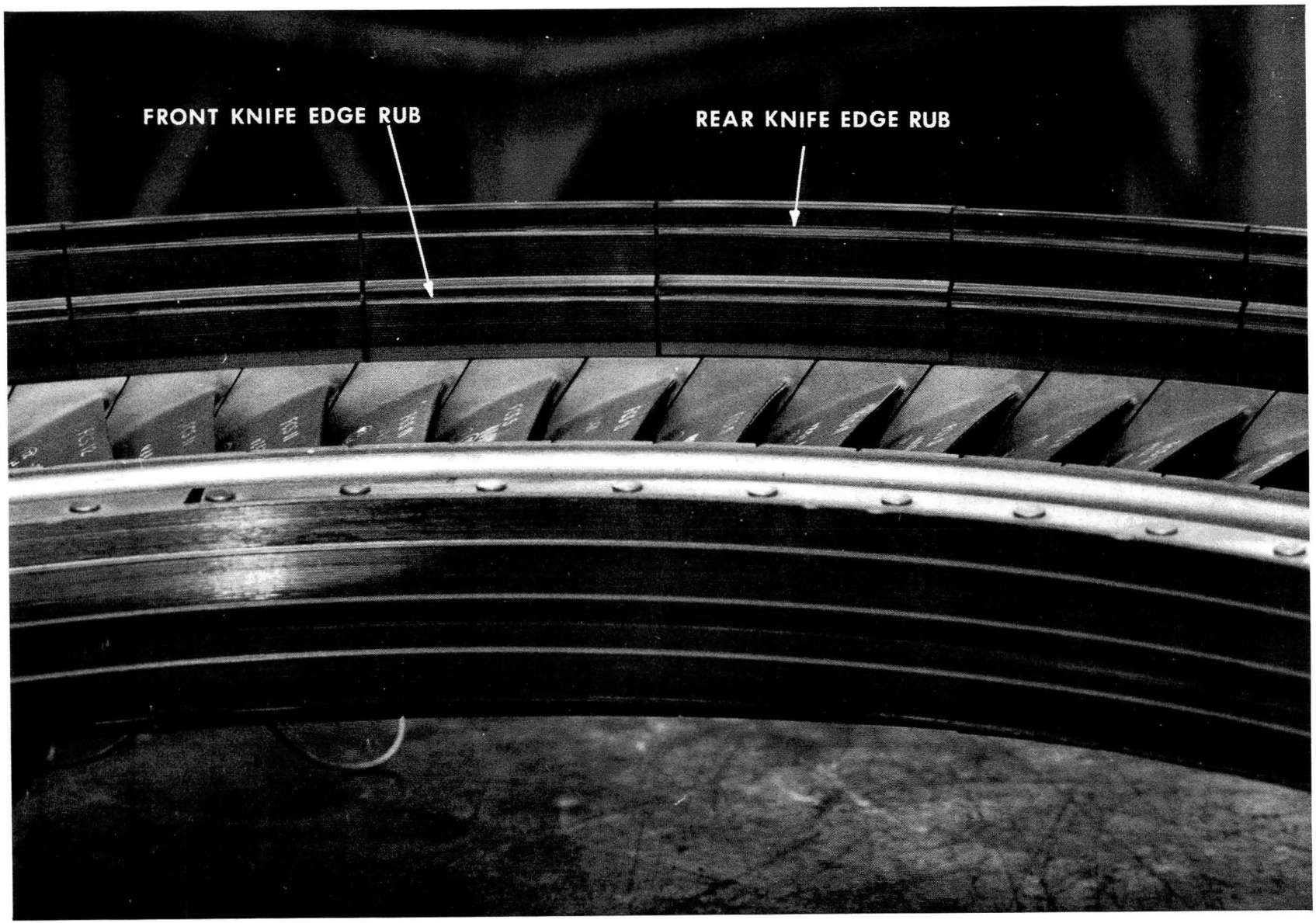

Second-Stage High-Pressure Turbine Outer Air Seal Assembly After Test Program.
(81C-153-1)

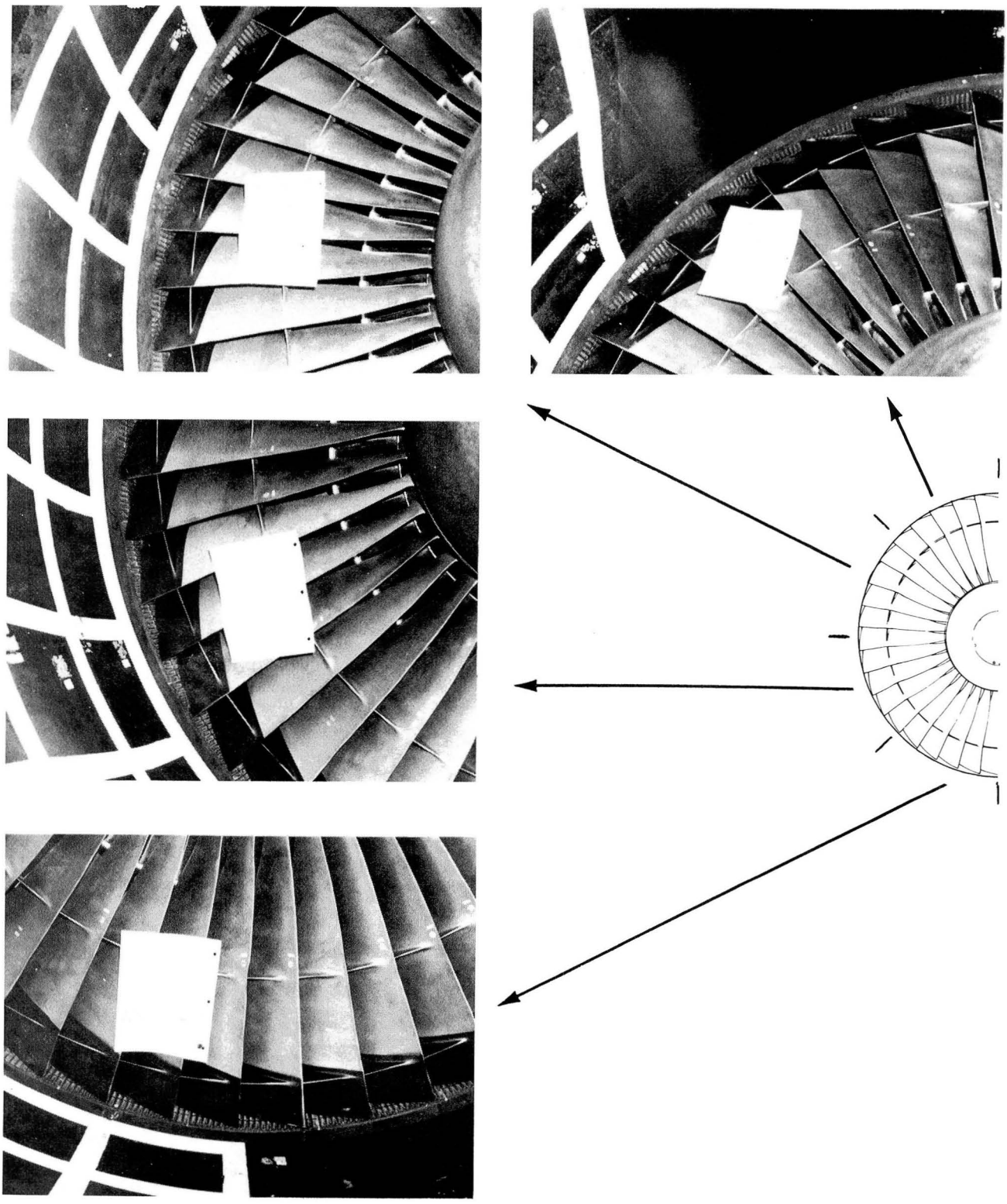

Fan Rub-Strip Wear on Position 3 Engine After Second Test Flight at 538,000-pound Take-Off Gross Weight with Flaps at 10 degrees; Left-Hand Portions. (Boeing, FA 123727 through FA 123730)

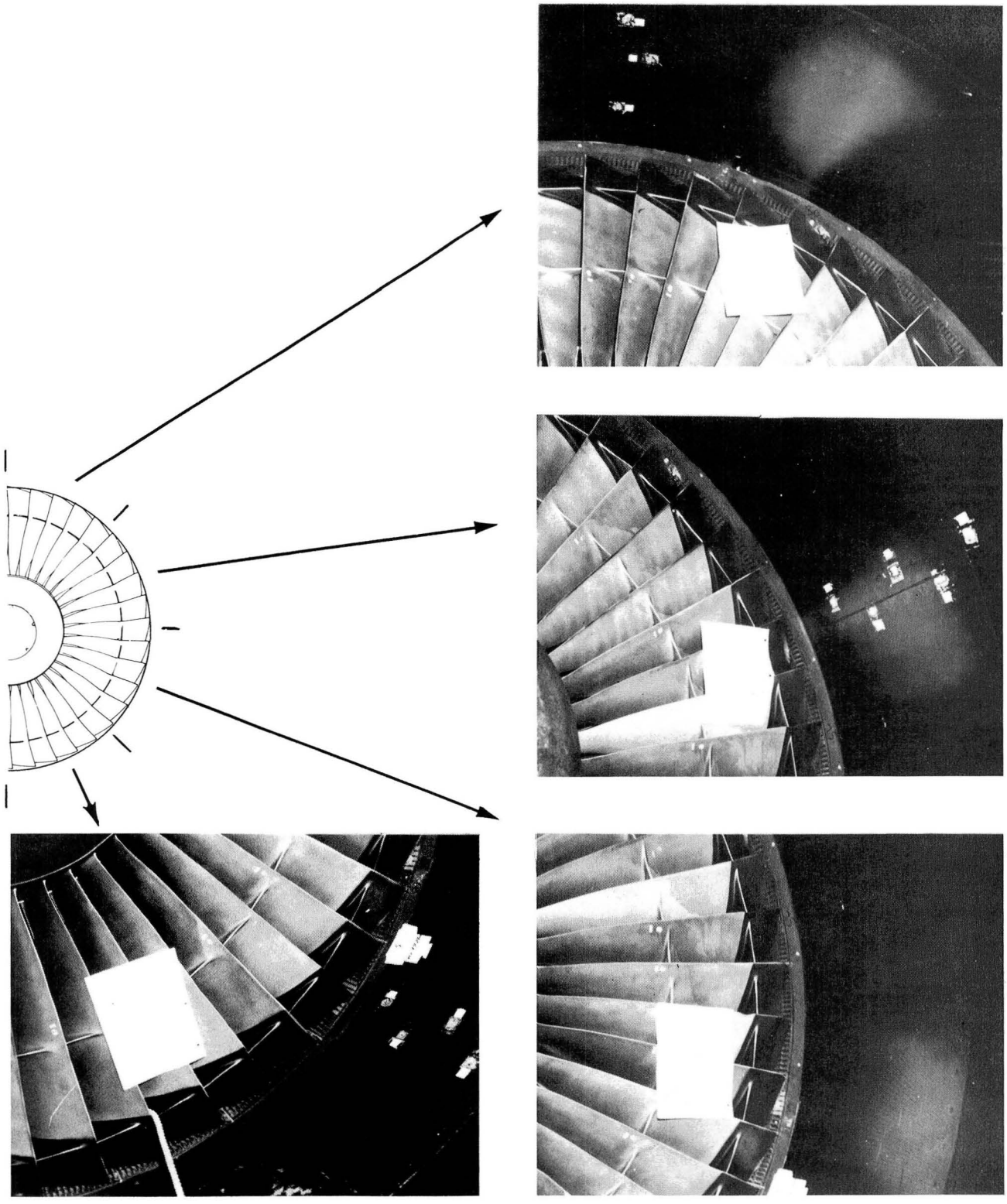

Fan Rub-Strip Wear on Position 3 Engine After Second Test Flight at 538,000-pound Take-Off Gross Weight with Flaps at 10 degrees; Right-Hand Portions. (Boeing, FA 123731 through FA 123734)

Fan Blade Clearance Measurement on Position 3 Engine After Test Program.
(81C-114-2)

Fan Blade Rub Depth Measurement During Disassembly of Position 3 Engine.
(81C-153-30)

APPENDIX B

ACRONYMS AND SYMBOLS

ACRONYMS (Oraganizations)

BCAC	Boeing Commercial Airplane Company
NASA	National Aeronautics and Space Administration
OPEC	Organization of Petroleum Exporting Countries
P&WA	Pratt & Whitney Aircraft

SYMBOLS

ACEE	Aircraft Energy Efficiency (Program)
ADAMS	Airborne Data Analysis and Monitoring System
APTDAC	Automatic Production Test Data Acquisition and Control
ECI	Engine Component Improvement (Program)
ECM	Engine condition monitoring (data)
EGT	Exhaust gas temperature (°C)
EPR	Engine pressure ratio
EVC	Engine vane control
FN, Fn	Net thrust (pounds)
G, g	Gravity, gravitational constant
gyro	Gyroscopic, gyroscope
HAPTS	High Accuracy Pressure and Temperature System
HOST	Hot Section Technology (NASA Program)
HPC	High-pressure compressor
HPT	High-pressure turbine
ID	Inside diameter
LPC	Low-pressure compressor
LPT	Low-pressure turbine
MATE	Materials for Advanced Turbine Engines (NASA Program)
Max Q, q	Airplane maximum dynamic pressure
MN, Mn	Mach number
N	Rotor speed (rpm)
NAIL	Nacelle Aerodynamic and Inertial Loads (NASA Program)
NASTRAN	NASA STRuctural ANalysis (computer program)
OD	Outside diameter
Opr	Operating (line)
P	Pressure (lb/in^2) (psia)
PIC	Plug-In Console (test system)

SYMBOLS (Cont'd.)

PLA	Power lever angle
RPM, rpm	Revolutions per minute
SLS	Sea level static
SP	Special Performance (Boeing 747SP airplane)
T	Temperature (°F) (°C)
TSFC	Thrust specific fuel consumption (lb/hr-lb)
TV	Television (monitor)
V	Airplane flight speed (Mach number)
W	Weight flow (lb/hr) (lb/min)
β	Vane angle (degrees)
Δ	Change

SUBSCRIPTS *

1	Undisturbed inlet (pressures and temperatures)
1	Low-pressure rotor (rotor speeds)
2	Fan inlet (pressures and temperatures)
2	High-pressure rotor (rotor speeds)
2.4	Fan blade discharge
2.5	Fan exit guide vane inlet
2.6	Fan exit guide vane discharge
3	Low-pressure compressor discharge
4	High-pressure compressor discharge
4.5	Combustor borescope location
5	High-pressure turbine inlet
6	High-pressure turibne discharge
7	Low-pressure turbine discharge
amb	Ambient
f	Fuel
i	Inner
S, s	Static
R	At take-off rotation
T, t	Stagnation (total)

* For simplicity, subscripts may be written "on the line" of type, especially in text.

REFERENCES

1. Sallee, G. P.: Performance Deterioration Based on Existing (Historical) Data. NASA CR-135448, 1978.

2. Olsson, W. J. and Sallee, G. P.: Performance Deterioration Based on In-Service Engine Data. NASA CR-159525, 1979.

3. Bouchard, R. J., Beyerly, W. R., and Sallee, G. P.: Short-Term Performance Deterioration in JT9D-7A(SP) Engine 695743. NASA CR-135431, 1978.

4. Jay, A. and Todd, E. S.: Effect of Steady Flight Loads on JT9D-7 Performance Deterioration. NASA CR-135407, 1978.

5. Jay, A. and Lewis, B. L.: Effect of Time-Dependent Flight Loads on JT9D-7 Performance Deterioration. NASA CR-159681, 1979.

6. Stromberg, W. J.: Performance Deterioration Based on Simulated Aerodynamic Loads Test. NASA CR-165297, 1981.

7. Sallee, G. P. and Martin, R. L.: Expanded Study of Feasibility of Measuring In-Flight 747/JT9D Loads, Performance, Clearance, and Thermal Data. NASA CR-159717, 1979.

8. Martin, R. L.: Nacelle Aerodynamic and Inertial Loads (NAIL) Project, Test Report. NASA CR-165760, 1981.

DISTRIBUTION LIST

AVCO LYCOMING DIVISION
550 SOUTH MAIN STREET
STRATFORD, CT 06497
ATTN: A. BRIGHT, ENG. PERFORM. (1)

AEROJET MANUFACTURING COMPANY
601 S. PLACENTIA
FULLERTON, CA 92634
ATTN: J. KORTENHOEVEN, VP ENG. (1)

AIR CALIFORNIA
OAKLAND INTL. AIRPORT
OAKLAND, CA 94614
ATTN: L. WUTH DIRECTOR ENGINEERING (1)

AIR RESEARCH MFG. CO. OF ARIZONA
DEPT. 93-200/503-3S
402 SOUTH 36TH STREET
PHOENIX, AZ 85010
ATTN: K. FLEDDERJOHN (1)

AIR RESEARCH MFG. CO. OF ARIZONA
DEPT. 93-010/503-48
PO BOX 5217
PHOENIX, AZ 85010
ATTN: DR. M. C. STEELE (1)

AIR TRANSPORT ASSOCIATION
1709 NEW YORK AVE., NW
WASHINGTON, DC 20056
ATTN: E. THOMAS, ASST. VP. ENG. (1)

ALASKA AIRLINES, INC.
BOX 68900
SEATTLE, WA 98188
ATTN: J. S. BRACELEN ENG. & MAINT. ADMIN. (1)

AMERICAN AIRLINES, INC.
TULSA MAINT. & ENGINEERING CENTER
3800 N. MINGO ROAD
TULSA, OKLAHOMA 74151
ATTN: KEITH GRAYSON (1)

ARNOLD ENGINEERING & DEVELOPMENT CENTER
AEDC/XRFX
ARNOLD AFS, TN 37389
ATTN: DR. JAMES G. MITCHELL, DIRECTOR OF FACILITY PLANS AND PROGRAMS (1)

ARNOLD ENGINEERING & DEVELOPMENT CENTER
AEDC/XRFX
ARNOLD AFS, TN 37389
ATTN: R. ROEPKE (1)

BOEING COMPANY
PO BOX 3707
SEATTLE, WA 98124
ATTN: R. MARTIN MS: 73-07 (2)

BRANIFF INTERNATIONAL, BRANIFF TOWER
PO BOX 35001
EXCHANGE PARK, DALLAS, TX 75235
ATTN: HANK NELSON, DIRECTOR - POWER-PLANT ENGINEERING (1)

CIVIL AERONAUTICS BOARD
WASHINGTON, DC 20428
ATTN: J. E. CONSTANTZ, CHIEF, ECONOMIC ANALYSIS DIVISION, B-68 (1)

CONTINENTAL AIRLINES, INC.
LOS ANGELES INTERNATIONAL AIRPORT
LOS ANGELES, CA 90009
ATTN: FRANK FORSTER, DIRECTOR - POWER PLANT ENGINEERING (1)

COOPER AIRMOTIVE, INC.
4312 PUTMAN STREET
DALLAS, TX 75235
ATTN: TERRY HARRISON (1)

DELTA AIRLINES, INC.
HARTSFIELD-ATLANTA INTERNATIONAL AIRPORT
ATLANTA, GA 30320
ATTN: JIM GOODRUM (1)

DEPT. OF TRANSPORTATION
21000 SECOND ST., SW
WASHINGTON, DC 20591
ATTN: HAROLD TRUE (1)

DEPT. OF TRANSPORTATION, FAA
21000 SECOND ST., SW
WASHINGTON, DC 20591
ATTN: R. S. ZUCKERMAN, ARD 550, AIRCRAFT NOISE PROJECT MANAGER (1)

DISTRIBUTION LIST (Cont'd.)

DETROIT DIESEL ALLISON DIV. GMC
PO BOX 894
INDIANAPOLIS, IN 46206
ATTN: R. A. SULKOSKE, DEPT. 8896 MS: V19 (1)

EASTERN AIR LINES, INC.
MIAMI INTERNATIONAL AIRPORT
MIAMI, FL 33148
ATTN: M. DOW, DIRECTOR PWRPLNT ENG. -MIAEW, BLDG. 21 (1)

EASTERN AIR LINES, INC.
MIAMI INTERNATIONAL AIRPORT
MIAMI, FL 33148
ATTN: ARTHUR FISHBEIN, PWR. PLNT. ENG.-MIAEW, BLDG. 21 (1)

EASTERN AIR LINES, INC.
MIAMI INTERNATIONAL AIRPORT
MIAMI, FL 33148
ATTN: P. M. JOHNSTONE VP ENGINEERING (1)

FEDERAL AVIATION ADMINISTRATION DOT/FAA/NAFEC
ANA-410, BLDG. 211
ATLANTIC CITY, NJ 08405
ATTN: GARY FRINGS, PROJECT ENGINEER (1)

FEDERAL EXPRESS CORP.
BOX 727
MEMPHIS, TN 38194
ATTN: J. R. RIEDMEYER, MAINT. AND ENGRG (1)

FLYING TIGER LINE, INC.
7401 WORLD WAY WEST, L. A. INTL. AIRPORT
LOS ANGELES, CA 90009
ATTN: J. DIMIN, POWERPLANT ENG. (1)

FLYING TIGER LINE, INC.
7401 WORLD WAY WEST, L. A. INTL. AIRPORT
LOS ANGELES, CA 90009
ATTN: B. LEWANDOWSKI (1)

FRONTIER AIRLINES, INC.
8250 SMITH ROAD
DENVER, CO 80207
ATTN: W. B. DURLIN ENGINEERING (1)

GENERAL ELECTRIC COMPANY, AIRCRAFT ENGINE GROUP
1 NEUMANN WAY
EVENDALE, OH 45215
ATTN: MR. A. F. SCHEXNAYDER (10)

HAMILTON STANDARD DIV. UTC
WINDSOR LOCKS, CT 06096
ATTN: LOUIS A. URBAN - SENIOR DESIGN PROJECT ENGINEER MS 3-2-36 (1)

HUGHES AIRWEST
SAN FRANCISCO INT'L AIRPORT
SAN FRANCISCO, CA 94128
ATTN: W. G. DRECHSLER, MAINTENANCE AND ENGINEERING (1)

LOCKHEED-CALIFORNIA CO.
PO BOX 551
BURBANK, CA 91520
ATTN: T. F. LAUGHLIN JR, DIRECTOR AIRCRAFT OPER. - TECH. (1)

MCDONNELL DOUGLAS
3855 LAKEWOOD BLVD.
LONG BEACH, CA 90846
ATTN: F. L. JUNKERMANN MC 36-41 (1)

MCDONNELL DOUGLAS
3855 LAKEWOOD BLVD.
LONG BEACH, CA 90846
ATTN: RONALD KAWAI MC 36-41 POWERPLANT ENGINEERING (1)

MCDONNELL DOUGLAS
3855 LAKEWOOD BLVD.
LONG BEACH, CA 90846
ATTN: TECH. LIB. ADTL 246-75 (1)

NASA
WASHINGTON, DC 20546
ATTN: W. S. AIKEN/R (1)

NASA
WASHINGTON, DC 20546
ATTN: DR. R. S. COLLADAY/RT-6 (3)

NASA
WASHINGTON, DC 20546
ATTN: P. G. JOHNSON/RJT-2 (1)

DISTRIBUTION LIST (Cont'd.)

NASA
WASHINGTON, DC 20546
ATTN: DR. J. L. KERREBROCK/R (1)

NASA
WASHINGTON, DC 20546
ATTN: C..R. NYSMITH/R (1)

NASA
WASHINGTON, DC 20546
ATTN: DR. W. B. OLSTAD/R (1)

NASA
WASHINGTON, DC 20546
ATTN: R. L. WINBLADE/RJT-2 (1)

NASA-HUGH L. DRYDEN FLIGHT RESEARCH CTR.
PO BOX 273, EDWARDS CA 93523
ATTN: DR. J. ALBERS MS E-PE (1)
ATTN: F. V. OLINGER/MS E-EAP (1)

NASA-HUGH L. DRYDEN FLIGHT RESEARCH CTR.
PO BOX 273, EDWARDS CA 93523
ATTN: HAROLD WASHINGTON, CHIEF - PROPULSION SYSTEMS BRANCH MS E-EA (1)

NASA-LANGLEY RESEARCH CENTER
HAMPTON, VA 23665
ATTN: DR. R. W. LEONARD/MS 158 (1)

NASA-LANGLEY RESEARCH CENTER
HAMPTON, VA 23665
ATTN: L. J. WILLIAMS/MS 249A (1)

NASA-AMES RESEARCH CENTER
MOFFETT FIELD, CA 94035
ATTN: J. ZUK/MS 237-11

NASA-LEWIS RESEARCH CENTER
21000 BROOKPARK ROAD
CLEVELAND, OH 44135
ATTN: DANIEL C. MIKKELSON/MS 86-7, HEAD SUBSONIC PROPULSION SECTION

NASA-LEWIS RESEARCH CENTER
21000 BROOKPARK ROAD
CLEVELAND, OH 44135
ATTN: MILTON A. BEHEIM/MS3-5, DIRECTOR OF AERONAUTICS (1)

NASA-LEWIS RESEARCH CENTER
21000 BROOKPARK ROAD
CELVELAND, OH 44135
ATTN: MILTON A. BEHEIM/MS 86-1, CHIEF, PROPULSION SYSTEMS DIV. (1)

NASA-LEWIS RESEARCH CENTER
21000 BROOKPARK ROAD
CLEVELAND, OH 44135
ATTN: CARL C. CIEPLUCH/MS 301-4, MGR. ENERGY EFFICIENT ENGINE PROGRAM (3)

NASA-LEWIS RESEARCH CENTER
21000 BROOKPARK ROAD
CLEVELAND, OH 44135
ATTN: MELVIN J. HARTMANN/MS 3-7, DIRECTOR OF SCIENCE & TECHNOLOGY (1)

NASA-LEWIS RESEARCH CENTER
21000 BROOKPARK ROAD
CLEVELAND, OH 44135
ATTN: LEWIS LIBRARY/MS 60-3 (2)

NASA-LEWIS RESEARCH CENTER
21000 BROOKPARK ROAD
CLEVELAND, OH 44135
ATTN: L. D. NICHOLS, CHIEF, FLUID MECHANICS & ACOUSTICS MAIL STOP: 5-3 (1)

NASA-LEWIS RESEARCH CENTER
21000 BROOKPARK ROAD
CLEVELAND, OH 44135
ATTN: NEAL T. SAUNDERS/MS49-1, CHIEF, MATERIALS DIVISION

NASA-LEWIS RESEARCH CENTER
21000 BROOKPARK ROAD
CLEVELAND, OH 44135
ATTN: TITO T. SERAFINI/MS 49-1, HEAD, POLYMER-MATRIX COMPOSITES SECTION

DISTRIBUTION LIST (Cont'd.)

NASA-LEWIS RESEARCH CENTER
21000 BROOKPARK ROAD
CLEVELAND, OH 44135
ATTN: D. L. NORED/MS 301-2, CHIEF, TRANSPORT PROPULSION OFFICE (1)

NASA-LEWIS RESEARCH CENTER
21000 BROOKPARK ROAD
CLEVELAND, OH 44135
ATTN: D. J. POFERL/MS 500-207 CHIEF, ENGINE SYSTEMS DIV. (1)

NASA-LEWIS RESEARCH CENTER
21000 BROOKPARK ROAD
CLEVELAND, OH 44135
ATTN: ANTHONY LONG/MS 500-305, CONTRACTING OFFICER (1)

NASA-LEWIS RESEARCH CENTER
21000 BROOKPARK ROAD
CLEVELAND, OH 44135
ATTN: REPORT CONTROL OFFICE/MS 5-5 (1)

NASA-LEWIS RESEARCH CENTER
21000 BROOKPARK ROAD
CLEVELAND, OH 44135
ATTN: R. J. ANTL/MS 301-4 (13)

NASA-LEWIS RESEARCH CENTER
21000 BROOKPARK ROAD
CLEVELAND, OH 44135
ATTN: J. A. ZIEMIANSKI/MS 49-6, CHIEF STRUCTURES AND MECHANICAL TECHNOLOGIES DIVISION (3)

NASA SCIENTIFIC AND TECHNICAL INFO. FACILITY
PO BOX 8757
BALTIMORE/WASHINGTON INTL. AIRPORT, MD 21240
ATTN: ACCESSIONING DEPT. (30)

NATIONAL AIRLINES, INC.
PO BOX 592055, AIRPORT MAIL FACILITY
MIAMI, FL 33159
ATTN: R. A. STARNER, DIRECTOR-ENGRG. (1)

NAVAL AIR PROPULSION CENTER
1440 PARKWAY AVENUE
TRENTON, NJ 08628
ATTN: W. L. PASELA - PE 63, PROJECT ENGINEER-TEST & EVAL. (1)

NORTHWEST AIRLINES, INC.
MINNEAPOLIS-ST. PAUL INT'L. AIRPORT
ST. PAUL, MN 55111
ATTN: A. RADOSTA - MS 838, ASSISTANT DIRECTR POWER PLANT MAINT. (1)

OZARK AIR LINES INC.
BOX 10007
ST. LOUIS, MO 63145
ATTN: E. E. BOOCK, MAINT & ENGINEERING (1)

PACIFIC AIRMOTIVE CORP.
2940 N. HOLLYWOOD WAY
BURBANK, CA 91503
ATTN: ODDVAR BENDIKSON, DIRECTOR, PROJECT ENGINEERING (1)

PACIFIC AIRMOTIVE CORP.
2940 N. HOLLYWOOD WAY
BURBANK, CA 91503
ATTN: J. R. GAST, SR. DIRECTOR ENGRG. (1)

PACIFIC SOUTHWEST AIRLINES
3225 HARBOR DR.
SAN DIEGO CA 92101
ATTN: L. NORWOOD, ENGINEERING (1)

PAN AMERICAN WORLD AIRWAYS, INC.
JOHN F. KENNEDY INTERNATIONAL AIRPORT
ROOM 312, HANGER 14; JAMAICA, NY 11430
ATTN: NIELS ANDERSEN, PROJECT ENGINEER (1)

PAN AMERICAN WORLD AIRWAYS, INC.
JOHN F. KENNEDY INTERNATIONAL AIRPORT
JAMAICA, NY 11430
ATTN: ANGUS MACLARTY, DIRECTOR - POWERPLANT ENGINEERING (1)

PAN AMERICAN WORLD AIRWAYS, INC.
JOHN F. KENNEDY INTERNATIONAL AIRPORT
JAMAICA, NY 11430
ATTN: VP & CHIEF ENGINEER (1)

PAN AMERICAN WORLD AIRWAYS
JOHN F. KENNEDY INTERNATIONAL AIRPORT
JAMAICA, NY 11430
ATTN: ROBERT E. CLINTON, JR. (1)

PIEDMONT AIRLINES
SMITH REYNOLDS AIRPORT
WINSTON-SALEM, NC 27102
ATTN: H. M. CARTWRIGHT, V.P. MAINT. & ENGINEERING (1)

DISTRIBUTION LIST (Cont'd.)

PIEDMONT AIRLINES
SMITH REYNOLDS AIRPORT
WINSTON-SALEM, NC 27102
ATTN: PAUL M. REHDER, SUPERVISOR-POWER PLANT ENGINEERING (1)

PRATT & WHITNEY AIRCRAFT GROUP
400 MAIN STREET
EAST HARTFORD, CT 06108
ATTN: J. P. MURPHY, CHIEF QUALITY PERFORMANCE BRANCH, AFPRO-OL-AA, DET. 8 (1)

PRATT & WHITNEY AIRCRAFT GROUP
400 MAIN STREET
EAST HARTFORD, CT 06108
ATTN: W. O. GAFFIN

REPUBLIC AIRLINES, INC.
3500 AIRLINE DR.
MINNEAPOLIS, MN 55450
ATTN: D. W. ATWOOD, MAINTENANCE & ENGINEERING (1)

SEABOARD WORLD AIRLINES, INC.
SEABOARD WORLD BUILDING, JFK INTL. AIRPORT
JAMAICA, NY 11430
ATTN: J. FARRAH, VP MAINTENANCE & ENGINEERING (1)

SEABOARD WORLD AIRLINES, INC.
SEABOARD WORLD BLDG., JFK INTL. AIRPORT
JAMAICA, NY 11430
ATTN: R. BARBA, MANAGER-POWERPLANT ENGINEERING (1)

SOUTHWEST AIRLINES, CO
BOX 37611
DALLAS, TX 75235
ATTN: J. A. VIDAL, MAINTENANCE & ENGINEERING (1)

TEXAS INTERNATIONAL AIRLINES, INC.
BOX 12788
HOUSTON, TX 77017
ATTN: R. STEPHENSON, ENGINEERING (1)

TRANS WORLD AIRLINES
PO BOX 20126, KANSAS CITY INTL. AIRPORT
KANSAS CITY, MO 64195
ATTN: KEN IZUMIKAWA 2-280 MCI (1)

TRANS WORLD AIRLINES
PO BOX 20126, KANSAS CITY INTL. AIRPORT
KANSAS CITY, MO 64195
ATTN: W. D. SHERWOOD (1)

USAIR
INTERNATIONAL AIRPORT
PITTSBURG, PA 15231
ATTN: W. G. PEPPLER, DEVELOPMENT ENGINEERING (1)

UNITED AIRLINES, INC.
SAN FRANCISCO INTERNATIONAL AIRPORT
SAN FRANCISCO, CA 94128
ATTN: JOHN CURRY (1)

UNITED AIRLINES, INC.
SAN FRANCISCO INTERNATIONAL AIRPORT
SAN FRANCISCO, CA 94128
ATTN: JAMES UHL (1)

WESTERN AIR LINES, INC.
6060 AVION DR. BOX 92005, WORLD WAY POSTAL CTR.
LOS ANGELES, CA 90009
ATTN: WALTER HOLTZ (1)

WIEN AIR ALASKA, INC.
4100 INT'L AIRPORT ROAD
ANCHORAGE, AK 99502
ATTN: J. E. COLBURN, OPERATIONS & MAINTENANCE (1)

WORLD AIRWAYS, INC.
BOX 2330
OAKLAND, CA 94614
ATTN: R. L. FUNK, MAINTENANCE & ENGINEERING (1)

WRIGHT-PATTERSON AFB
DAYTON, OH 45433
ATTN: E. BAILEY, AFWAL/NASA PO (1)

WRIGHT-PATTERSON AFB
DAYTON, OH 45433
ATTN: LT. COL. D. S. DICKSON, ASD/YZI (1)

WRIGHT-PATTERSON AFB
DAYTON, OH 45433
ATTN: C. M. HIGH, ASD/YZE (1)

WRIGHT-PATTERSON AFB
DAYTON, OH 45433
ATTN: MAJ. C. KLINGER, ASD/YZET (1)

~~WRIGHT-PATTERSON AFB~~
~~DAYTON, OH 45433~~
~~ATTN:~~ E. C. SIMPSON (RETIRED)